

POLITECNICO DI TORINO

Collegio di Ingegneria Chimica e dei Materiali

**Master of Science Course
in Materials Engineering**

Master of Science Thesis

Graphene-based biosensor for the detection
of bacteria



Supervisor

Prof. Marco Sangermano

Hosting University Supervisor

Prof. Ivan Mijakovic

Candidate
Alessandra Merlo

July 2018

*“Quando inizia a capire
Che sei solo e in mutande
Quando inizi a capire
Che tutto è più grande
C’era chi era incapace a sognare
E chi sognava già.
Tra una botta che prendo
E una botta che dò
Tra un amico che perdo
E un amico che avrò
Che se cado una volta
Una volta cadrò
E da terra, da lì, mi alzerò
C’è che ormai che ho imparato a sognare,
non smetterò.”*

- Negrita

Contents

Sommario esteso	1
1. Introduction.....	1
2. Graphene	3
2.1 Properties of graphene.....	3
2.2 Antibacterial properties of graphene	8
2.3 Graphene field effect transistor	16
2.3.1 MOSFET	16
2.3.2 G-FET.....	18
3. CVD Graphene Biosensor	21
3.1 The working principle	21
3.2 Device fabrication process	23
3.3. Characterization	34
3.3.1 Raman spectroscopy.....	34
3.3.2 R- V_G characteristics.....	38
3.4 Set-up	40
3.5 Bacterial colonization	43
3.5.1 Gram-positive and Gram-negative bacteria	43
3.5.2 Biofilm formation.....	45
3.6 Single bacteria test	46
3.6.1 P. aeruginosa	47
3.6.2 Staphylococcus Epidermidis	54
3.6.3 Escherichia coli	57
3.6.4 Staphylococcus Aureus.....	60
3.7 Discussion of results	63
4. Conclusions.....	68
Appendix I: Boron doped graphene Biosensor.....	71
I. The working principle	71
II. The structure of the flakes	73
III Preparation for testing	74
III.I Samples preparation.....	74
III.II The setup	77
IV. Verification of induced magnetism	79
V. Conclusions and future prospects.....	80
References.....	81
List of symbols and acronyms.....	89

Aknowledgments..... 91
Ringraziamenti..... 93

Sommario esteso

Il grafene, dopo la sua prima sintetizzazione da parte di Geim e Nosedov nel 2004 ^[1,2] ha conosciuto grossa fortuna nel campo della ricerca per le sue peculiari proprietà, tra le quali ad esempio l'ottima conduttività elettrica ^[19,30-38] e termica ^[39-41], notevoli proprietà barriera nei confronti sia di sostanze gassose che liquide ^[24-25] e un modulo elastico di circa 1TPa ^[16,23], solo per citare alcuni esempi. Tali caratteristiche hanno permesso lo sviluppo di numerose tecnologie innovative basate sull'utilizzo del grafene e dei suoi derivati (quali ad esempio grafenossido e grafenossido ridotto) in numerosi campi di applicazione quali l'aeronautica ^[4,5], l'elettronica ^[7,8] e la medicina ^[10] (Figura 1). La possibilità di combinare differenti caratteristiche del materiale ha suggerito il suo utilizzo sia a sè, ad esempio sotto forma di nanotubi di carbonio per il rilascio mirato di farmaci, sia integrato in dispositivi atti alla rilevazione di specifiche sostanze chimiche o biologiche, generalmente noti come biosensori. Una trattazione più ampia e approfondita delle caratteristiche del materiale è consultabile nel Capitolo 2 dell'elaborato di tesi.

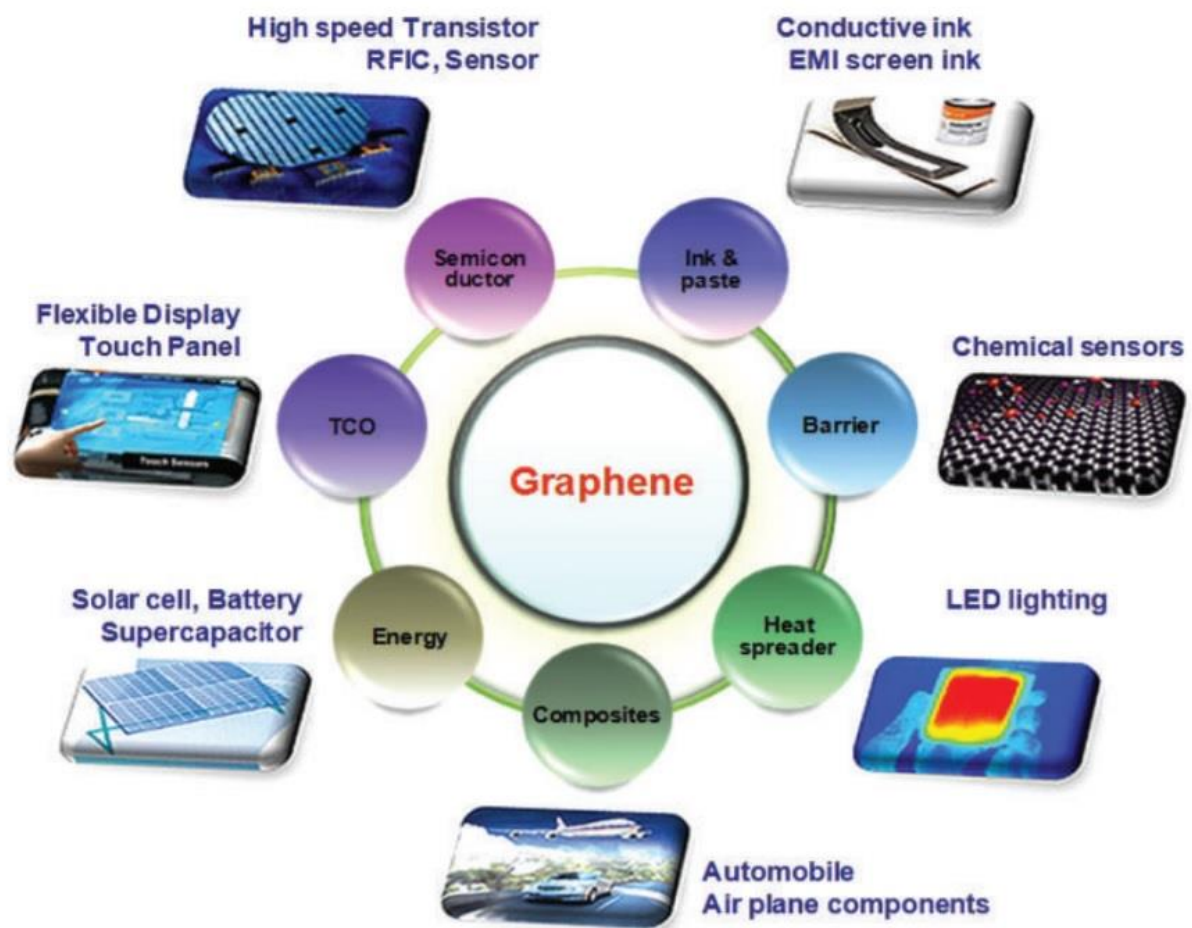


Figura 1. Quadro d'insieme delle applicazioni del grafene in differenti campi di ricerca. [3]

Nella presente relazione, il grafene è stato integrato in un dispositivo elettronico analogo, per comportamento, ad un transistor ad effetto di campo (FET), al fine di realizzare un dispositivo in grado di rilevare, in tempo reale, l'inizio, e possibilmente il tipo, di una infezione batterica.

Come in un comune Metal-Oxide-Semiconductor FET, e similmente a quanto riportato in letteratura per altri biosensori contenenti grafene ^[87-90], la struttura del dispositivo è a strati: sopra un substrato di silicio (in grigio in Figura 2), un secondo strato di ossido di silicio, in blu, viene accresciuto, cui segue la realizzazione dei contatti metallici per i terminali di Source, Drain e Gate. La configurazione finale del biosensore è ottenuta col trasferimento del grafene sul substrato, come mostrato in Figura 2.

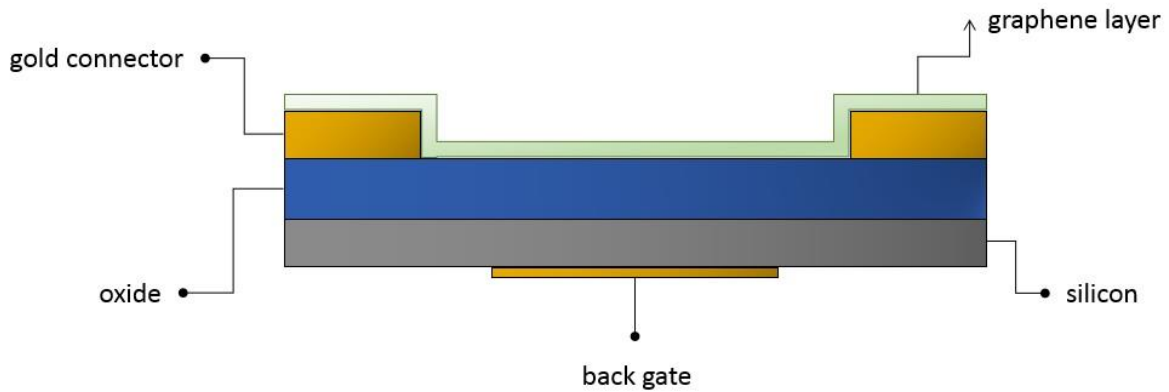


Figure 2. Panoramica della struttura e dei materiali utilizzati per realizzare il biosensore.

Il principio di funzionamento del dispositivo è simile a quello di un MOSFET: in assenza di differenza di potenziale tra i contatti, non vi è possibilità di passaggio di corrente tra Source e Drain. Viceversa, in presenza di una differenza di potenziale tra Gate e Source e Source e Drain, si ha la formazione di un canale elettronico che permette il passaggio di corrente (la cui intensità è controllata dalla ddp tra Gate e Source) tra Source e Drain. Per i graphene-FET in generale, e per questo caso nello specifico, il canale elettronico non si forma, come nel MOSFET, all'interno dell'ossido, ma è costituito dal singolo strato di grafene trasferito sulla superficie. Questa differenza ha necessariamente un impatto sulle curve caratteristiche del dispositivo, in particolare nei grafici $I_D - V_G$, dove il grafico assume una caratteristica forma a V ^[98], indice di un comportamento ambipolare. Tuttavia, il minimo di tale curva può essere traslato rispetto alla sua posizione teorica in presenza di molecole adsorbite sulla superficie o difetti e impurità insorti durante produzione o trasferimento del grafene ^[99]. Tali curve caratteristiche sono dunque un ottimo strumento per la valutazione qualitativa del dispositivo.

Il sensore è stato realizzato con tecnica litografica, ampiamente diffusa per la realizzazione di componenti elettronici di elevata qualità, secondo diversi passaggi esemplificati graficamente in Figura 3: a partire da un normale substrato per componenti elettronici di silicio e ossido di silicio, sono dunque stati realizzati prima i contatti in oro e dunque il trasferimento del grafene, poi limitato alla zona di connessione tra i diversi contatti. Un primo coating permette la protezione del circuito sottostante e ne favorisce il riutilizzo. Il montaggio sul supporto, la realizzazione dei contatti e la stesura di un ulteriore strato polimerico protettivo portano il sensore alla sua configurazione finale.



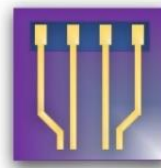
Si substrate



Si + SiO₂



coating with parylene
and window realization



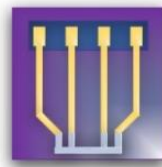
deposition of
gold contacts



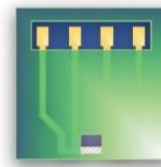
graphene
transfer



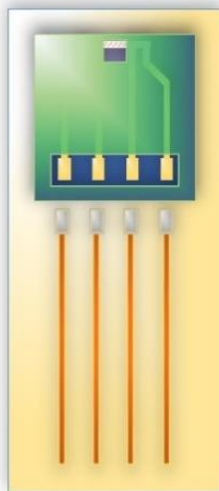
PMMA is
cleansed off



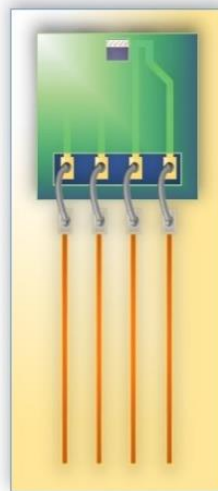
graphene is taken off
from undesired areas



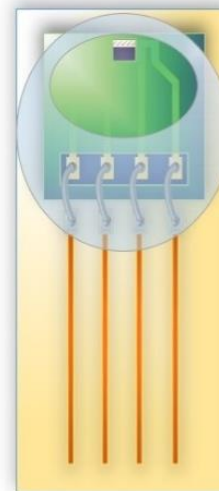
graphene area is exposed and
chip protected with LOR3A



chip is mounted on support



Contacts in silver paste are realized



PDMS is used to cover the
fragile areas of the sensor

Figura 3. Sommario 2D delle diverse fasi del processo litografico necessarie alla realizzazione del sensore.

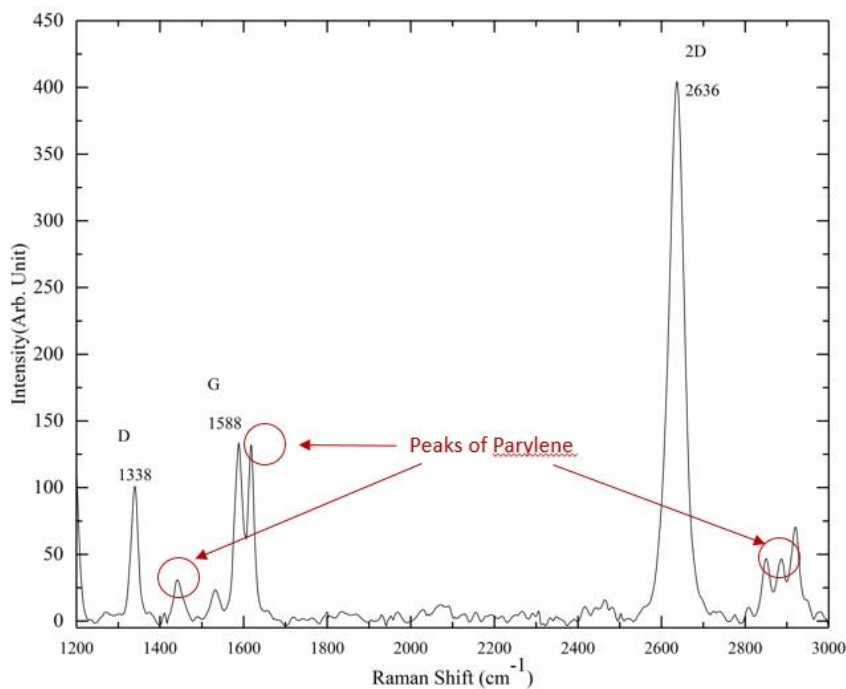
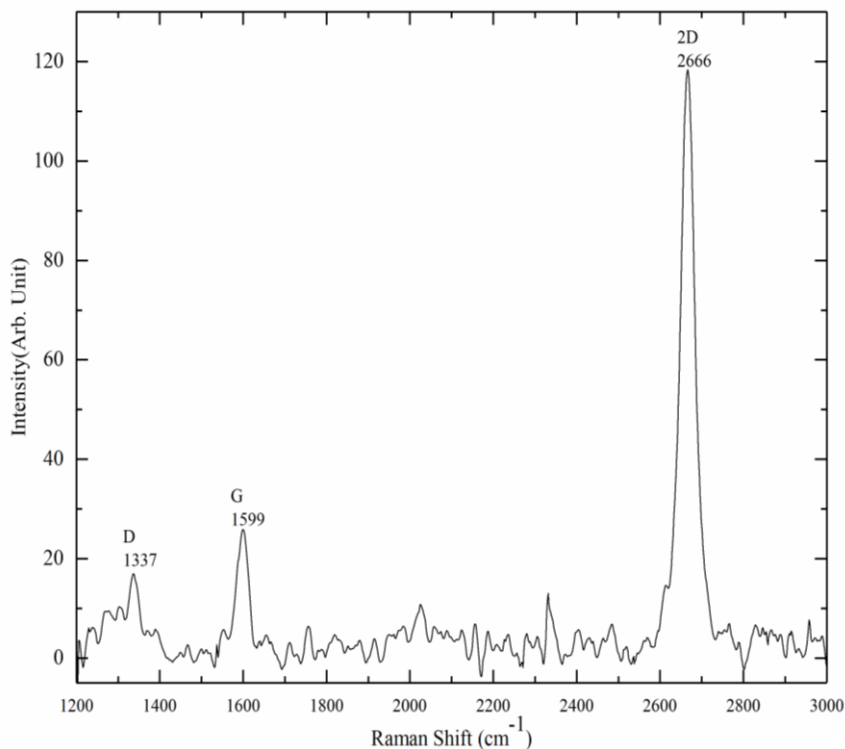


Figure 4. Spettri Raman di grafene cresciuto per Chemical Vapour Deposition su un substrato di rame (a, in alto) e del grafene in seguito al trasferimento sul substrato del biosensore (b).

Al completamento del processo litografico, i sensori sono stati adeguatamente testati per garantirne il corretto funzionamento sia con tecniche di spettroscopia Raman, la quale fornisce informazioni sulla struttura e configurazione elettronica del materiale [17,117], sia con valutazione delle caratteristiche $R-V_G$, grazie alle quali si ottengono indicazioni qualitative sulla qualità del processo di fabbricazione e sull'affidabilità del dispositivo. Il rapporto tra i picchi caratteristici della grafite, a circa 1580 e 2700 cm^{-1} , ottenuti dalle analisi spettroscopiche mostrate in Figura 4, confermano la presenza di un monolayer di grafene [117,118]. Tuttavia, la presenza di picchi secondari, già visibili nella spettroscopia sul substrato di rame (a), ma ancor più evidenti dai risultati ottenuti in seguito al trasferimento (b), indica tuttavia la presenza di alcuni difetti nel materiale, ulteriormente accentuati dal processo di trasferimento, dove la presenza di picchi

riconducibili al parylene suggerisce la formazione di ulteriori difetti e disomogeneità nel monolayer. Tali ipotesi vengono ulteriormente corroborate dai risultati ottenuti dalle curve caratteristiche dei dispositivi fabbricati, non riportate in questo estratto ma consultabili al Capitolo 3 dell'elaborato di tesi, dove la traslazione delle curve $I_D - V_G$ rispetto al punto teorico di minima conduttanza [120] conferma la presenza di difetti sulla superficie del grafene.

I dispositivi funzionanti sono stati dunque collegati al circuito di misurazione (mostrato in Figura 5) e utilizzati per i diversi test con soluzioni batteriche: l'immersione del biosensore in soluzione acquosa, infatti, implica l'interazione tra i composti organici costituenti le barriere cellulari batteriche e il monolayer, con conseguente colonizzazione della superficie e formazione di biofilm. I fenomeni di interazione e adsorbimento sul monolayer implicano allora una variazione nella densità e nella mobilità dei portatori lungo il canale. Di conseguenza, anche in presenza di un V_G costante, la differenza di potenziale tra Source e Drain V_{DS} non sarà costante a causa della variazione di resistenza del grafene. Tale variazione di potenziale nel tempo, riconducibile alla variazione di resistenza in funzione del tempo, viene monitorata costantemente per un periodo di otto ore, ritenuto adeguato per la riproduzione batterica e la formazione del biofilm.

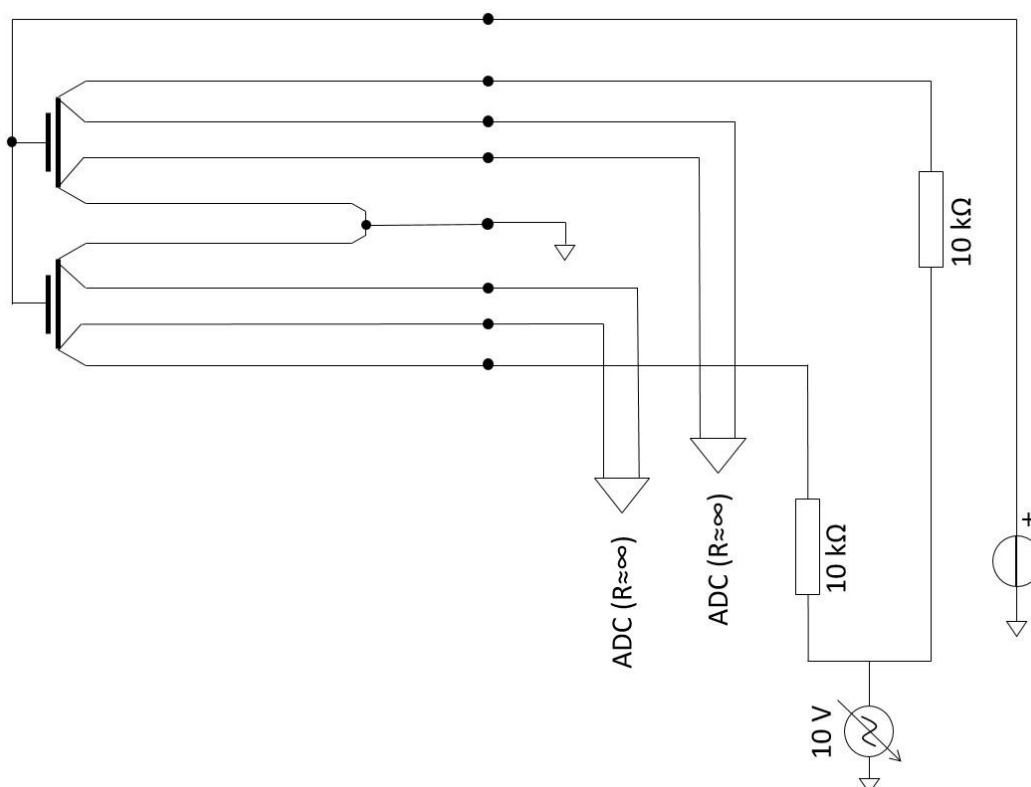


Figura 5. Visione d'insieme del circuito del biosensore.

Di particolare interesse sarebbe la possibilità di distinguere il batterio causa dell'infezione in corso grazie a specifici trend della curva di resistenza rispetto al tempo. Tale ipotesi garantirebbe infatti la possibilità di una diagnosi e somministrazione antibiotica più mirata, così da sfavorire la formazione di ceppi batterici resistenti, in sempre più rapida diffusione.

Una volta collegato al circuito e valutata la resistenza iniziale, il dispositivo può essere immerso (vedi Figura 6) per i dovuti test in 12 ml di soluzione acquosa composta come segue:

- 6 ml of di acqua de-ionizzata sterilizzata;
- 6 ml of LB media;
- 20 μ l di soluzione batterica.

Tale soluzione batterica è ottenuta grazie all'inoculazione di due colonie batteriche in 6 ml di media, poi mantenuti per 8h a 37°C così da permettere la riproduzione batterica.

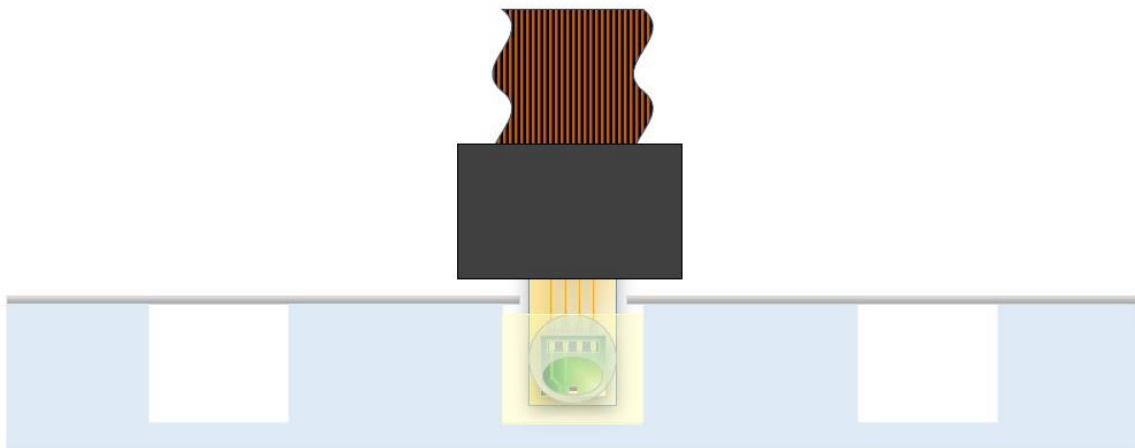


Figura 6. Rappresentazione 2D del sistema utilizzato per l'immersione del biosensore nella soluzione batterica.

Il sistema descritto in Figura 6 è dunque interamente inserito all'interno di una incubatrice, così da permetterne il mantenimento alla temperatura di 37°C. Ogni esperimento ha avuto una durata totale di 8 ore, con campionamento dei valori di resistenza ogni trenta secondi: per le prime cinque ore le condizioni del campione vengono mantenute come descritto, e la variazione di resistenza nel tempo è da imputarsi alla moltiplicazione e colonizzazione batterica. Dopo 5 ore, l'aggiunta di 120 µl di antibiotico, chiaramente visibile nei grafici finali a causa di una improvvisa impennata del valore di resistenza, permette invece di valutare l'impatto sul sistema di tale aggiunta sulla riproduzione batterica e formazione del biofilm.

Come ampiamente discusso nella Sezione 3.5 *Biofilm formation* dell'elaborato di tesi, la quasi totalità dei batteri può essere suddivisa in due macrocategorie in base agli esiti di un metodo di colorazione, noto come "colorazione di Gram", che distingue i batteri tra Gram-positivi e Gram-negativi in funzione dei costituenti della loro membrana cellulare esterna, come graficamente descritto in Figura 7.

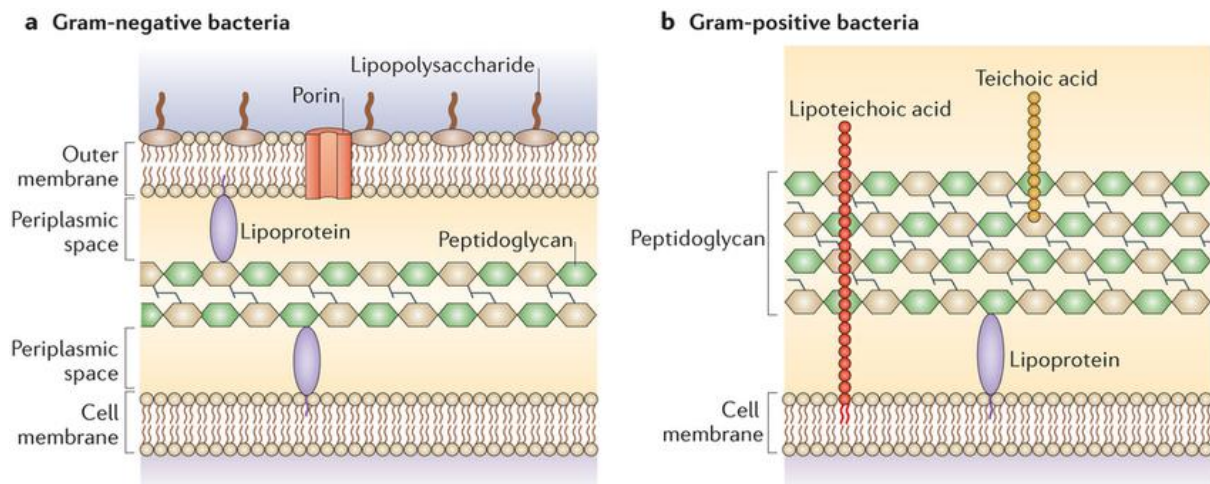


Figura 7. Rappresentazione della differente composizione e struttura della membrana cellulare di batteri Gram-negativi (sulla destra) e Gram-positivi (sulla sinistra) [modificato da125].

Tale differenza, e l'impatto che questa potrebbe avere nei fenomeni di adsorbimento superficiale dei batteri sul grafene, ha richiesto di effettuare test su batteri appartenenti ad entrambi i gram-tipi. In questo modo, è stato possibile trarre conclusioni sull'impatto che la composizione della membrana cellulare esterna ha sulla variazione di resistenza nel tempo. In aggiunta a questa prima macrodistinzione, si è scelto di testare due differenti batteri per ogni gram-tipo, così da valutare la

possibilità di individuare delle caratteristiche dei grafici finali dei rimandi univoci ad un singolo batterio, come da proposito iniziale per una somministrazione antibiotica più mirata.

Conseguentemente, sono allora stati oggetti di esperimenti quattro batteri:

- Pseudomonas Aeruginosa (Gram-)
- Staphylococcus Epidermidis (Gram+)
- Escherichia Coli (Gram-)
- Staphylococcus Aureus (Gram+)

Dai grafici Resistenza – Tempo risultanti da tali esperimenti, esemplificati in Figura 8, è stato possibile trarre delle conclusioni sulle capacità e sui limiti del dispositivo. Comparando gli esiti ottenuti per il

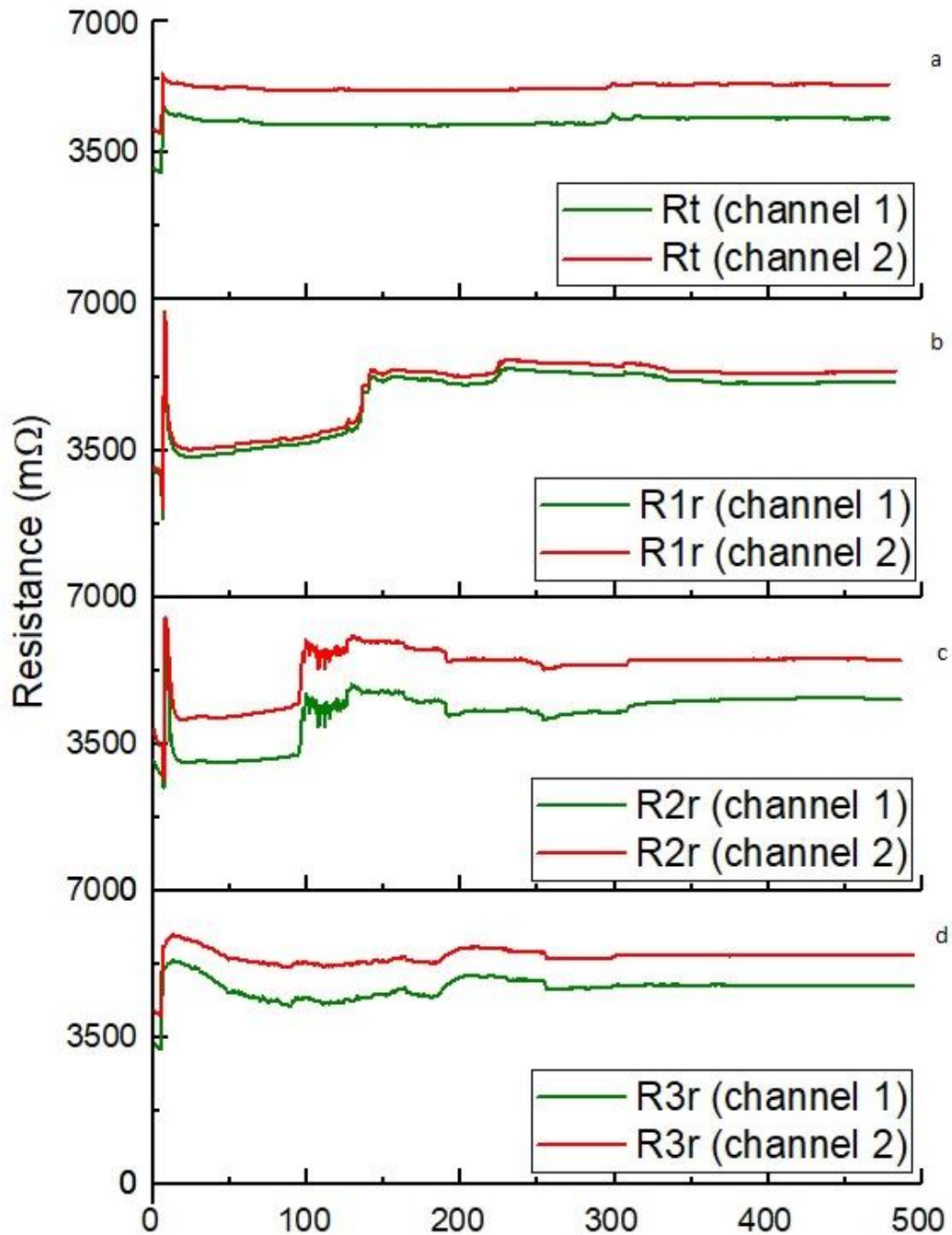


Figura 8. Paragone verticale dei grafici resistenza-tempo per LB media (a) and 1° (b), 2° (c) and 3° (d) test condotto con immersione del biosensore in una soluzione contenente 20 μl di soluzione batterica con Escherichia Coli.

batterio Escherichia Coli, si possono fare diverse osservazioni: anzitutto, la rilevazione della presenza batterica è confermata dalla differenza tra il grafico in Figura 8.a, con soluzione di brodo LB scevro di contenuto batterico e utile al controllo del comportamento del biosensore in soluzione, e quelli in Figura 8.b/c/d, dove invece sono presenti 20µl di soluzione batterica. In aggiunta, la variazione di resistenza nel tempo segue un andamento simile tra i differenti test, con la presenza di un repentino cambio di resistenza tra i minuti 100 e 200, possibilmente riconducibile all'inizio di formazione del biofilm. Il picco ricorrente a 300 minuti è invece da attribuirsi alla turbolenza causata dall'aggiunta dell'antibiotico.

Risultati analoghi, consultabili alla Sezione 3.9 *Discussion of Results* dell'elaborato di tesi, sono stati ottenuti con il batterio di stesso gram-tipo, Pseudomonas Aeruginosa. Non vi sono tuttavia, tra i grafici ottenuti per i due batteri, differenze tali nell'andamento o picchi caratteristici che possano permettere la discriminazione inequivocabile di un determinato batterio.

Per poter valutare una correlazione tra la variazione di resistenza nel tempo e determinate fasi della curva di crescita batterica, si è fatto ricorso alla tecnica di conto colonie, una procedura comune in microbiologia: quantità definite di una soluzione batterica sono "impiattate" in diluizioni progressive su dei terreni di coltura, allo scopo di ottenere su tali terreni colonie batteriche singole facilmente contabili. Il numero di colonie presenti nel piatto, relazionabile al numero di colonie nella soluzione di partenza, permette di ottenere delle indicazioni sulle fasi e sull'entità della crescita batterica.

A partire da una soluzione batterica del tutto analoga a quella utilizzata per i test sul biosensore, 100 µl di soluzione batterica sono stati prelevati con scadenza oraria e diluiti progressivamente fino ad ottenere concentrazioni batteriche tali da garantire l'effettiva singolarità delle colonie, e dunque "impiattate". Dopo ogni prelievo, la soluzione batterica è stata riposta nell'incubatrice a 37°C, così che le condizioni di crescita potessero eguagliare al meglio quelle ottenute nell'esperimento con il biosensore. Al termine dell'impattamento i terreni di coltura sono stati mantenuti per 20 ore a 37°C, così da permettere la crescita batterica, al termine delle quali si è potuto procedere alla conta. Noto il tempo e la diluzione del piatto analizzato è possibile ottenere il numero di colonie nella soluzione batterica di partenza secondo la formula:

$$\begin{aligned} & \# \text{ numero di colonie presenti nella soluzione diluita al tempo } t \\ & * \text{ fattore di diluizione rispetto alla soluzione batterica iniziale} \\ & = \# \text{ di colonie batteriche presenti nella soluzione iniziale al tempo } t \end{aligned}$$

Un esempio dei risultati ottenuti da tale metodo è fornito in Tabella 1.

Tabella 1. Conto colonie per una soluzione per biosensore contenente 20 µl di soluzione batterica con Escherichia Coli.

time	CFUs
0	3,21E+05
1	2,95E+05
2	8,90E+05
3	5,30E+06
4	2,63E+07
5	1,31E+08
1h, a	5,47E+05
2h, a	2,87E+06
3h, a	2,86E+06

I risultati ottenuti dalla procedura di conto colonie sono rappresentati graficamente nell'istogramma in Figura 9.

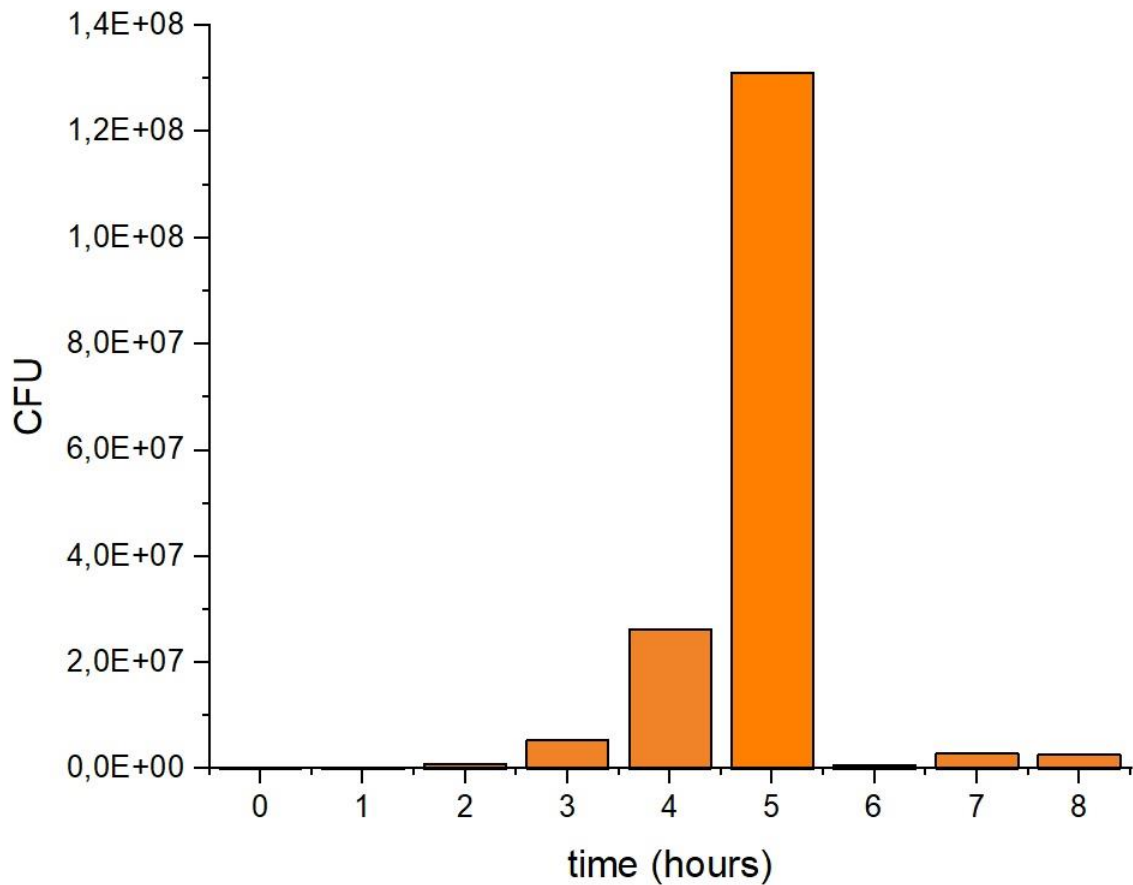


Figura 9. Conto colonie in funzione del tempo per una soluzione per biosensore contenente 20 μ l di soluzione batterica con Escherchia Coli.

E' interessante notare come, confrontando i dati sulla crescita batterica ottenuti da conte colonie e le variazioni di resistenza nel tempo, non sembra esserci alcuna correlazione evidente: la fase di crescita esponenziale dei batteri continua ben oltre il periodo di 100/200 minuti per i quali si individua un picco di resistenza nei grafici R-t. Sebbene questo risultato neghi una correlazione tra le due curve, potrebbe tuttavia indicare che, raggiunta una soglia di batteri tale da garantire saturazione della superficie del grafene, l'ulteriore crescita ed evoluzione della popolazione batterica non sia rilevante nella variazione complessiva di resistenza.

Per quanto concerne invece i batteri gram-positivi, quali Staphylococcus Aureus e Staphylococcus Epidermidis, il biosensore non è in grado di rilevare la presenza di tali batteri in soluzione. Facendo riferimento alla Figura 10, che mostra un paragone dei grafici R-t ottenuti per lo Staphylococcus Epidermidis, non si nota alcuna differenza significativa tra la soluzione di controllo, priva di batteri (Figura 10.a) e i test in presenza di batteri in soluzione (Figura 10.b/c). In aggiunta, non vi è un andamento similare per i diversi test, e, diversamente dai gram-negativi, nessun picco caratteristico ad indicare la presenza di tale Gram-tipo di batterio in soluzione.

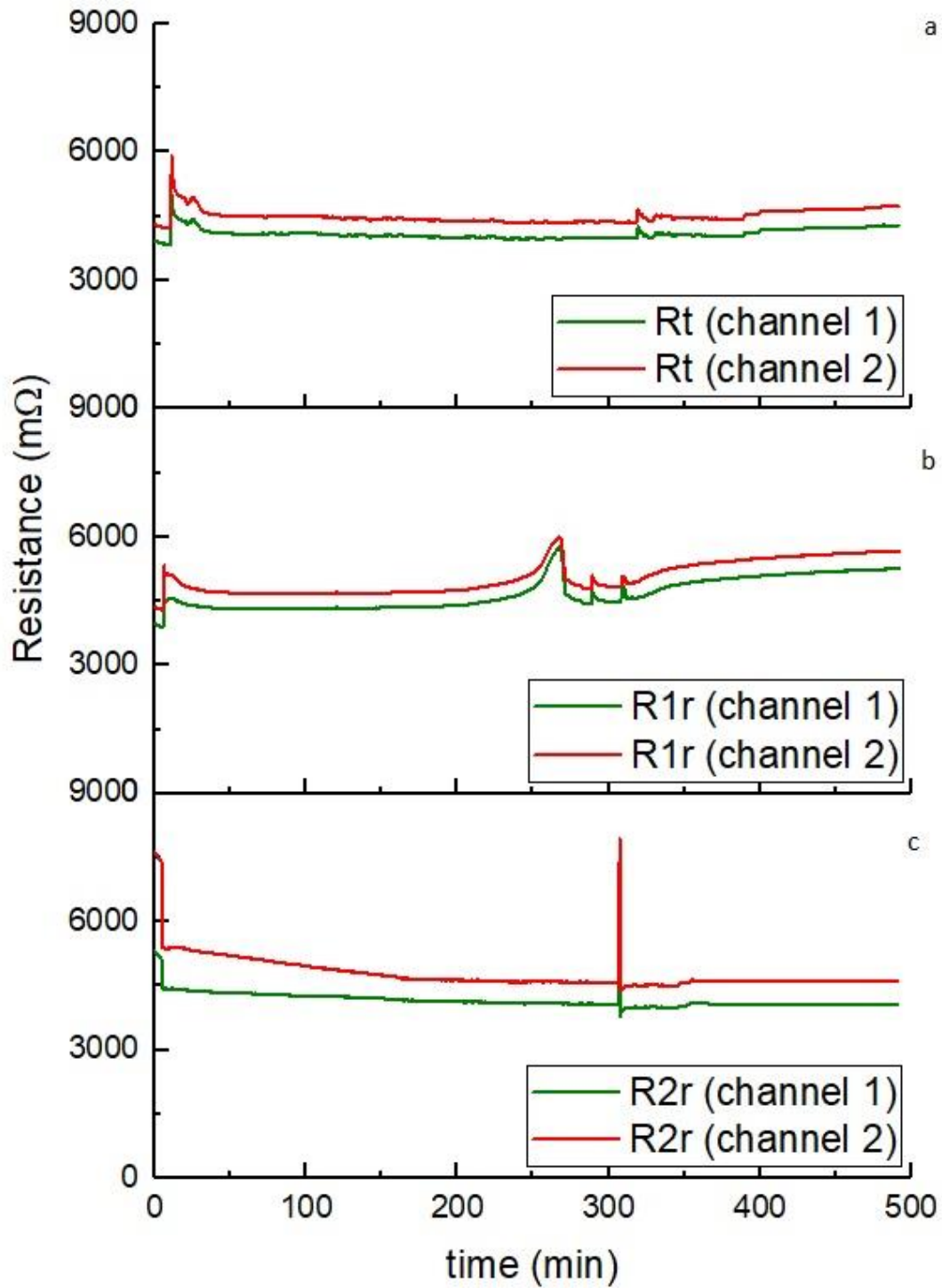


Figura 10. Paragone verticale dei grafici resistenza-tempo per TSB media (a), 1° (b) e 2° (c) test condotto con immersione del biosensore in una soluzione contenente 20 μ l di soluzione batterica con *Staphylococcus Epidermidis*.

A conferma di una normale crescita dei batteri in soluzione, e dunque dell'incapacità del biosensore di rilevare la presenza del batterio presente, si riportano gli esiti ottenuti dai conti colonie per il batterio *Staphylococcus Epidermidis* in Figura 11.

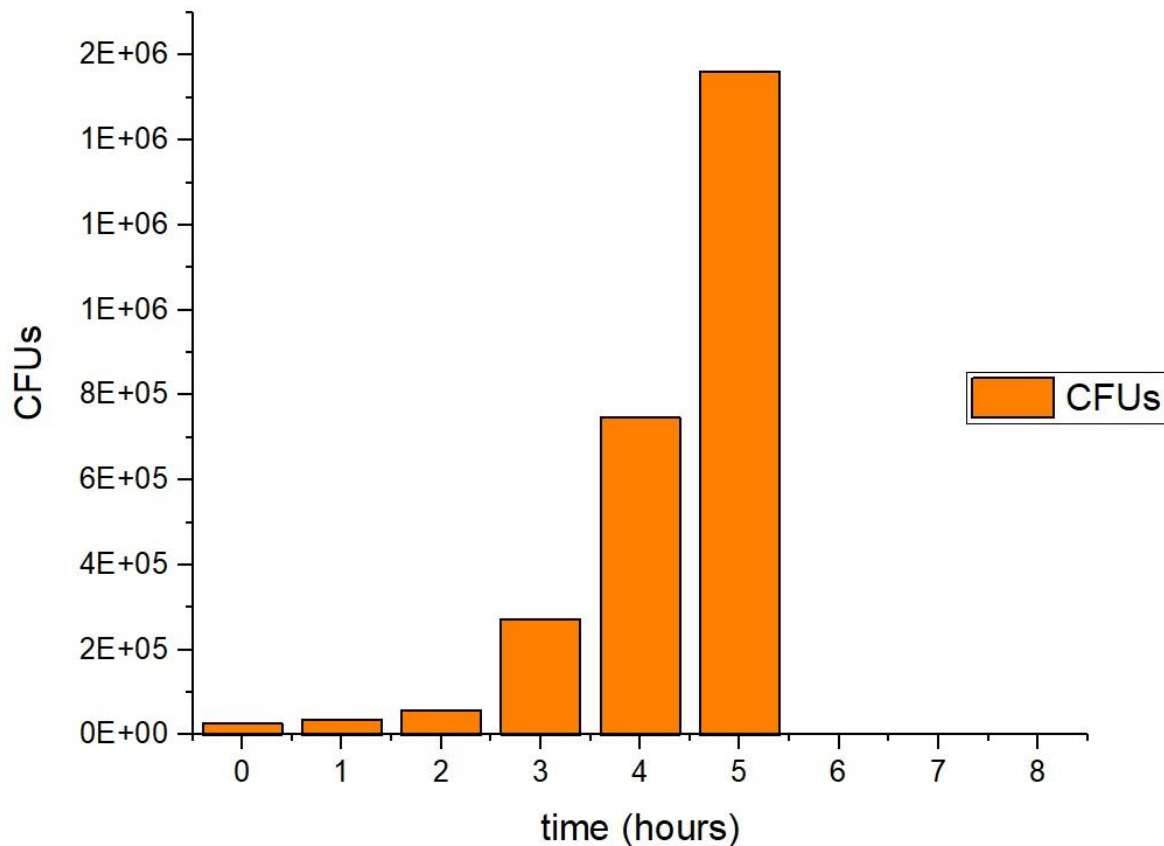


Figura 9. Conto colonie in funzione del tempo per una soluzione per biosensore contenente 20 μ l di soluzione batterica con *Staphylococcus Epidermidis*.

Come nel caso del batterio *Escherichia Coli*, la curva di crescita batterica è conforme a quella attesa, indice di una normale progressione nella replica dei batteri. A differenza di quest'ultima tuttavia, l'assenza di colonie dopo l'aggiunta dell'antibiotico lascia presumere una differente efficacia dello stesso sui diversi batteri. L'ipotesi è corroborata ulteriormente se si paragonano i due istogrammi a quelli ottenuti per gli altri due batteri e consultabili nel Capitolo 3 dell'elaborato di tesi.

In conclusione, in seguito alle analisi svolte è possibile concludere che il grafene sia una buona scelta, in termini di materiale, per la realizzazione di un biosensore per analisi in tempo reale, vista la facilità di integrazione grazie alla tecnica di trasferimento e alle peculiari qualità che esso possiede. Inoltre, come discusso nel Capitolo 3.3 *Antibacterial properties of graphene* dell'elaborato, l'utilizzo di grafene ottenuto per Chemical Vapour Deposition garantisce l'assenza di proprietà antibatteriche e permette di concludere, in combinazione con gli esiti dati dai conti colonie, che la riproduzione e colonizzazione batterica seguono un andamento concorde con quelli ottenuti per substrati inerti, e che la decrescita o totale assenza di colonie in soluzione dopo cinque ore sia da attribuirsi unicamente all'utilizzo dell'antibiotico.

Il dispositivo risulta affidabile nel rilevare la presenza di batteri gram-negativi in soluzione, giacchè nei grafici di resistenza in funzione del tempo ottenuti per batteri tale gram-tipo ricorre la presenza di una

netta variazione di resistenza, compresa tra i minuti 100 e 200, che non è invece presente nei grafici per i quali la soluzione non contiene batteri (vedi Figura 9). Tale riconoscimento non avviene invece, facendo riferimento ai dati attuali, in presenza di batteri gram-positivi, come lo *Staphylococcus*, dove non sono riconoscibili picchi o andamenti della curva attribuibili con certezza alla presenza di batteri.

Sebbene sia dunque attestata la possibilità di distinguere tra gram-tipi diversi, rimane da accertare l'eventualità di distinguere invece tra diversi batteri dello stesso gram-tipo, poichè non risultano, per i dati a disposizione, elementi della curva distintivi per un singolo batterio. Inoltre, come osservabile dai dati ottenuti, uno stesso antibiotico, per giunta in una quantità volutamente di molto superiore alla concentrazione critica, non ha un eguale efficacia sui differenti batteri, nemmeno su quelli dello stesso gram-tipo (si vedano nell'elaborato di tesi le Figure 3.39 e 3.53). Perchè il dispositivo possa sopperire al suo scopo di assistere nell'identificazione di una infezione e garantire una somministrazione antibiotica mirata, risulta allora di cruciale importanza l'identificazione del singolo batterio. Di conseguenza, ulteriori test saranno necessari per definire la ragione per la quale i batteri gram-positivi non possano essere rilevati, e quali soluzioni dovrebbero essere adottate per poter distinguere tra batteri dello stesso gram-tipo.

Infatti, sebbene i risultati dei grafici di resistenza in funzione del tempo mostrino una marcata dipendenza dalla struttura della membrana cellulare esterna dei batteri, altre variabili potrebbero dimostrarsi rilevanti nella definizione di un andamento specifico della curva per un singolo batterio. I batteri, ad esempio, si nutrono dei costituenti dei brodi di coltura per sopravvivere e proliferare, e conseguentemente un diverso tenore di costituenti nel brodo potrebbe indurre risultati differenti sulla curva finale di Resistenza – Tempo in termini di tempi di formazione del biofilm.

Al contempo, altre variabili secondarie come la qualità dei processi di deionizzazione e sterilizzazione dell'acqua, così come statistici errori casuali nella normale routine di laboratorio sono tutti fattori che potrebbero avere una rilevanza più o meno importante sul risultato finale, e in ogni caso non permettono una reiterazione dell'esperienza in condizioni completamente analoghe. Tali differenze potrebbero dimostrarsi ancora più importanti alla luce del fatto che, nel caso di test in tempo reale, il media sarebbe sostituito presumibilmente da sangue o plasma sanguigno, la cui composizione è molto più diversificata e complessa di quella del brodo di coltura. In conclusione, sebbene la composizione della membrana esterna dei batteri sembri essere una variabile di notevole importanza, la non perfetta corrispondenza tra curve indica comunque la presenza di variabili secondarie, non completamente individuate allo stato attuale, incidenti sul risultato finale.

Due questioni irrisolte meritano una nota a parte: la definizione di un processo di pulitura efficace del dispositivo e la riproducibilità dei risultati ottenuti.

Per quanto concerne la prima questione, il biosensore, dopo ogni utilizzo, è stato risciacquato in etanolo e poi immerso in acqua bollente per 5 minuti, seguiti da un rapido risciacquo in acqua distillata e asciugatura con gas inerte in pressione. Tale metodo si è dimostrato non del tutto efficace per due motivi distinti: anzitutto, il processo di pulitura non garantisce una completa rimozione del biofilm dal dispositivo, variando la resistenza iniziale del dispositivo per ogni nuovo test. In secondo luogo, alcune componenti del biosensore, e in special modo quelle più delicate ed esposte alla soluzione batterica durante i test, potrebbero danneggiarsi durante le diverse fasi del lavaggio. E' necessaria, di conseguenza, la definizione di un processo di pulitura del dispositivo che risulti meno aggressivo nei confronti dello stesso, e possibilmente più efficace nell'eliminazione del biofilm: in tal modo si combinerebbe una efficienza di lavaggio ad un minore impatto sulle componenti del sensore, aumentando di conseguenza la riproducibilità dei risultati. Quest'ultimo fattore è fortemente influenzato dalla necessità, per lo più economica, nella fase di sviluppo, di ri-utilizzo dei dispositivi. La produzione manuale dei dispositivi, per giunta, implica un'intrinseca differenza dei risultati ottenuti: unicamente nel processo di trasferimento del grafene, che è solo uno dei diversi passaggi nella produzione litografica del sensore, la qualità del monolayer finale viene determinata dalla qualità del processo manuale, che può generare la formazione di difetti superficiali, con risultante

danneggiamento e morte della cellula batterica secondo le modalità elencate al Capitolo 3 della tesi. Un processo di produzione automatizzato e su più larga scala permetterebbe allora una migliore riproducibilità dei risultati.

In ultima analisi, dunque, sebbene sia possibile ottimizzare alcune fasi del processo di produzione e sia necessario indagare ulteriormente le variabili che agiscono sul sistema in modo da definirne la rilevanza, i risultati finora ottenuti sono incoraggianti: il primo e più importante nodo da risolvere riguarda la conferma dei dati ottenuti per i batteri gram-negativi e l'individuazione di parametri che possano permettere la rilevazione di batteri gram-positivi e la distinzione tra differenti tipi di batterio.

Come prospettive future, sarebbe interessante valutare i risultati ottenuti dal biosensore nel caso di soluzione contenenti delle combinazioni batteriche, fenomeno ricorrente nella realtà, in modo da poter definire se il risultato del grafico Resistenza-tempo risulti una combinazione lineare dei risultati o viceversa il risultato finale non permetta distinzioni tra infezioni singole e multiple.

1. Introduction

The possibility of producing single layers of graphite was first developed in 2004 by Geim and Noselov^[1,2], when the duo managed to divide a single layer of graphite, then called graphene, from a bulk by using a reiterated process of mechanical exfoliation with adhesive tape. The just synthesized material constituted a unicum on the market: while the possibility of synthesizing 2D material was already theorized in previous years^[3], many doubts still remained on the possibility of obtaining such materials in an equilibrium state, necessary to their industrial use.

The confirmation of the stability of graphene, then, opened the door to numerous and innovative ideas for their applications both in their pristine form and integrated in composites for the most different fields of research: aeronautic^[4,5], automotive^[6], electronics^[7,8], optics^[9] and medicine^[10], just to list a few. While other interesting 2D materials, like boron nitride^[11,12] and transition metal dichalcogenides^[13,14], can nowadays be more easily synthesized, processed and studied, graphene still remains the planar material most researched upon. In fact, numerous techniques allow the production of graphene with relatively cheap costs, factor which favors its diffusion in numerous researches that find their goal in the exploitation of its peculiarities, unparalleled when compared to the common materials used on the market. The present work aimed at analyzing how the interaction with bacteria and subsequent formation of a biofilm would change the resistance of graphene when integrated into a Field-Effect Transistor-like device. The detection of specific patterns for specific bacteria in the resulting resistance vs time curves, and their correlation with the system variables, would permit the use of the device as a real-time biosensor for the detection of on-going bacterial infection and thus allow immediate treatment.

A brief overview of graphene properties is provided in Chapter 2, with a specific focus on the controversial antibacterial properties of graphene. The latter topic raised growing interest in the biomedical sector because of the pioneering applications that the combination between graphene properties and bactericidal ability may accord. In addition, basics on the working principle of MOSFETs and G-FETs are explained, so to have a general understanding of all the components that come into play in the following analysis.

The device fabrication and characterization introduce, in Chapter 3, the discussion of results obtained during the testing on four different strains of bacteria. Drawn conclusions, suggestions on improvements of the testing for the definition of relevant variables and future prospects are addressed in chapter 4.

Appendix I offers instead a short summary of the first steps of a pilot project aimed to produce a label-free biosensor using boron-doped graphene, the preliminary results and future prospects.

2. Graphene

2.1 Properties of graphene

Carbon is an abundant element in nature, essential for the development and evolution of life on Earth. While it is present in countless organic compounds with the most diverse functions, it is also possible to find it in its pristine state in many different allotropic forms. The common natural forms are graphite, constituted by stacked layers of atomic planes organized in a hexagonal lattice, and diamond (Figure 2.1). To these two, it is possible to add synthetic forms like fullerenes, carbon nanotubes and graphene, whose relatively recent discovery widened the horizons in many scientific fields, paving the way for readapted or entirely new applications.

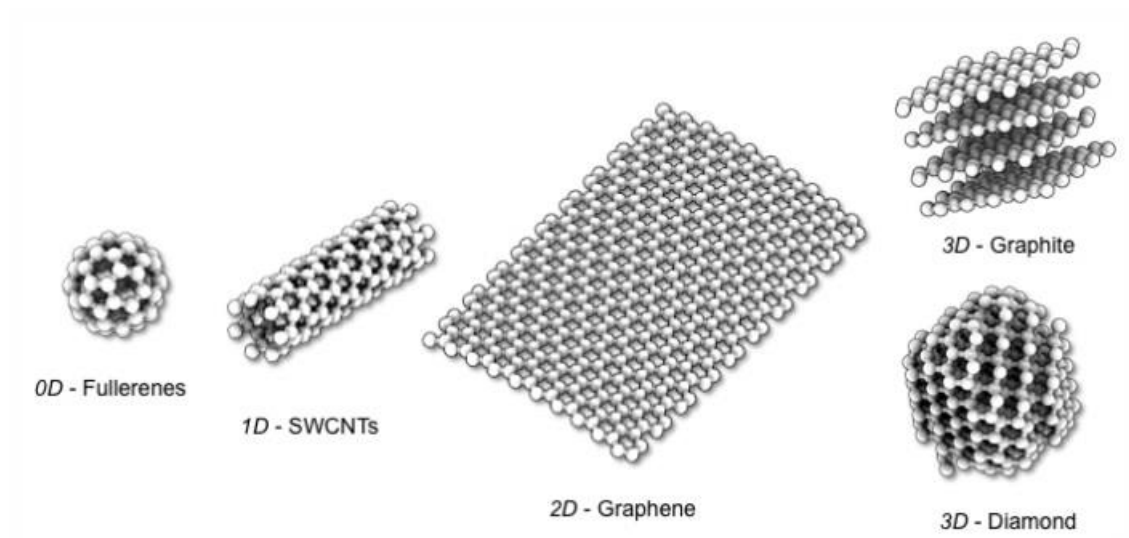


Figure 2.1 Overview of the allotropic forms of graphene. [15]

Among the others, graphene in particular holds a noteworthy relevance for its 2D structure: it is a single layer of carbon atoms arranged in a planar honeycomb lattice (see Figure 2.2), where the atoms are sp^2 hybridized and the bonds form a flat structure with consistent bond length around 0,142 nm ^[16]. Its importance is also underlined by the continuously increasing investigations on this material and its possible applications in various fields ^[17] (see Figure 2.3).

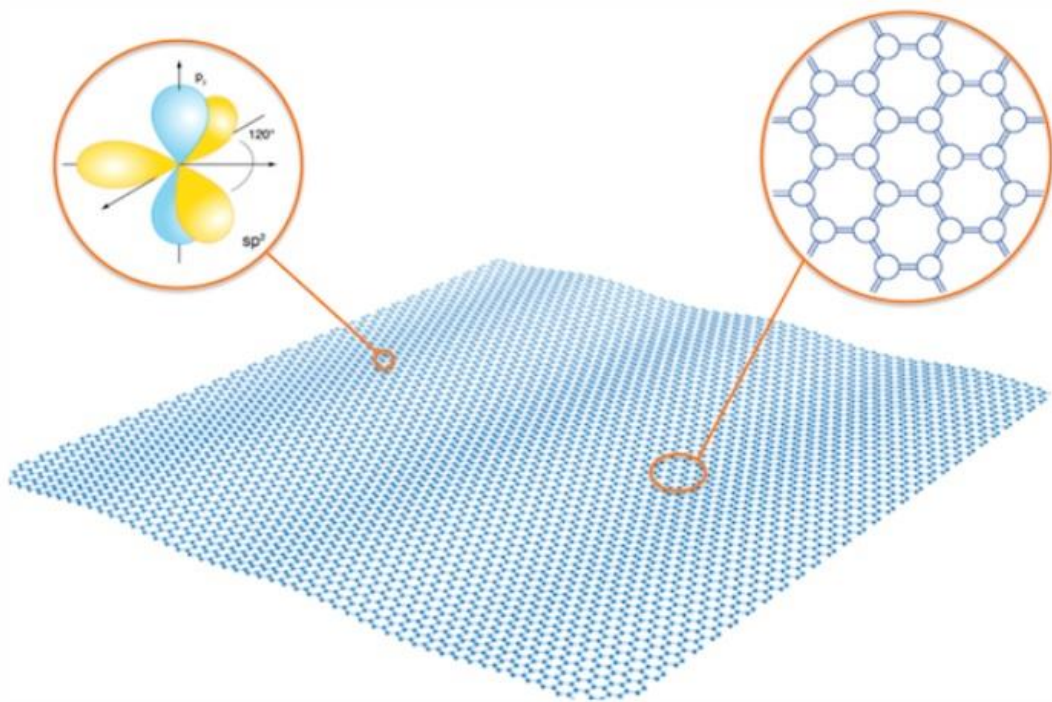


Figure 2.2 Representation of the planar structure and bonding of graphene, depicted in the bubble on the left of the image. [15]

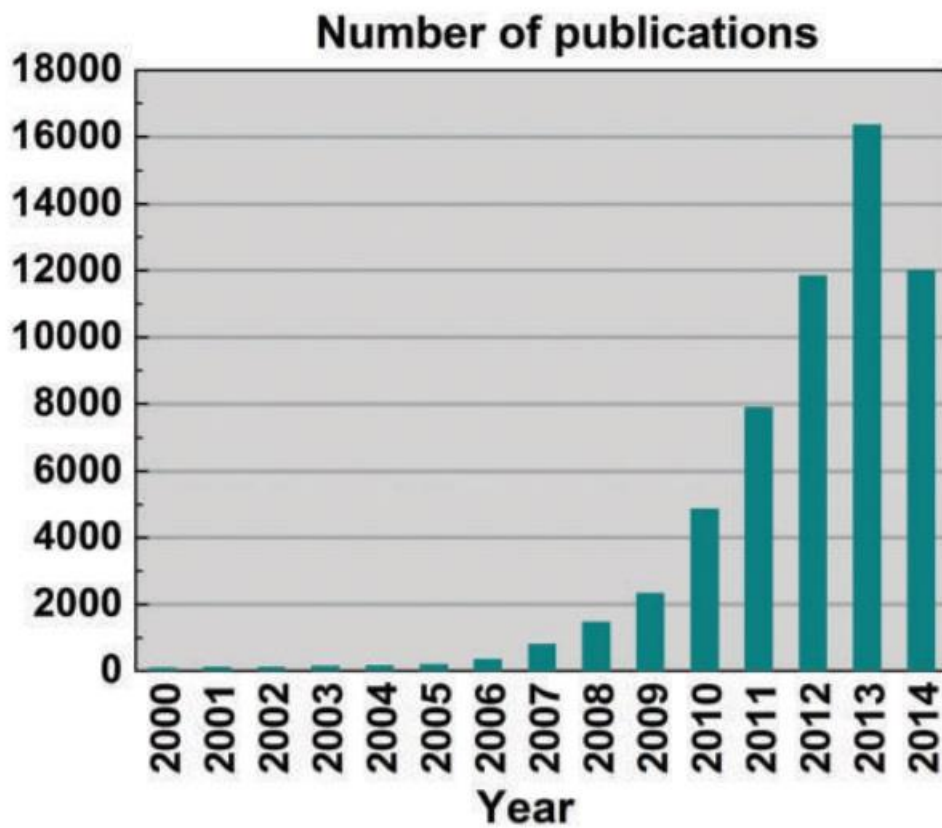


Figure 2.3 Number of publications per year (from 2000 until 2014) regarding graphene. [17]

Graphene can be synthesized in numerous ways, briefly summarized in Figure 2.4 [18,19,20,21]. In general, techniques can be divided in two categories, characterized by a different approach to the fabrication of the layer: the bottom up subgroup is made up of those techniques that seek to form graphene starting from precursors, while the top down approach groups all those methods that deliver graphene from graphite.

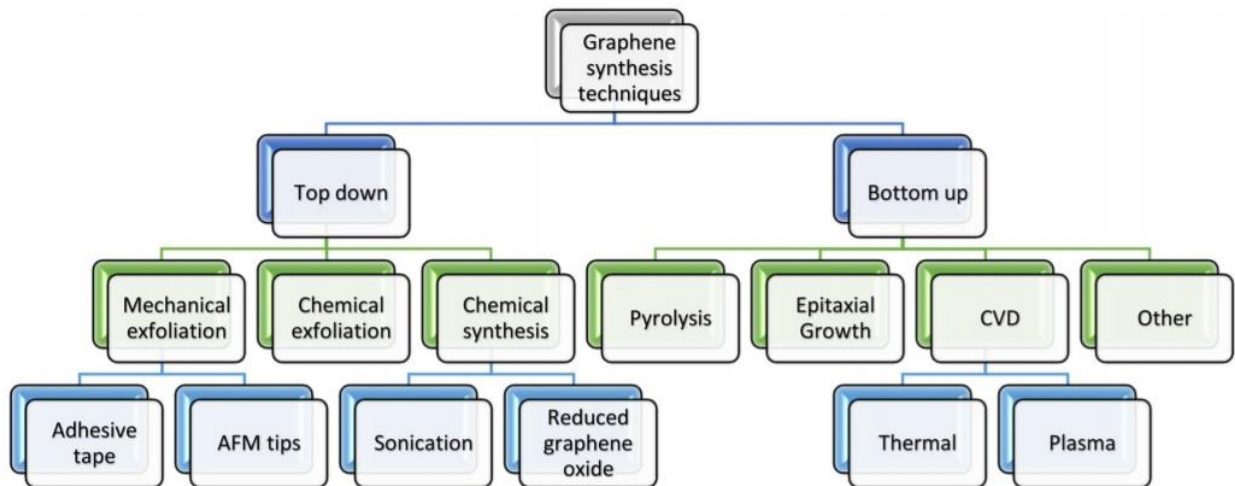


Figure 2.4 The tree diagram represents the synthesis techniques of graphene: on the left the top down approaches, on the right the bottom up ones. [18]

These different approaches, although, do not deliver a material with consistent properties among the various possibilities: graphene, in fact, differs in many variables such as number of layers, surface quality, scalability and obviously costs [22], as shown in Table 2.1. Such discrepancies imply distinct possibilities of employment for such material, according to the intrinsic requirements of the application for which they are produced.

	Ref.	Electronic quality of layers	Cost	Number of layers	Throughput	Nature of produced graphene	Size of layers	Compatibility with chip fabrication Process	Precursor
Mechanical Exfoliation	1	High	Low	Single and multiple	Low	Pristine	10 μm	No	Graphite
Liquid suspension graphene oxide followed by chemical reduction	8	Low	Low	Single and multiple	High	Chemically modified	Several hundred nm	No	Graphite oxide
Liquid-phase exfoliation	9	High	Low	Single and multiple	High	Pristine	Tens of μm to much smaller fragments	No	Graphite
Epitaxial growth by thermal desorption of Si atoms from the SiC surface	10	High	High	Single and multiple	Low	Pristine	>50 μm	Yes	Silicon carbide
Epitaxial growth by chemical vapor deposition on transition metals	11,12	High	High	Single and multiple	Low	Pristine	> 100 μm (can be wafer-size)	Yes	Hydrocarbons
Solvothermal synthesis	13	Not available	Low	Single and multiple	High	Chemically modified	Tens of μm to much smaller fragments	No	Ethanol
Unzipping carbon nanotubes	14	Inferior compared to Ref. 1.	Low	Single and multiple	High	Chemically modified	Nano ribbon with length of 4 μm	No	Multi-walled carbon nanotubes

Table 2.1 The table provides a brief summary of the different synthesis techniques and correlates them with some relevant properties such as electronic quality of layers, their number and size. [22]

The reason why graphene has known such a wide outburst in recent times is primarily due to its fairly unique properties^[23], whose exploitation makes the material adapt for many different applications. The most significant characteristics are sketched in Figure 2.5.

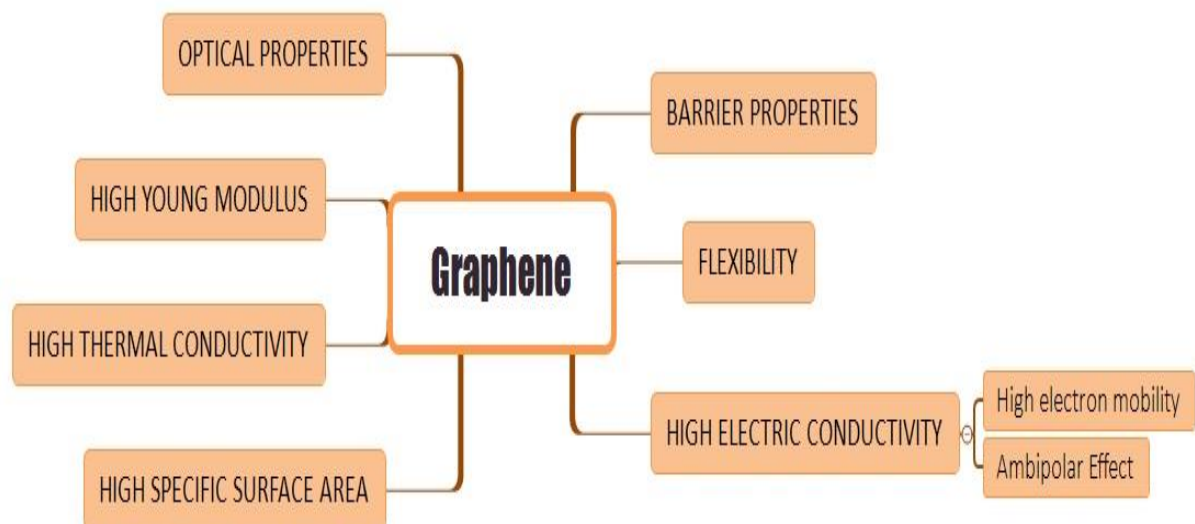


Figure 2.5 The graph synthesizes the most significant properties of graphene.

The most relevant properties summarized in Figure 2.5 are described in more detail in Table 2.2.

Barrier Properties		Impermeable to gases and liquids	[24, 25]
High Specific Surface Area		Theoretical specific surface area of about 2600 m ² /g	[16]
Optical Properties		Transmittance is > 70% for thickness around 10 nm, up to 95% for 2nm	[26]
Flexibility		Atomic layer thick, can be easily folded	[27]
High Young's Modulus		Young's Modulus is attested around 1TPa	[16, 23]
High Electrical Conductivity	High Electron Mobility	Ultrahigh electron mobility, up to 10 ⁵ cm ² V ⁻¹ s ⁻¹	[19, 23, 28, 29]
		Saturation velocities as high as 5×10 ⁷ cm/s	[19, 30]
	Ambipolar Effect	Charge carriers can be tuned by applying voltage	[31, 32, 33]
		High mobility at high carrier density (ballistic transport)	[34, 35, 36, 37, 38]
High Thermal Conductivity		High Thermal Conductivity was shown to be proportional to 1/T above 100K	[39]
		RT values for single-layer G can reach up to 5300W/mK	[40, 41]

Table 2.2 Brief sum up of the most relevant properties of graphene.

This incredible variety of peculiar properties, and the chance to combine them and take advantage of their synergetic effects opened the door for numerous and diversified applications (see Figure 2.6): in microelectronics, mechanically-enhanced composites, high temperature applications, coatings but also in the biomedical field.

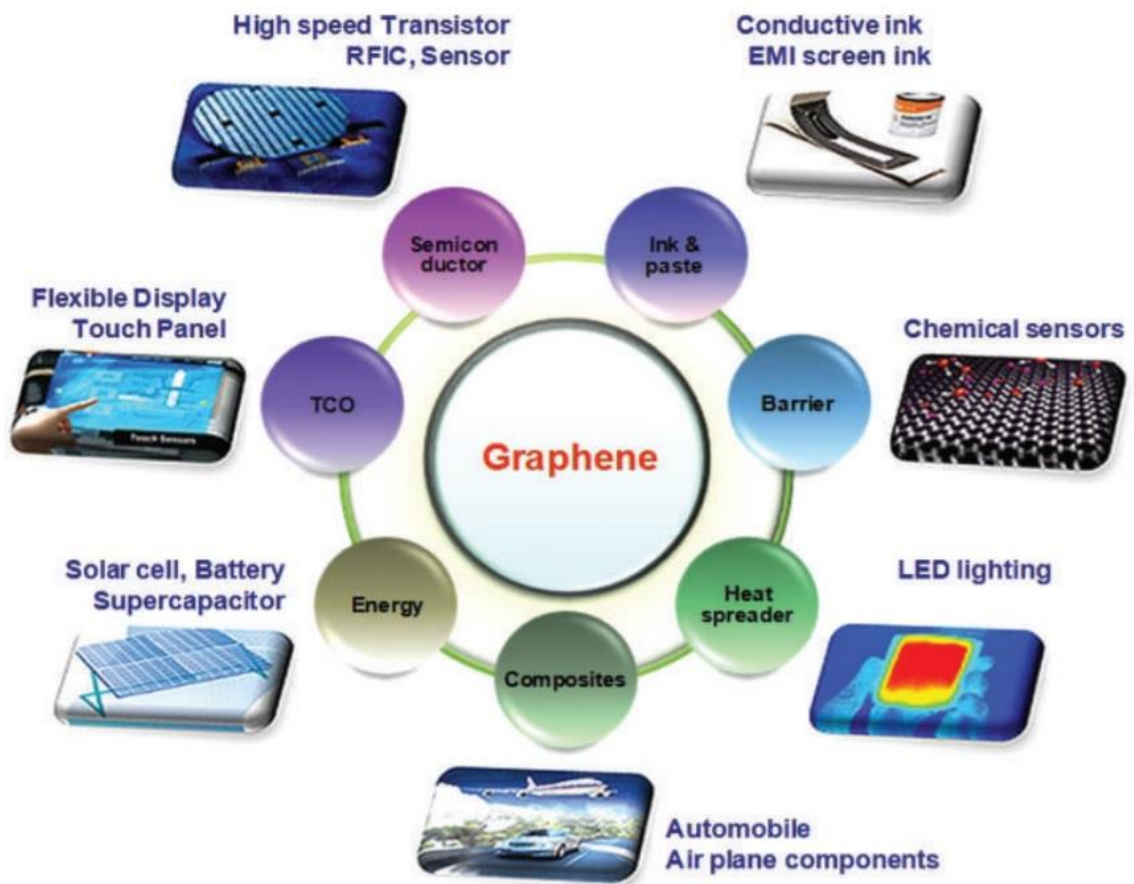


Figure 2.6 Overview of graphene applications in different fields of research. [3]

2.2 Antibacterial properties of graphene

The attested antibacterial properties of numerous nanomaterials, e.g. silver nanoparticles [42,43], combined with the peculiar characteristics of carbon compounds such as graphene and graphene oxide, lit a spark of interest for the application of nanosized graphene-based materials in the biomedical field [44, 45].

The intrinsic properties of graphene and its derivatives, like high thermal conductivity, ease of surface functionalization and response to IR radiation, if combined with good toxicity towards bacterial cells, would permit its exploitation in different areas: bioimaging [46], drug delivery [47,48], antibacterial coatings [49], antibacterial and antifouling membranes [50,51], just to cite a few.

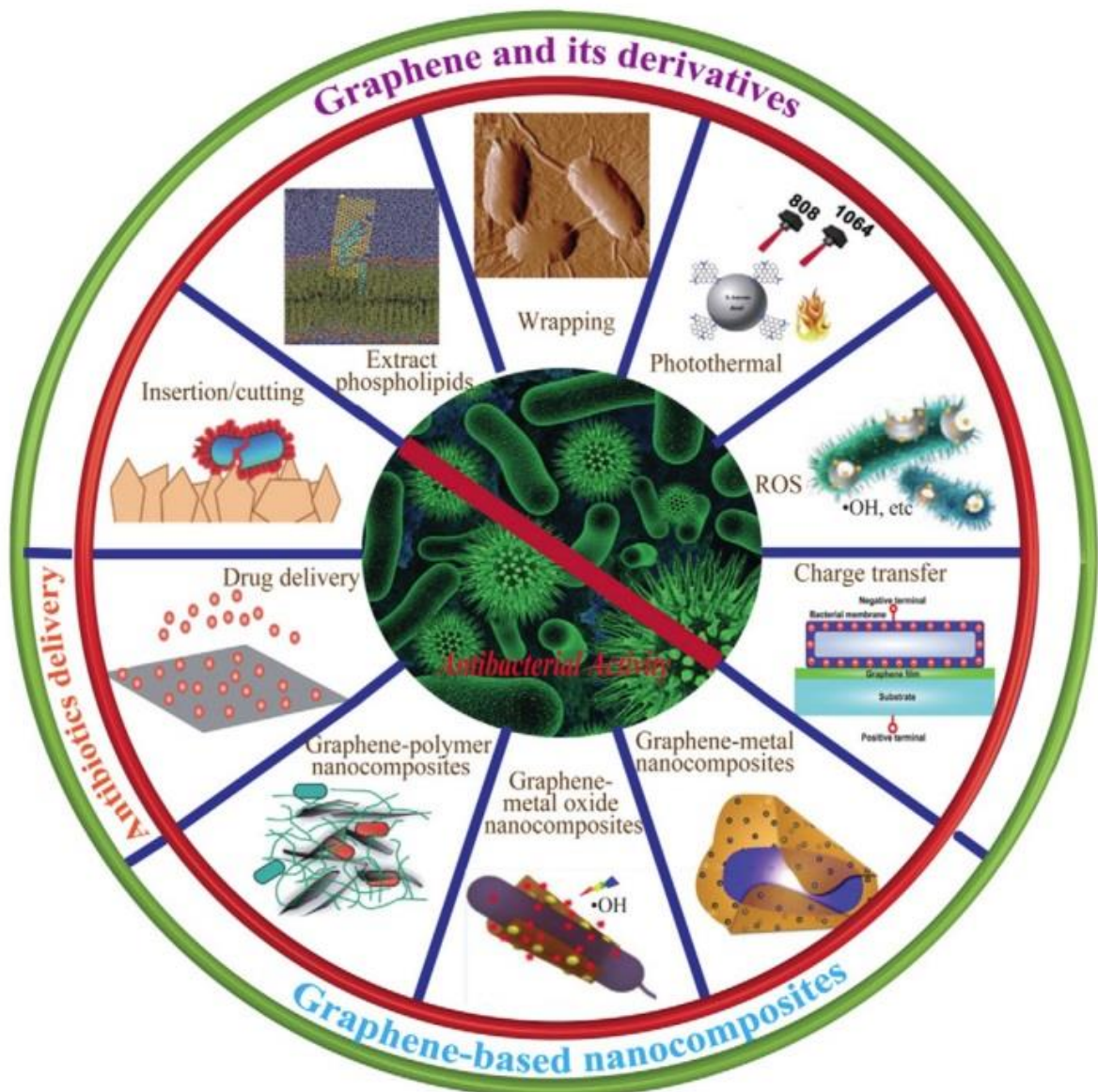


Figure 2.7 Schematic illustration of the antibacterial applications of graphene-based nanomaterials. [52]

Differently from other nanomaterials, although, bactericidal properties of graphene remain, presently, quite controversial: the presence of antibacterial properties, their quantitative value, as much as the type of bacteria mined by them, is not yet defined univocally [53, 54, 55].

The dispute cannot be settled without taking into considerations some variables that, as already proven for non-graphene-based nanomaterials, have an impact on the microbial properties: among those, for importance, shape, size, surface functionalization and stability [56, 57]. In addition to those, G-based materials seem to express different antibacterial effects according to the mechanism of interactions between the material and the bacterial cells [55]. These interactions are, in turn, strongly dependent on the phase and structure of the material: pristine material in dispersion [53, 54], as part of a composite [58,59,60,61], in membranes [62,63,64] and

hydrogels ^[65,66]. It is reasonable to presume that if all these parameters are involved in the definition of the material's toxicity, a huge dispersion of outcome is possible.

Firstly, it's important to underline how the macroscopic category of G-based nanomaterials comprises not only graphene, but also its derivatives, like reduced-graphene oxide (r-GO), graphene oxide (GO), graphite (Gt) and graphite oxide (GtO). These derivatives and graphene itself differ, among each other, in some properties that can prove to be quite relevant in the biomedical field. The difference in surface charge and hydrophilicity, for example, are two variables that determine a different interaction with the biological matter. Besides these inherent characteristics, the surface properties, number of layers, purity and size of these materials also strongly differ depending on the fabrication method adopted to produce them: graphene only, for example, can be produced through different methods such as exfoliation, sonication and centrifugation or chemical vapor deposition (see Section 2.1). These techniques deliver final products with different quirks depending on the adopted method, but also within the same production protocol small differences in procedure can lead to different end results.

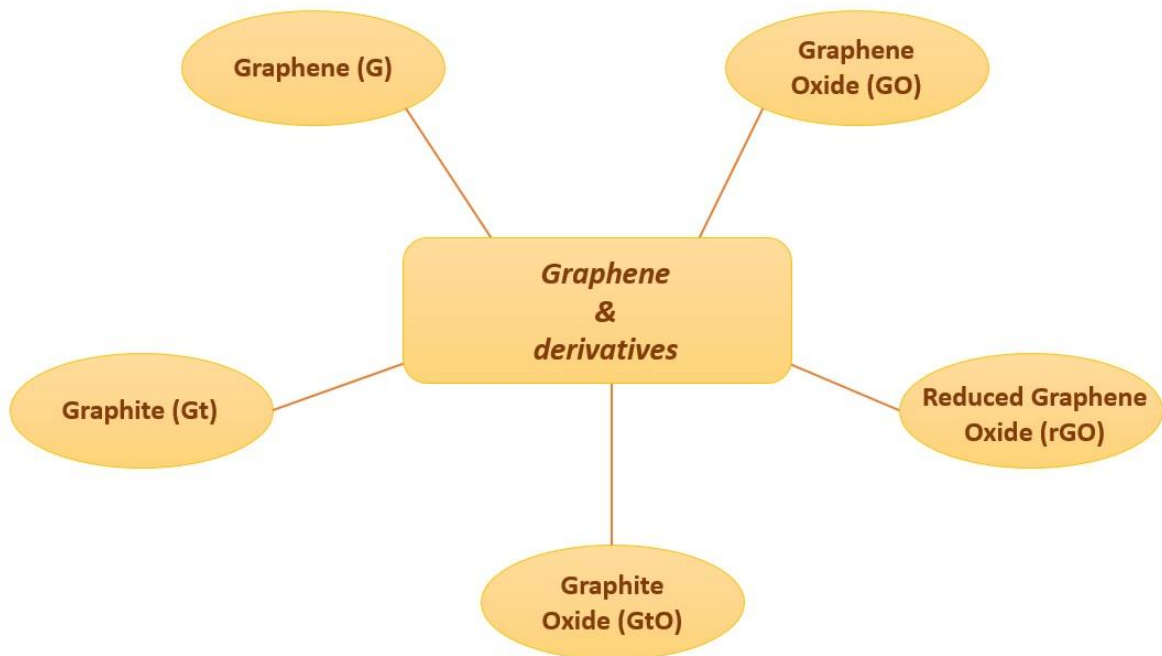


Figure 2.8 Overview of graphene and its derivatives.

For what concerns the bacterial cell – G-based material interaction, four major mechanisms could be underlined ^[52]:

- Cellular Membrane Stresses
- Capturing and Killing
- Oxidative Stresses
- Wrapping isolation

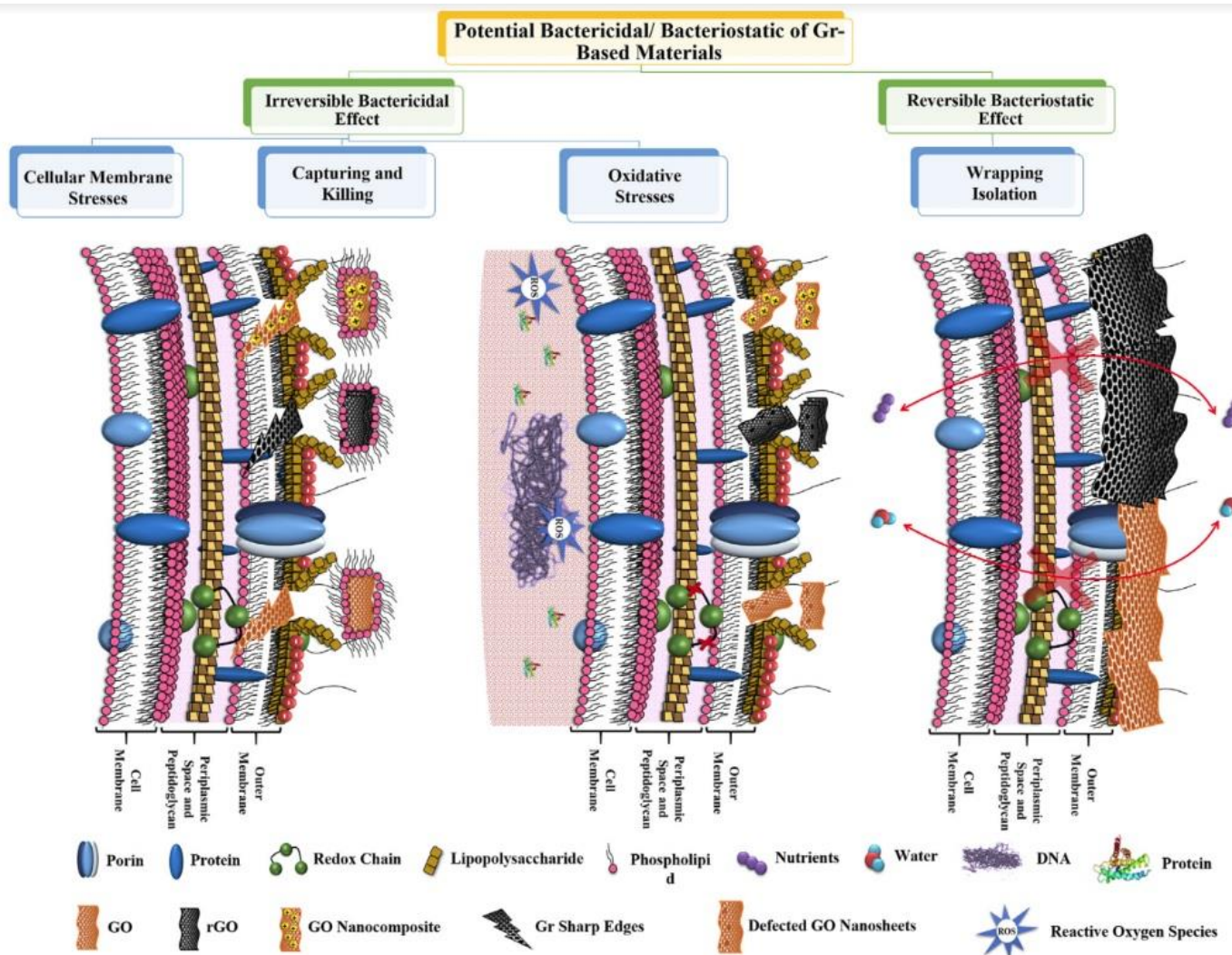


Figure 2.9 Summary of the possible methods of interaction between bacterial cells and G-based materials. [52]

Any of these mechanisms, best summarized in Figure 2.9, can act separately or in combination with each other, and is influenced by some variables that characterize either the nanomaterials or the bacteria. For example, cellular membrane stress is strongly connected with the orientation and size of the nanoparticles interacting with the bacteria: the piercing of the external membrane (different according to the type of bacteria), induced by the presence of sharp edges, causes the extraction of phospholipids, leakage of the cytoplasm and death of the cell [67, 68, 69].

Oxidative stress and Reactive Oxygen Species (ROS) production seems to be connected with the internalization of the nanoparticle, easier in case of smaller particles, while bigger particles in sheet form would instead facilitate the wrapping phenomenon [70]. Strong impact on the interaction is also attributed to the surface charge and surface properties of both the particles and the bacteria, that may affect the interaction directly or indirectly through aggregation phenomena of the suspension [71].

As already discussed, moreover, some surface and geometric variables strongly impact the biocidal activity of graphene-based nanomaterials, and in particular, among those, five parameters seem to be of most importance [55]:

- Geometric parameters (like shape, size and surface area)
- Hydrophilicity
- Dispersibility
- Surface functionalization
- Orientation

Graphene research in general, and specifically in biomedical applications, has known a boost in the last few years thanks to both the extraordinary possibilities this material provides and the innovative and stimulating demands of the medical sector. However, the researches lead on the topic strongly differ in so many aspects, from the production method, to the surface functionalization, from the orientation and size of the nanoparticles to the type of bacteria tested, that would be an oversimplification to reduce the behaviour of such material to a single word. The parameters that may determine a change in behaviour are so numerous, and their combination or overlapping with other properties so significant, that differences in even a single parameter may lead to opposite outcomes during the testing.

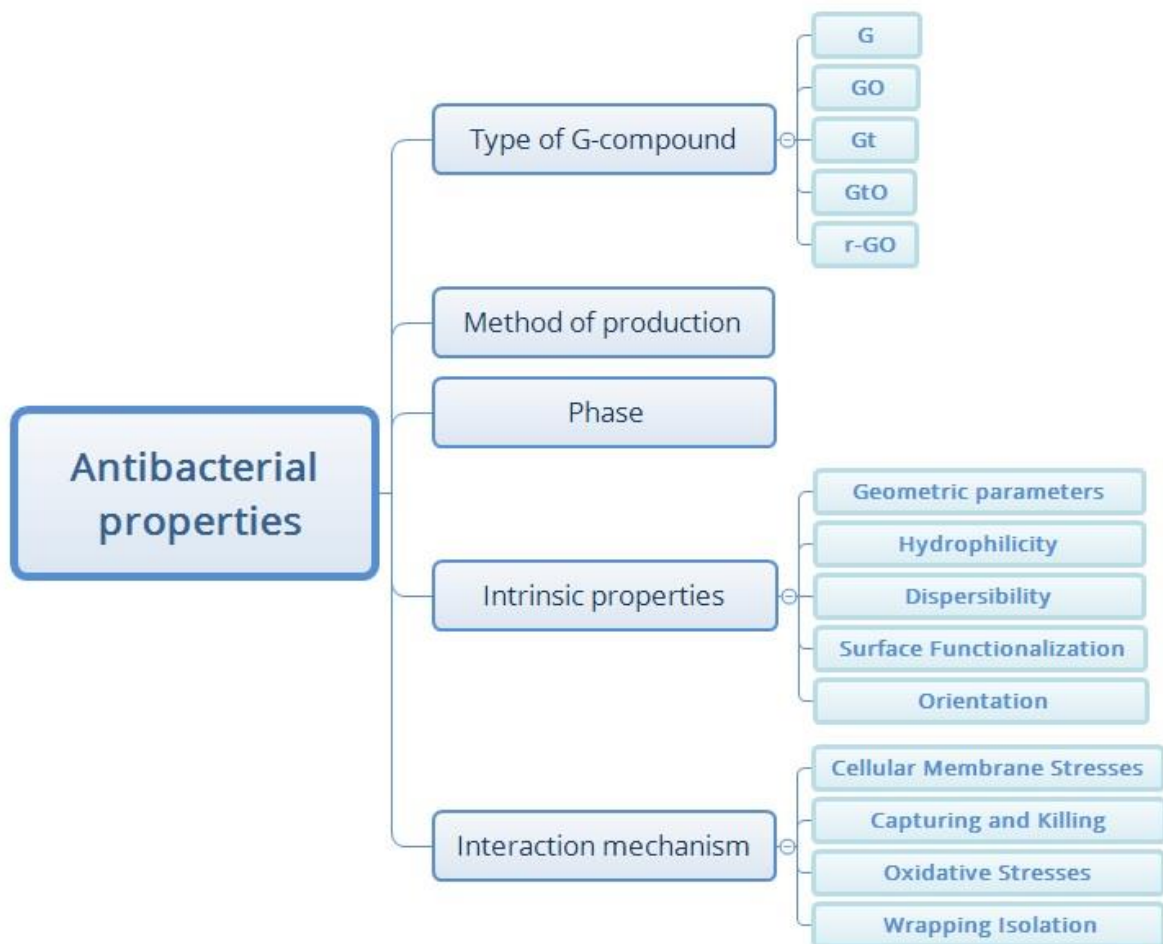


Figure 2.10 A synthetic résumé to describe the five core variables that impact the antibacterial properties of G-based materials.

To give the faintest idea of such dispersibility in up to date researches, Table 2.3 shows a brief summary of some of the newest researches on the antibacterial applications of G-based nanomaterials.

Table 2.3 This table exemplifies, by a short selection of articles, the dispersity of results obtained on the bactericidal properties of graphene and its derivatives: big discrepancies are present in terms of size (second column), bacteria tested (third columns) and consequently final results (fifth and sixth column) [52].

Formulations	Size	Toxicity	Function	Advantages	Disadvantages	Ref.
rGO	From nm to μm	<i>E. coli</i> : 90% viability loss	Cell membrane damage due to contact interaction	Longer and lasting antibacterial activity, physical damage, shows little bacterial resistance	Tendency to agglomerate, thus reducing their antimicrobial activities by altering their surface and edge properties	[33]
GO	Lateral dimensions	<i>E. coli</i> : 98.5% viability loss	Insertion/cutting of cell membranes and destructive extraction of lipid molecules	Physical damage	Bacteria can be reactivated after removing the sheets	[24]
GO	500, 200, and 50 nm	<i>E. coli</i> : 90.9%, 51.8%, and 40.1% viability loss	Trap bacteria and isolate them from their environment	Can focus on a targeted area for effective treatment	Limited deeper tissue penetration	[38]
GO	$0.753\text{--}0.010\ \mu\text{m}^2$	<i>E. coli</i> : larger sizes present stronger activities	Photothermal ablation upon NIR laser irradiation	ROS is a broad-spectrum bactericide	Antibacterial properties will be considerably inhibited when basal plane is masked	[44]
rGO	No data	<i>S. aureus</i> : 99.6% viability loss <i>E. coli</i> : 99.9% viability loss	ROS generation		High toxicological risk	[47]
GO	0.525 μm	<i>P. aeruginosa</i> : 87% viability loss				
rGO	3.40 μm	<i>P. aeruginosa</i> : 86% viability loss				
GO–AgNPs	AgNP: 18 and 5 nm	<i>X. perforans</i> : 99% viability loss	The adhesion of bacteria to GO–Ag composites is increased, and the size, distribution, and aggregation of AgNPs are controlled.	Synergistic antimicrobial effect; silver ions and AgNPs have excellent antibacterial activity		[32]
GO–AgNPs	AgNP: 30–50 nm	<i>C. albicans</i> : 38.9% viability loss	Controlled release of silver ions			[26]
CNSs–AgNPs		<i>C. albicans</i> : 78.6% viability loss				
rGO–Cu	CuNPs: 10–50 nm	<i>E. coli</i> : 99.990% viability loss <i>S. aureus</i> : 99.581% viability loss	Increase the stability of copper nanoparticles and control the release of Cu^{2+}	Synergetic antimicrobial effect; copper is of low cost	High toxicological risk	[102]
rGO–Au	AuNPs: 8–45 nm	<i>S. aureus</i> and <i>P. aeruginosa</i> : 100% viability loss <i>B. subtilis</i> : 99.76% viability loss <i>E. coli</i> : 97.47% viability loss	Oxidation stress on both the antioxidant systems and membrane	Synergistic antimicrobial effect; Good biocompatibility	High costs	[82]
GO–TiO ₂	3D ordered porous structure 1.6-nm thickness	<i>P. aeruginosa</i> and <i>E. coli</i> : 7.5-fold stronger than bare TiO ₂ film	TiO ₂ can generate ROS when illuminated and graphene can improve the efficiency of photoinactivation	Synergistic antimicrobial effect; TiO ₂ possess excellent chemical stability and photocatalytic efficiency	Low photoinactivation efficiency in visible region	[113]
GO–ZnO	ZnO: 4 nm	<i>E. coli</i> : about 200-fold stronger than ZnO NPs	GO facilitated the dispersion of ZnO NPs and enabled close contact with bacteria, thus increasing the local zinc concentration and the bacterial membrane permeability.	Synergistic antimicrobial effect; low cytotoxicity	Low photoinactivation efficiency in visible region	[120]
GO–PVK	Average grain size was about 160 nm	<i>E. coli</i> , <i>C. metallidurans</i> , <i>B. subtilis</i> and <i>R. opacus</i> : 57% (biofilms) and 30% (planktonic cells) higher than GO alone	Encapsulate bacteria to reduce their microbial metabolism	Form well-defined and homogenous coating on various surfaces	Difficult to completely eradicate bacteria	[61]
GO–PLL	No data	the bacterial inhibition is much higher than PLL alone	The composite possesses a positively charged high surface area and tends to strip the bacterial outer membrane	Promote the growth of human cell	Limited stability	[62]

In conclusion, it seems possible to deduce that graphene and its derivatives possess antibacterial properties, but under specific conditions. Further studies are necessary to investigate how relevant a single property is for a specific effect, how the combination of properties come into play, what impact the method of production might have on the biocompatibility of the final product, and how all of the previously investigated variables interconnect. Once these questions are answered, the antibacterial properties of graphene and its derivatives can clearly be defined.

Aside from the antibacterial properties, the use of graphene in bio-related fields such as dentistry, drug delivery and antibacterial coatings would still require further investigation on the eco-physiological toxicity of the material. If the bactericidal properties were to be combined with a more general toxicity towards mammalian cells, the use of graphene would not be as safe in medical applications. Toxicity of carbon nanotubes was widely reported [72,73,74], while, for other G-based nanomaterials, toxicity seems to be both time- and concentration-dependant [75,76], and further discrepancies can be found if different cell lines are considered [77] (vedi Figura 2.11). The mechanisms of interaction between the mammalian cells and G-based nanomaterials seem consistent with the ones observed for bacterial cells [78], but the internalization of the particles inside the nucleus may cause some genotoxic effects [79,80]. While the use of surface functionalization may limit the contingent toxic effects, it may also hinder the positive results induced by the nanomaterials. In any case, desorption of the functionalizing agent would still be possible, and that wouldn't call the toxic effects off. In addition to in vitro tests, in vivo experiments would also be necessary to define the pharmacokinetics of the nanomaterials to determine whether and how fast they can be eliminated from the body.

The complexity of interactions and interconnections between the different variables already underlined for the bacterial effect analysis stands true also for the effect of such nanomaterials on mammalian cells, to which the above underlined conditions must be applied. Thus, the same conclusions about the necessity of ulterior researches, possibly comparable, to come to a definitive conclusion applies also in this case.

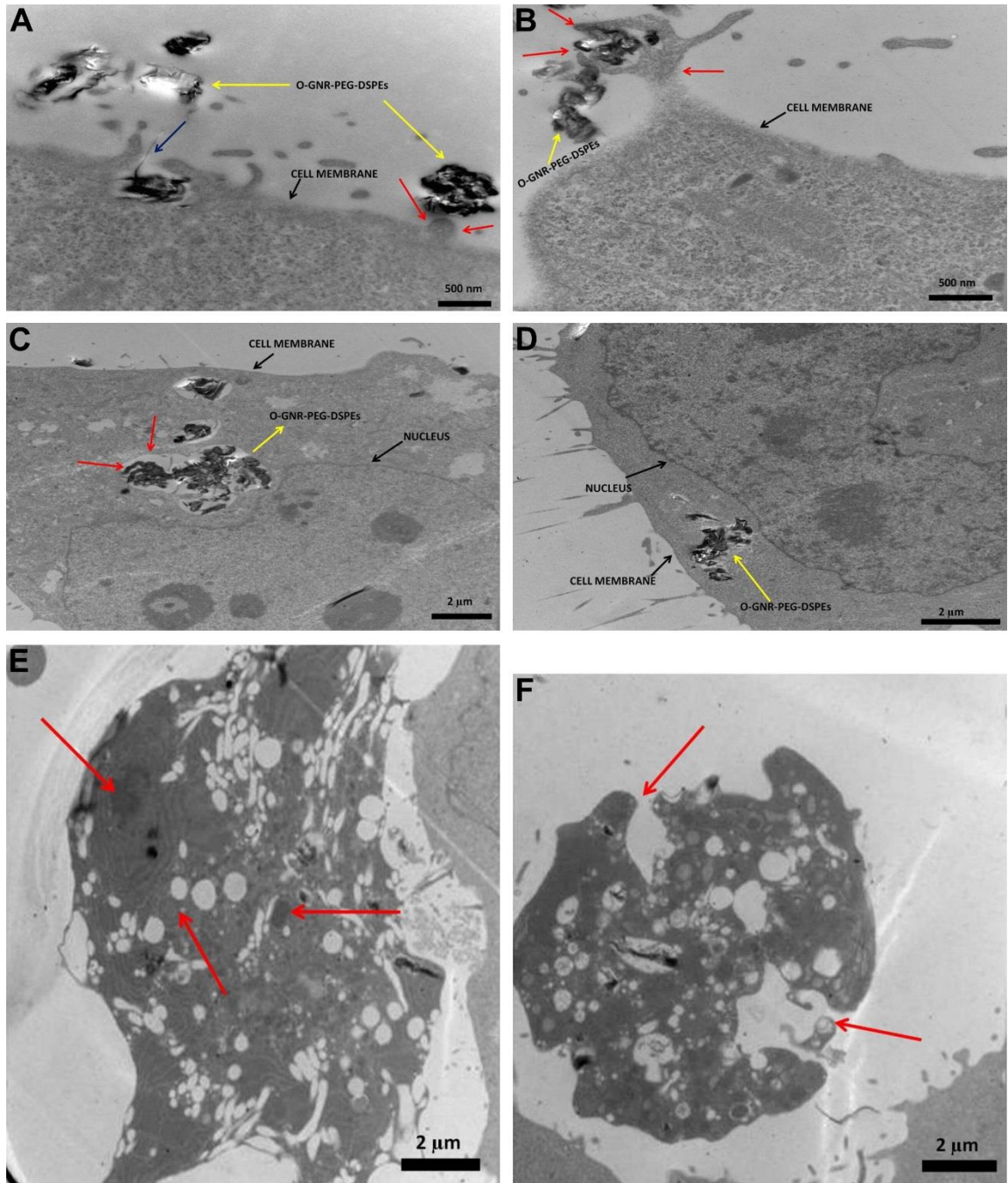


Figure 2.11 TEM images of a HeLa cell incubated with 20 µg/ml oxidized graphene nanoribbons water-solubilized with PEG-DSPE (O-GNR-PEG-DSPE) for 3 h. In Figure (A) O-GNR-PEG-DSPE aggregate at the periphery of the cell (blue arrows). (B) Cell membrane protrudes toward and engulfs the particles aggregates (red arrows). (C and D) O-GNR-PEG-DSPE aggregates are contained in large cytoplasmic vesicles (red arrows). (E and F) HeLa cells after 24h exposure to 20 µg/ml O-GNR-PEG-DSPEs (yellow arrow): (E) swollen vesicles, and (F) ruptured plasma membrane (red arrows), symptom of necrosis. [77]

2.3 Graphene field effect transistor

G-FETs, acronym of Graphene Field Effect Transistors, are an innovative application that adapts widely diffused electronic components, such as transistors, combining them with new possibilities accorded by the use of graphene. G-FETs production and operating principle generally find their basis in the fabrication techniques and working process of Metal Oxide Semiconductor Field-Effect Transistors (MOSFETs), electronic devices whose electric conductivity can be controlled through the difference in voltage applied between its parts.

2.3.1 MOSFET

MOSFETs are a specific type of Field-Effect Transistors, generally referred as FETs. FETs are microelectronic components fabricated through photolithographic techniques, whose electric conductivity can be tuned by controlling the voltage applied between the gate and source. The macrocategory can be generally divided in two subcategories: Junction Field Effect Transistors (JFETs) and MOSFETs, as shown in Figure 2.12.

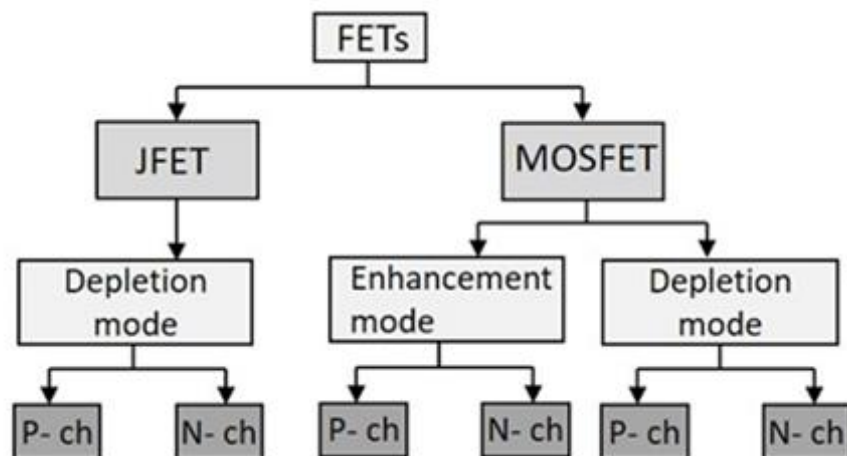


Figure 2.12 Tree diagram illustrating the different types of field effect transistors. [81]

MOSFETs are characterized by a layered structure as the one presented in Figure 2.13. First, a silicon substrate, generally p-doped, is implanted in two small areas with n-doping atoms, in order to have an inversion in the type of carriers in that region. On this base layer a second insulating oxide layer (in SiO_2) is grown, followed by the fabrication of the metal contacts for source (S), drain (D) and gate (G). If no difference in potential is applied between the gate and the source, no current will pass between the source and drain. In case of a difference in voltage between both the gate and the source and the source and the drain, the transistor behaves almost like a capacitor: the negative charges present in the substrate are attracted toward the oxide because of the presence of the gate oxide, and thus form a conductive channel. The formation of said conductive channel permits the passage of current between source and drain. The difference in voltage between gate and source (V_{GS}) determines the stability and carrier density of the channel, and thus controls the device output current.

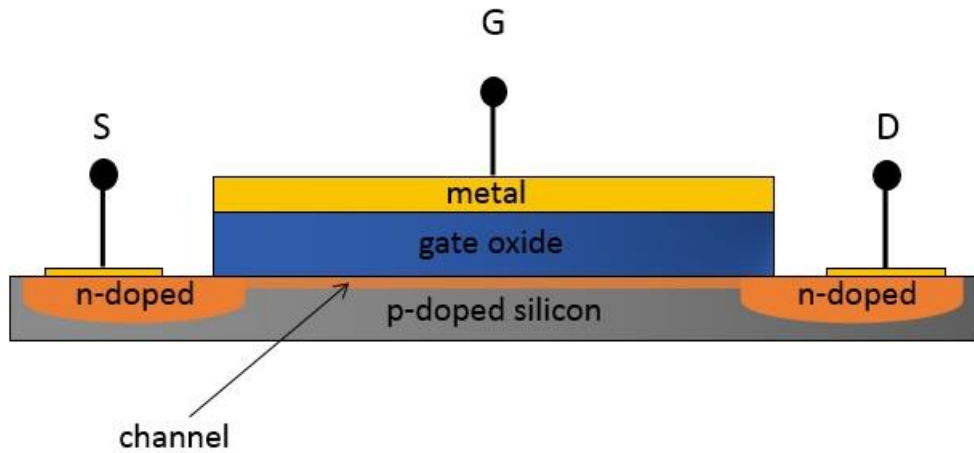


Figure 2.13 Overview of the layered structure of a MOSFET.

To describe more precisely how drain current i_D and voltage are connected, it is possible to refer to two characteristic plots: the drain current versus gate voltage (i_D vs V_{GS}) and the drain current vs source-to-drain voltage (i_D vs V_{DS}).

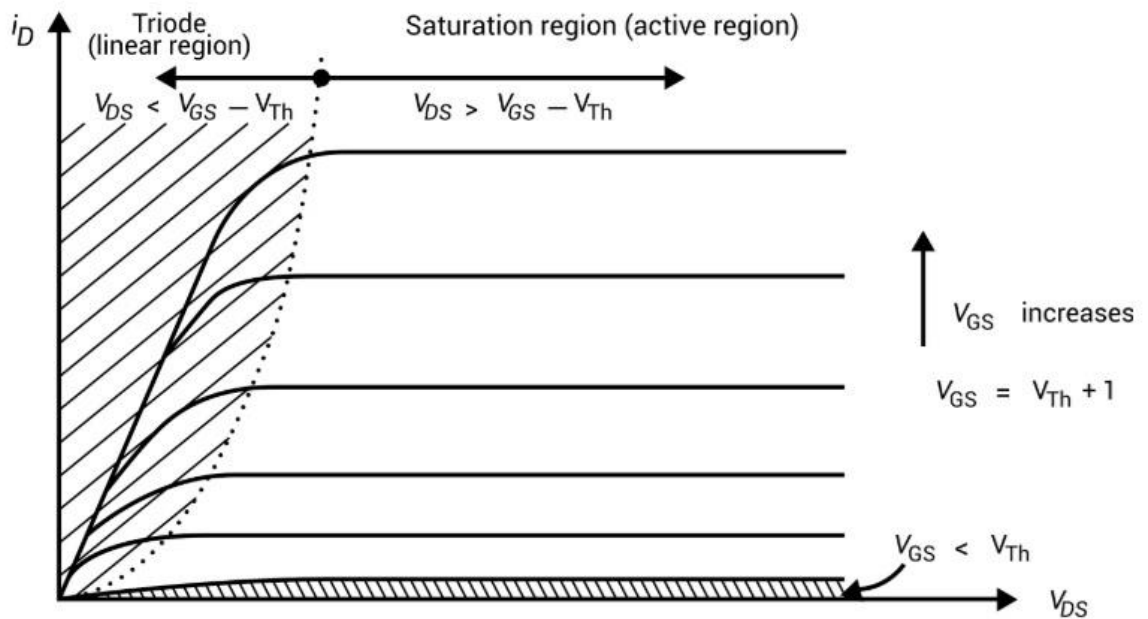


Figure 2.14 Typical i_D vs V_{DS} curve of a MOSFET. [82]

Below a certain voltage, defined threshold voltage V_{th} , the channel is not yet formed, or, if formed, not stable, and the current between the source and drain i_D is approximately null. When the V_{GS} increases, so does the i_D , for the channel formed is richer in carriers. With increasing V_{DS} , instead, two areas are identifiable: the linear region and the saturation region. In the linear region the relation between V_{DS} and i_D is linear, and higher differences of potential correspond to higher output current.

2.3.2 G-FET

The use of graphene and its derivatives in their various allotropes in electronics has known a boost in the recent years because of unique possibilities offered by graphene, best described in Section 2.1 *Properties of Graphene*, that make it adapt to different sensing applications for both medical and chemical applications.

The first devices that tried to combine the working principle of FET with the qualities of graphene used carbon nanotubes (CNTs) [83,84,85]. Controlling the diameter of carbon nanotubes still remains, although, a critical issue of such devices: the electrical properties of CNTs strongly depend on their diameter [86], factor that determines a high dispersity of results. An alternative path was then considered by substituting the carbon nanotubes with monolayer graphene [87,88,89,90].

Different configurations were considered, some developing towards enhanced electronic applications and others oriented to biological and chemical use as biosensors: top-gated G-FETs, back-gated G-FETs, bilayer G-FETS (where both a top-gate and a back-gate are present) [91], but also electrolyte-gated graphene FETs [92,93,94,95], where the gate and the graphene are divided by a liquid solution (see Figure 2.15).

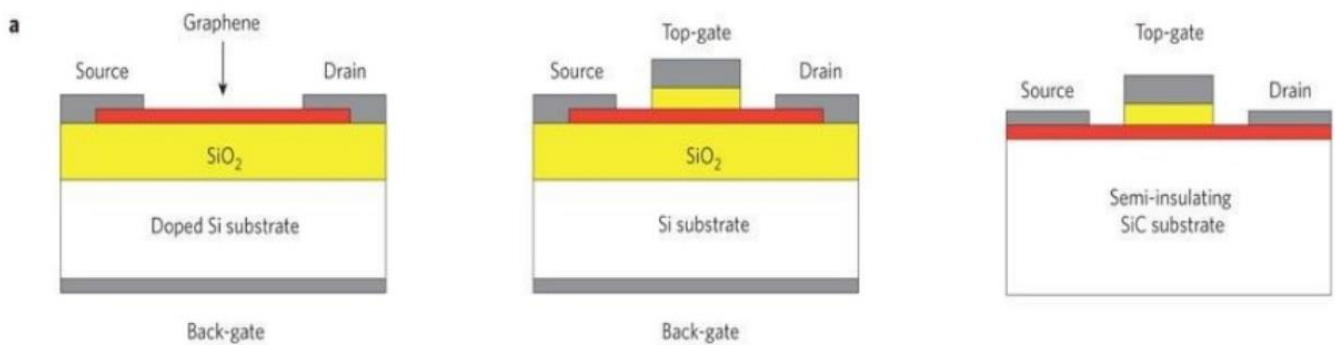


Figure 2.15 Overview of the different types of G-FET with solid gate. From left to right: back-gated G-FET, bilayer G-FET, top-gated G-FET. [96]

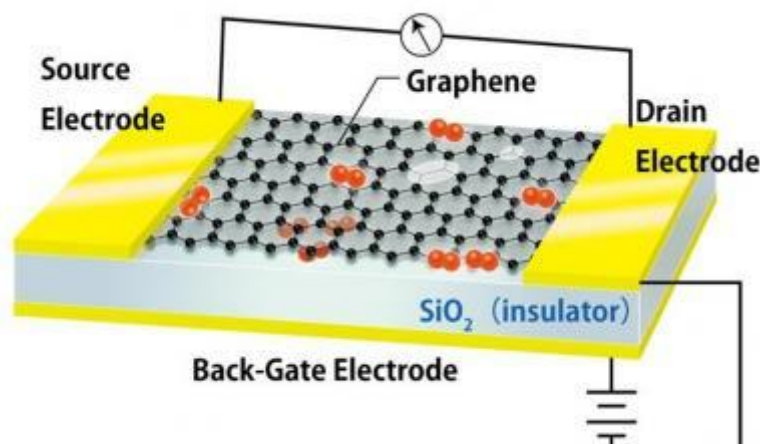


Figure 2.16 Representation of a standard structure of a G-FET: the graphene layer connects the source and drain electrodes. [97]

The common ground of the technology is that G-FETs are generally realized by using graphene as the channel connecting Source and Drain, as in Figure 2.16.

The working principle of G-FETs is similar to the one described in Section 2.3.1

MOSFET: by changing the gate voltage V_G at a constant V_{DS} , the conductivity of graphene can be controlled. A typical transfer curve for such devices can be found in Figure 2.17: the graph is generally V-shaped, confirmation of the ambipolar characteristics of graphene.

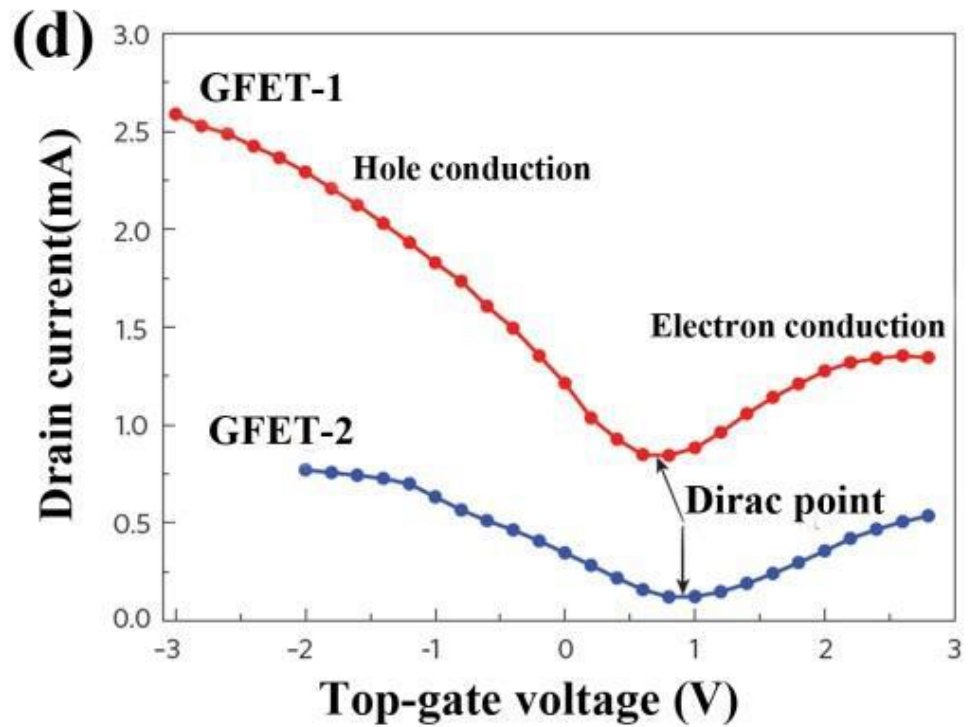


Figure 2.17 Representative transfer characteristics curves for two G-FETs with large-area-graphene channel [modified from 98]

The point of minimum conductance of graphene corresponds to the Dirac point, pointed at by black arrows in Figure 2.17: the Dirac point represents the potential at which the number of holes and electrons is equal, and should be around 0V for ideal graphene. If in pristine graphene the energy of the Fermi level corresponds to the Dirac Point, the presence of surface defects or adsorbed molecules (due to engineered surfaces or statistical formation of impurities and defects during the processing) results in doping-type effects, which change the conductivity of graphene shifting their characteristics toward different voltages (see Figure 2.18).

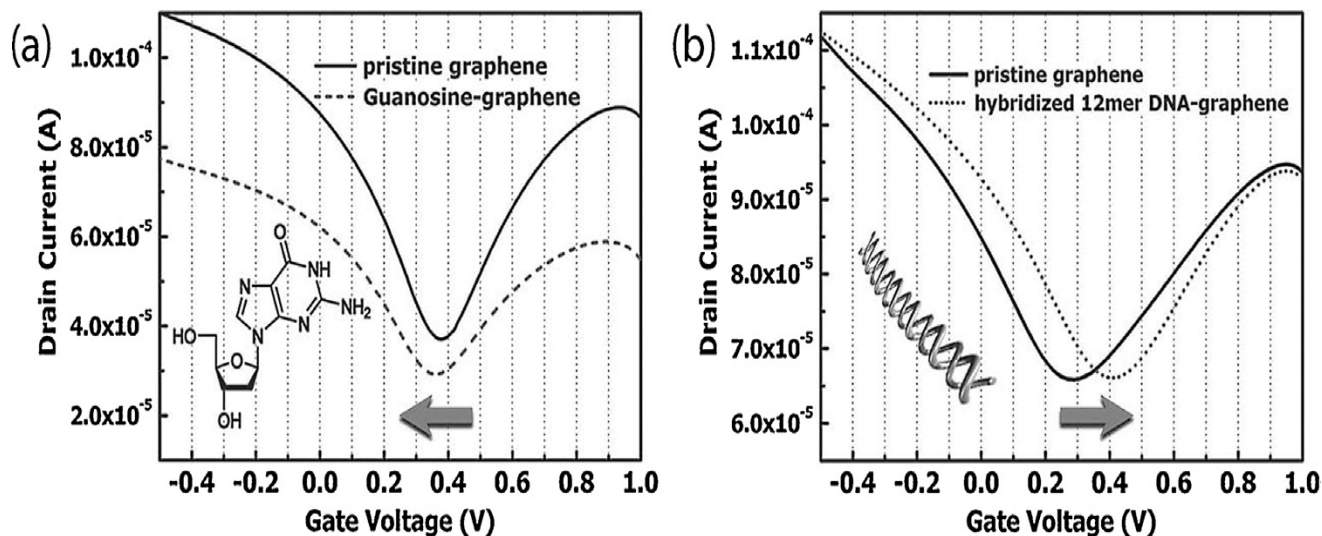


Figure 2.18 The transfer curves for a graphene device before and after interacting with (a) the guanosine nucleoside and (b) a dsDNA hybridized from the probe and complementary DNA [modified from 99]. Notice the shifts in the Dirac Point due to the adsorption of molecules on the graphene surface.

Such differences of graphene field effect transistors with respect to the ideal behavior can be investigated through both Raman spectroscopy, which allow a better understanding of the purity of quality of the graphene layer, and $R-V_G$ characteristics, that instead represent how the carrier population was affected by the manufacturing steps, and where the Dirac Point is subsequently located.

For these reasons, graphene appears to be a validate candidate for integration in FET for the sensing of a huge variety of both organic and inorganic compounds: DNA^[100,101], microRNA^[102], dopamine^[103], NO^[104], Ebola Virus Disease^[105] and biofilm growth^[106], glucose^[107], pH^[108] just to give a few examples.

3. CVD Graphene Biosensor

3.1 The working principle

Over the last few decades, the development of multi-resistant bacterial strains drew more and more attention in the scientific world. Inappropriate or excessive use of drugs [109,110] prescribed in the treatment of diseases even if not strictly required, combined with a misuse in large part of the agricultural world [111, 112], induced the formation of multi-resistant bacterial strains. These strains can develop through statistical genetic mutations that are passed over onto next generations or transferred horizontally to other cells via plasmids.

Antibiotics cannot be replaced, at the moment, given their most relevant role played in guaranteeing a progressive healing of the patients by preventing bacterial colonization in many routine medical practices like chemotherapy, surgical operations and organ transplants. The formation of drug-resistant bacteria, on the other hand, requires the adoption of new solutions like longer treatments, and thus longer hospitalization, with the linked problems, but most importantly an increase in the drug dosage prescribed to the patient, with a higher degree of toxicity. In addition, the number of antibiotics available on the market is limited. Even if alternative and preventive measures are being developed, it would be extremely important to limit the use of broad-spectrum antibiotics and identify the type of bacteria causing the infection. The treatment of such infection with narrow-spectrum antibiotics would limit the development of drug-resistance in bacteria.

The goal of this inquiry is to evaluate whether graphene would qualify as an efficient material in this specific application, and in order to do so, graphene is integrated in FETs. The working principle of Graphene Field-Effect Transistor is described in more detail in *Chapter 2. Graphene*, but the general functioning of the device can be understood, in broad terms, through an analogy with a MOSFET.

In its most basic form, a MOSFET is constituted by a layer of semi-conductive material, generally Silicon (Si), either n or p doped. On this first layer, two more are grown, an insulating di-electric layer of SiO₂, and a third layer made of metal.

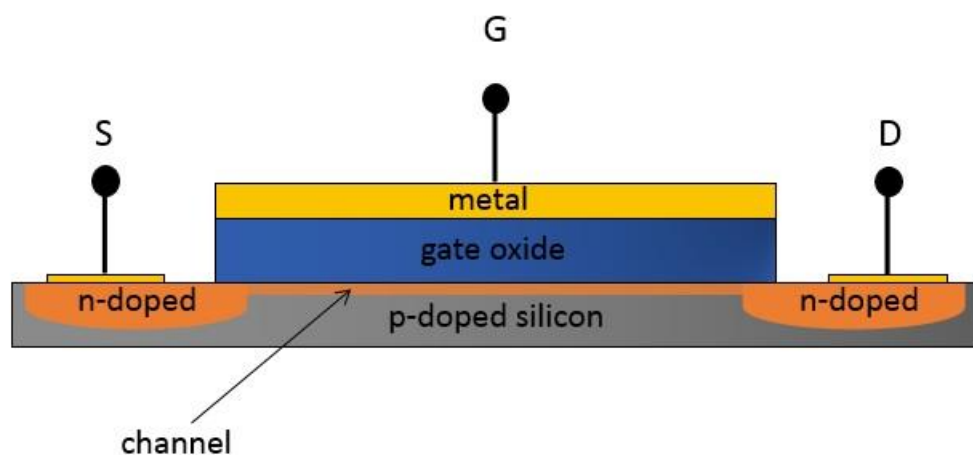


Figure 3.1 Structure of a standard n-gated MOSFET.

When the gate voltage applied is null, no current can pass between drain and source, but when the voltage assumes a positive value, then the negative charges present in the p-doped silicon are drawn toward the oxide, and a conductive channel forms. The formation of such channel allows the passage of current, whose intensity is controlled through the gate voltage.

In the case of Graphene-FETs, the principle is similar. When a voltage is applied to the back gate connected to the silicon, a channel forms, but this time in the graphene: the passage of current from drain to source is then again possible.

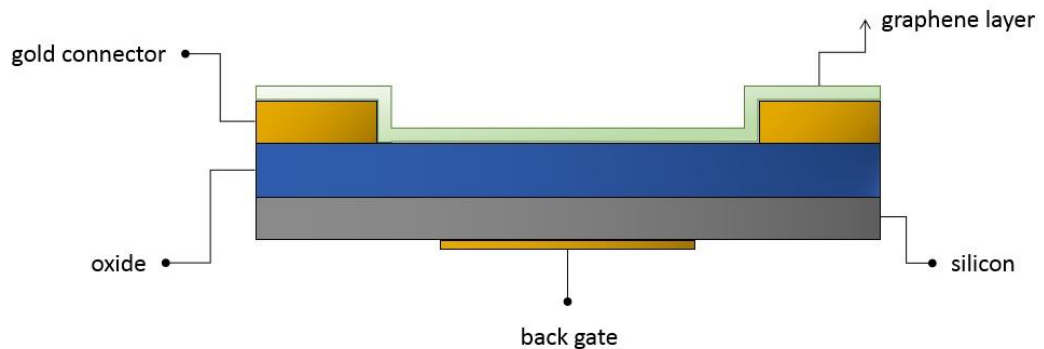


Figure 3.2 Overview of the materials used for the fabrication of a G-FET.

The exposure of graphene to the liquid bacterial solution constitutes, although, the key difference with other sensors: bacterial cell walls are made of organic compounds of different nature (lipids, polyglycans...) which interact with the graphene layer, colonizing the surface to form a biofilm. The adhesion phenomena on the graphene surface exposed to the solution results in a change in carrier density and mobility across the channel.

Because of these adhesion phenomena and the following formation of a bacterial biofilm, the resistivity of graphene is not constant, and its change can be monitored over time.

Practically speaking the G-FET is integrated inside the circuit shown in Figure 3.3: given a defined constant V_G , the V_{DS} measured between S and D depends, subsequently, from the resistance between source and drain, which, as said, changes over time because of the formation of a biofilm. Such resistance is in series with another resistor, referred as R_0 , which implies that the current between Source and Drain can be defined through the formula:

$$I_{SD} = \frac{R_{SD} * 10V}{R_{SD} + R_0} \quad \text{referred as current bias.}$$

Being $R_{SD} \ll R_0$, then I_{SD} can be approximately estimated as:

$$I_{SD} = \frac{R_{SD} * 10V}{R_0}$$

More precisely, the ΔV initially imposed between S and D is a periodic function in the form:

$$V_0 = 10V * \sin(2\pi * f * t)$$

where the frequency $f = 37$ Hz.

That results in an output variable $V(t) = V_{SD} * \sin(2\pi * f * t + \phi)$, where ϕ takes into account the possible capacitive or inductive phenomena that may originate in the device or circuit. An *ad hoc* program fits the measured variable so to obtain a more precise value of V_{SD} . By the ratio between V_{SD} and I_{SD} , one can obtain the value of the resistance R_{SD} . The change in resistivity of the graphene can be thus related to a change in voltage over the source-drain, which is more precisely measured through a four-wires measurement.

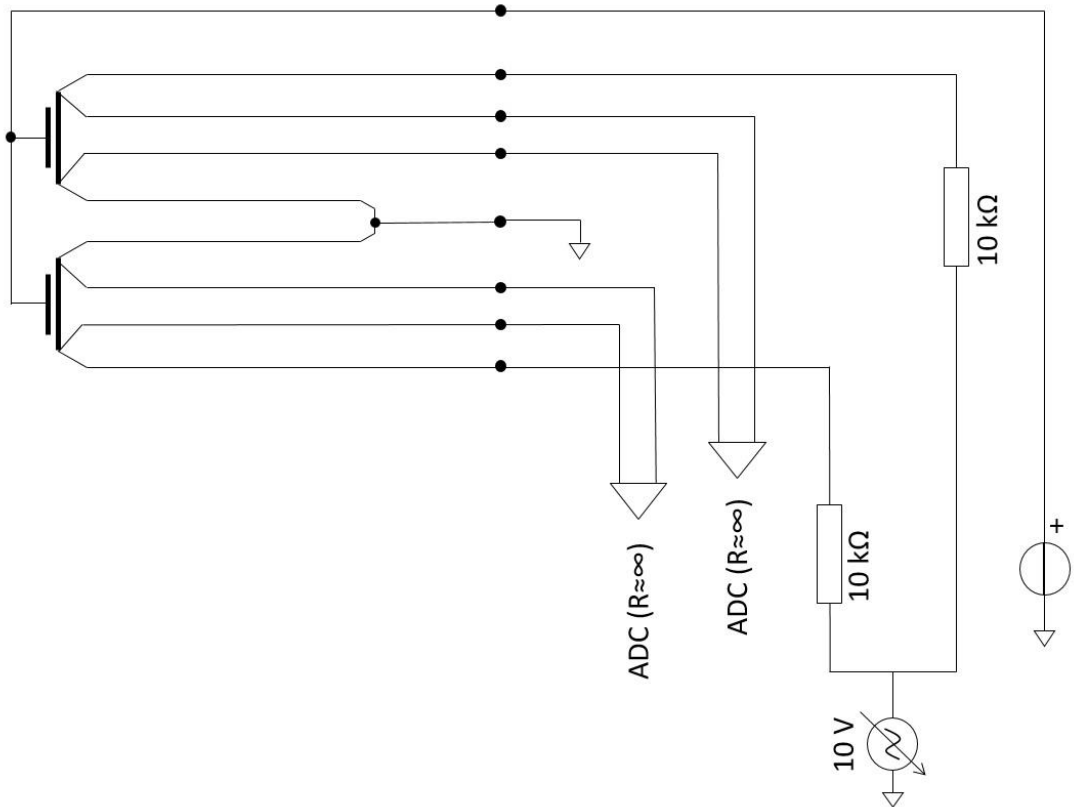


Figure 3.3 A representation of the circuit of the biosensor.

The resulting resistance vs time plots can be analyzed in order to point out specific trends for similar bacteria or unique trends connected to specific properties of a single bacteria. If specific trends can be underlined, it would then be possible to use the biosensor in case of infection to treat the patient not with broad-spectrum antibiotics, but to define a targeted drug treatment, thus reducing the risks underlined in the introduction of the Section.

3.2 Device fabrication process

The biosensor is realized through photolithography, a technique widely diffused for the production of high precision microelectronic components. A basic photolithographic process is made up of several steps^[113], as summarized in Figure 3.4:

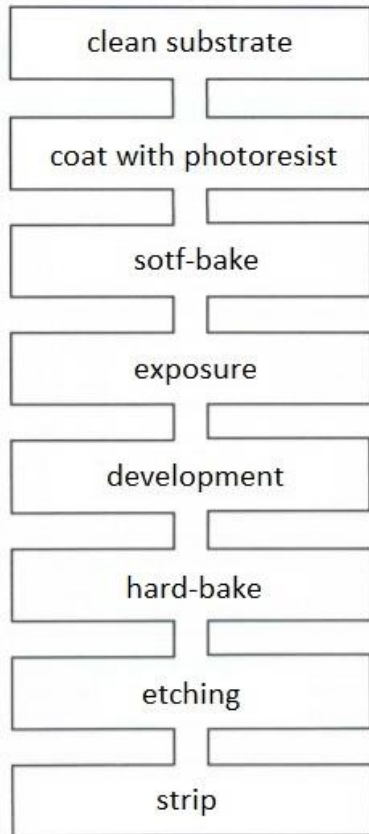


Figure 3.4 Chart flow of a standard lithographic process for electronic components.

- First, a substrate preparation is required to clean it from contaminants. This step proves also to be useful in order to improve the adhesion of the photoresist in the following step.

- The substrate is then *covered* with a uniform layer of *photoresist* through a spin coating process. The resist's thickness can be generally defined a priori thanks to the resist thickness – spin speed curves provided in the material datasheet.

- Given that the photoresist spun on the substrate is generally in liquid form, the resulting resist will still contain a considerable amount of solvent. Consequently, the coated substrate undergoes a baking process in order to eliminate most part of the solvent and stabilize the dimensions of the formed film for the subsequent processes.

- After the soft-bake, the substrate is ready to be exposed to radiation, generally UV light: such exposition results in a change in solubility of the resist in a given developer (more soluble in case of positive photoresist, the opposite for a negative one). The use of photolithographic masks containing defined patterns leads to the replications of these patterns on the substrate.

- Once the desired patterns are re-created, the photoresist is developed in a given solution: the different degree of solubility of the resist in the

developer caused by the exposure to UV light determines the obtainment of the desired pattern “carved” in the resist.

- A hard-bake is then necessary to harden the resist and grants its integrity and shape for the following steps.
- The patterns copied through photolithography from the mask to the resist are now transferred on the substrate, generally though subtractive techniques like etching. Additive deposition and ion implantation can be viable options in case of specific requirements.
- Once the etching process is completed, the remaining photoresist is removed through the use of solvents (wet stripping), generally acetone, or plasma (dry stripping).

In the specific case of the considered biosensor, the fabrication process requires, first, the identification of an adapt substrate. For such purposed a Si (p-doped)/SiO₂ substrate, a commercial product easily attainable given its use in the productions of many electronic components, was chosen.

On the Si/SiO₂ substrate, a layer of parylene is deposited through sublimation of 1,85g of parylene-N, for a final thickness of 150 nm of polymer.

The parylene, though, would not allow a proper fixing of the golden connector necessary to create the biosensor circuit, thus the formation of a small window is required to optimize the adhesion between the golden electrodes and the initial substrate.

This small opening in the parylene layer is realized through a photolithographic process:

- first a layer of the positive photoresist S1813 is made through spin coating at 3000 rpm; a post-apply bake process at 95°C for 2 minutes follows;
- final photoresist development step of 70 seconds in Microposit™ MF319, a metal ion free, tetramethyl-ammonium hydroxide-based developer [114].

MICROPOSIT S1800 PHOTO RESIST UNDYED SERIES
Figure 1. Spin Speed Curves

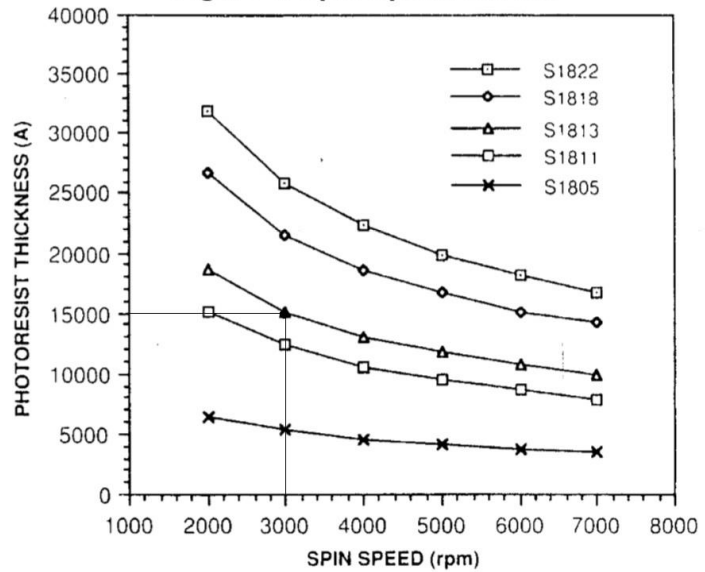


Figure 3.5 Thickness - Spin speed curve for Microposit S1800 Photoresist series. [115]

The final thickness of the S1813 layer, obtained by the resist thickness – spin speed curves, is about 1500 nm (see Figure 3.5).

The parylene covering the window section is etched through O₂ plasma treatment at 40 watts for 3 minutes. No hard bake step is necessary for the S1813. The photoresist is eventually removed through combined washing steps:

- in acetone at room temperature for 10 minutes;
- acetone at 50°C for 10 minutes;
- stirring in isopropyl alcohol (IPA);
- blow drying with inert gas;

The results of the described photolithographic step are represented in Figure 3.6.

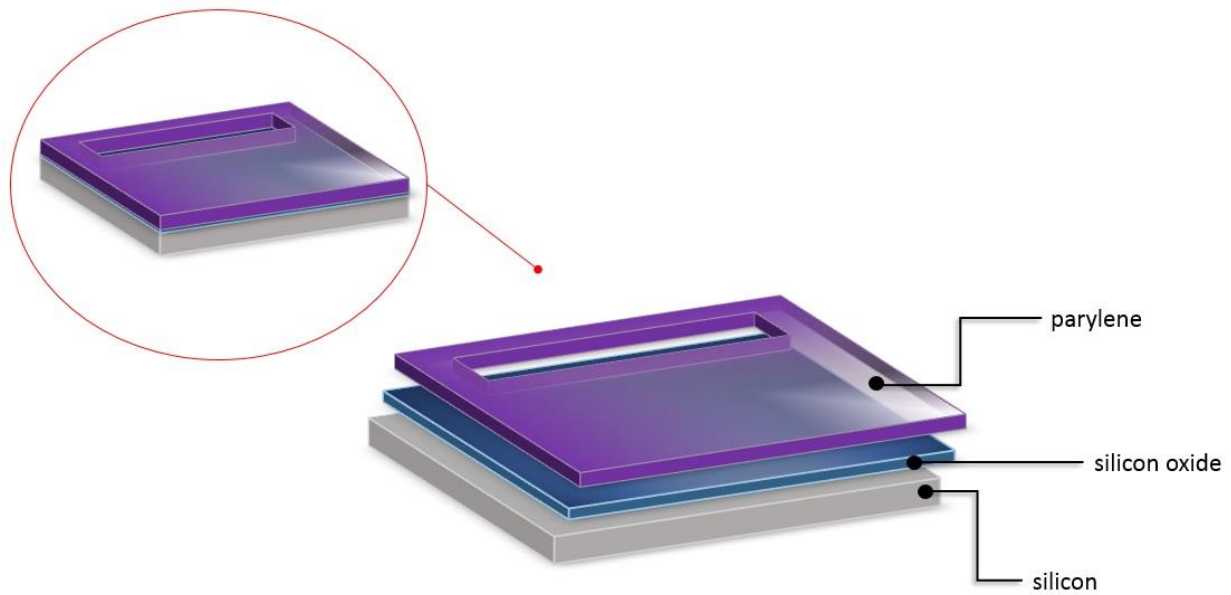


Figure 3.6 Overview of the biosensor appearance and structure after the realization of a window in parylene.

The following step of the process allows the realization of the circuit electrodes through photolithography, through a process, represented in the image on the side, almost identical to the one described above:

- a layer of LOR3A is spin-coated on the substrate at 3000 rpm, followed by soft-baking for 10 minutes at 130°C. The final thickness of the layer should be around 320 nm (see Figure 3.8).
- a second layer of the positive photoresist S1813 is made through spin coating at 3000 rpm, followed by soft-baking at 95°C for 2 minutes, to obtain a final thickness of about 15000 nm (see Figure 3.5);
- photoresist development step of 55 seconds follows.

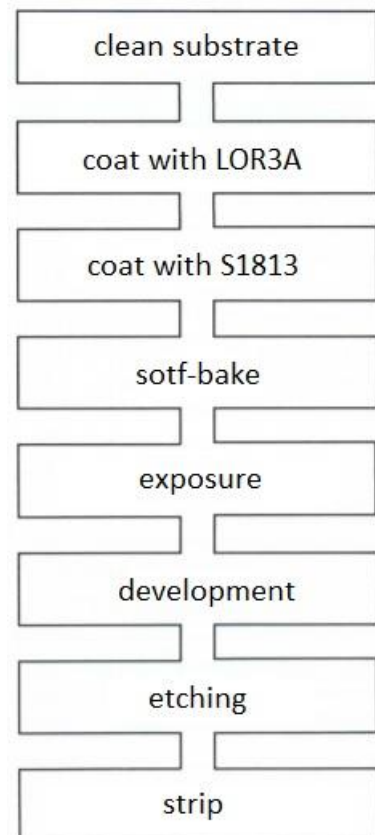


Figure 3.7 Flow chart description of the photolithographic process for the realization of circuit electrodes.

Spin speed vs film thickness for LOR A series resists.

Other film thicknesses available upon request.

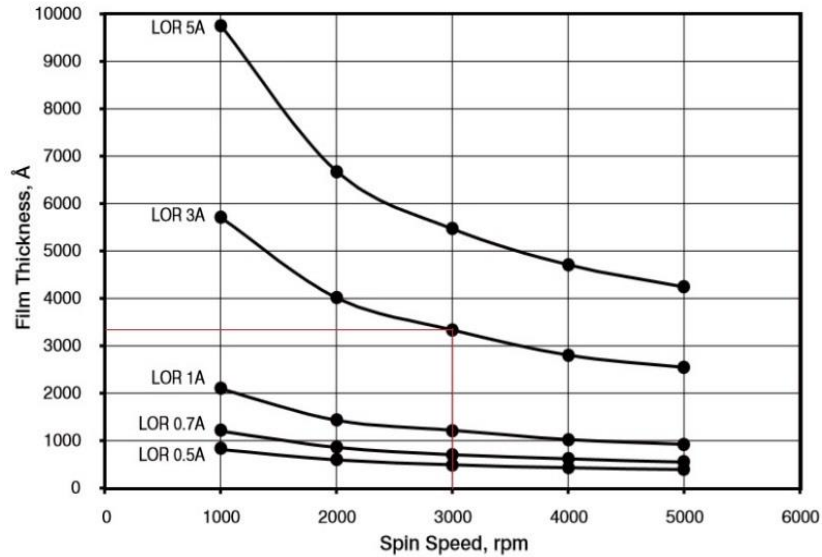


Figure 3.8 Thickness - Spin speed curve for LOR A series resists. [116]

LOR is a lift-off resist with multiple uses: not only it allows a bi-layer processing with no further exposition or development steps necessary, but its most interesting characteristic is the isotropic development. Developing isotropically (see Figure 3.9), LOR3A creates a reentrant sidewall profile, that excludes the possibility of damages to the wanted profiles during lift-off [116].

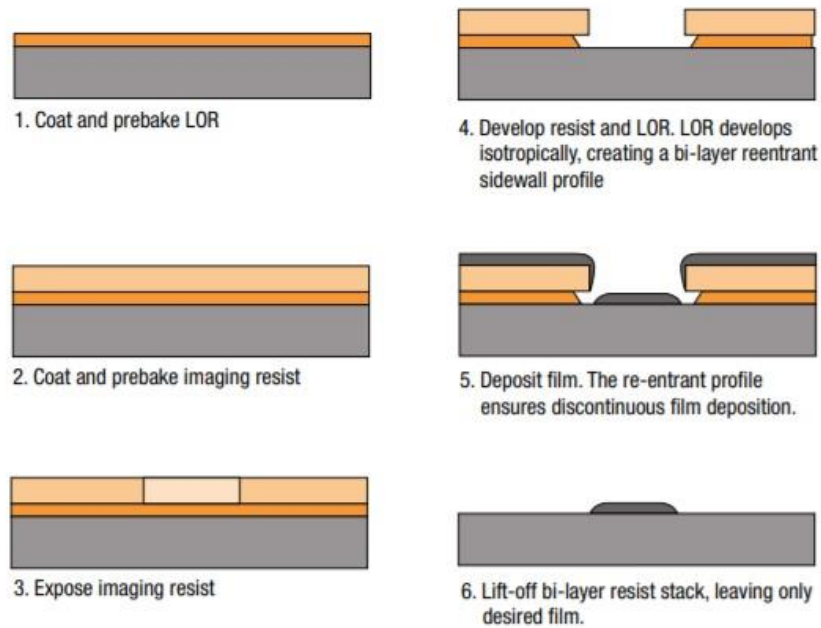


Figure 3.9 Overview of the photolithographic process and lift-off using LOR3A. Notice in particular picture 5, which describes how the isotropic development guarantees a better reproduction of the wanted profiles on the substrate. [116]

Electrodes growth is realized by evaporation: to improve the adhesion of gold to the substrate, a thin layer of chromium or platinum is used. In the current process, the said electrodes are realized through:

- a very thin layer (5nm) of Cr;
- a thicker layer of Au of 180 nm.

The lift-off process is carried out in acetone, as previously described. The results of this step are show in Figure 3.10.

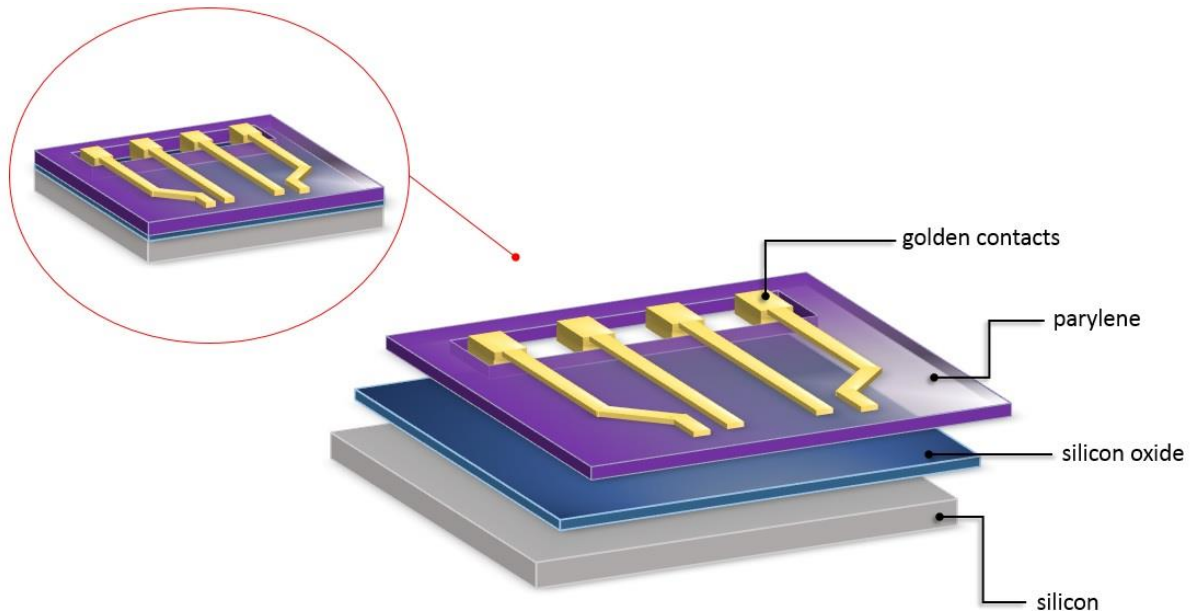


Figure 3.10 Overview of the biosensor appearance and structure after the realization of the gold contacts.

Graphene is then grown on a copper substrate by CVD process and then coated with two layers of PMMA through spin-coating at 1000 rpm, then baked at 50°C for 30 minutes.

The copper is etched through a combined process:

- washing in diluted ammonium persulfate (APS) for two hours;
- cleansed in de-ionized water for 2 hours.

Graphene is then vertically transferred by a droplet of IPA, and the processed substrate is left to rest overnight.

The PMMA on top of the graphene is removed through the following steps:

- washing in acetone at room temperature for 15 minutes;
- washing in acetone at 50°C for 15 minutes;
- stirring in IPA;
- blow drying with inert gas.

The results of the graphene transfer process are illustrated in Figure 3.11.

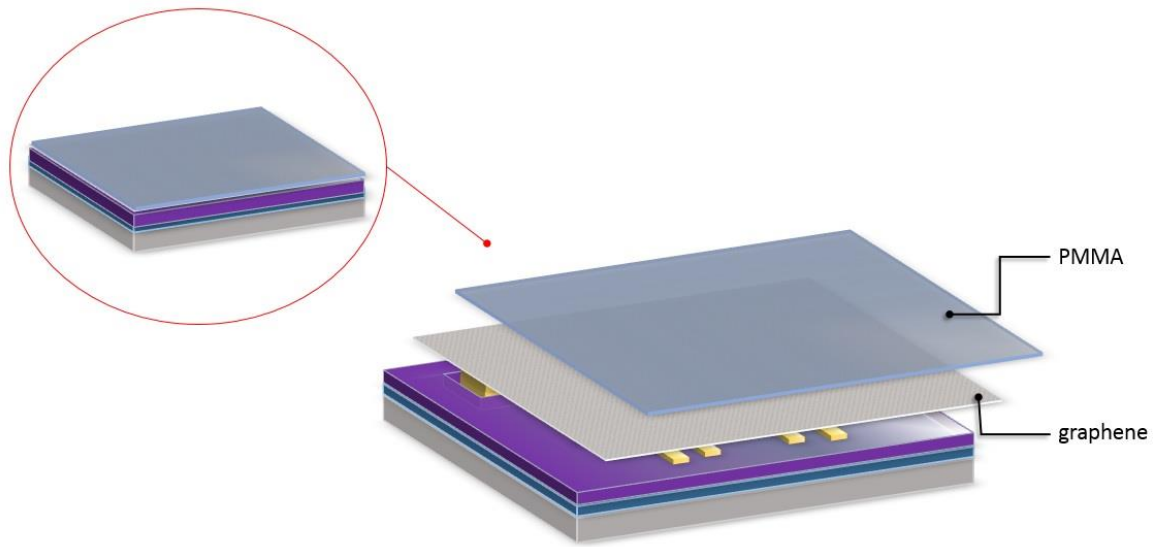


Figure 3.11 Overview of the biosensor appearance and structure after the graphene transfer process.

An ulterior step of photolithography is necessary in order to guarantee the coverage, by graphene, of only a specific area of the substrate, as shown in Figure 3.12. In preparation of the treatment, different steps are required.

- 2 layers of PMMA 2A obtained through a spin-coating process at 6000 rpm, then prebaked at 60°C for 3 minutes, attaining a thickness of about 60 nm;
- a layer of LOR3A is spin-coated on the substrate at 4000 rpm, then pre-baked for 10 minutes at 130°C for a final thickness of around 300 nm (see Figure 3.8).
- another layer of the positive photoresist S1813 is made through spin coating at 4000 rpm, then pre-baked at 95°C for 2 minutes, to obtain a final thickness of about 1300 nm (see Figure 3.5).
- resists are exposed to UV light in order to select specific areas for patterning;
- photoresist development step of 55 seconds.
- PMMA and graphene are here etched in O₂ plasma at 100W for 1minute, then the substrate undergoes flux exposure with UV light for 40 seconds, so that the LOR and the photoresist remained can be dissolved in the developer for 30 secs.

The results of such photolithographic step are shown in Figure 3.12.

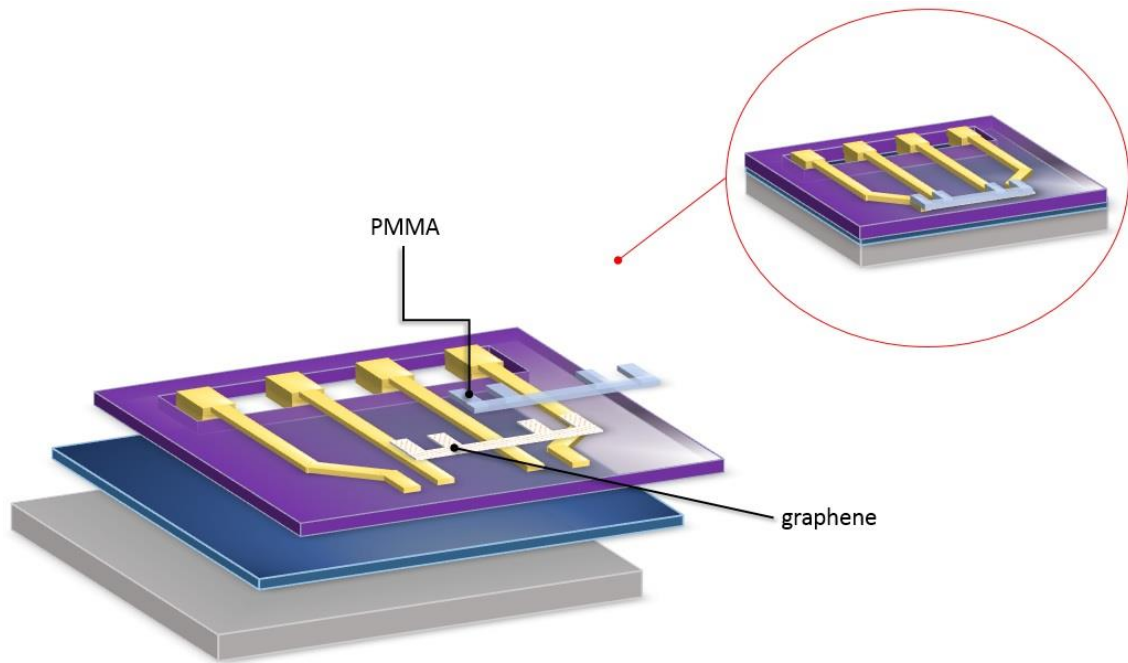


Figure 3.12 Overview of the biosensor appearance and structure after the etching of PMMA and graphene in specific areas.

To realize a protection layer and allow the sensor to be reusable, a protection layer is created through:

- a layer of LOR3A is spin-coated on the substrate at 3000 rpm, then pre-baked for 10 minutes at 130°C, for a final thickness of around 300 nm (see Figure 3.8);
- another layer of the positive photoresist S1813 is made through spin coating at 3000 rpm, then pre-baked at 95°C for 2 minutes, to obtain a final thickness of about 1500 nm (see Figure 3.5);
- exposure of desired area and photoresist development for 60 seconds.

The process is concluded through the removal of remaining PMMA after the final cleansing: the substrate is stirred in acetone for 1 min.

The appearance and structure of the substrate after this step are shown in Figure 3.13.

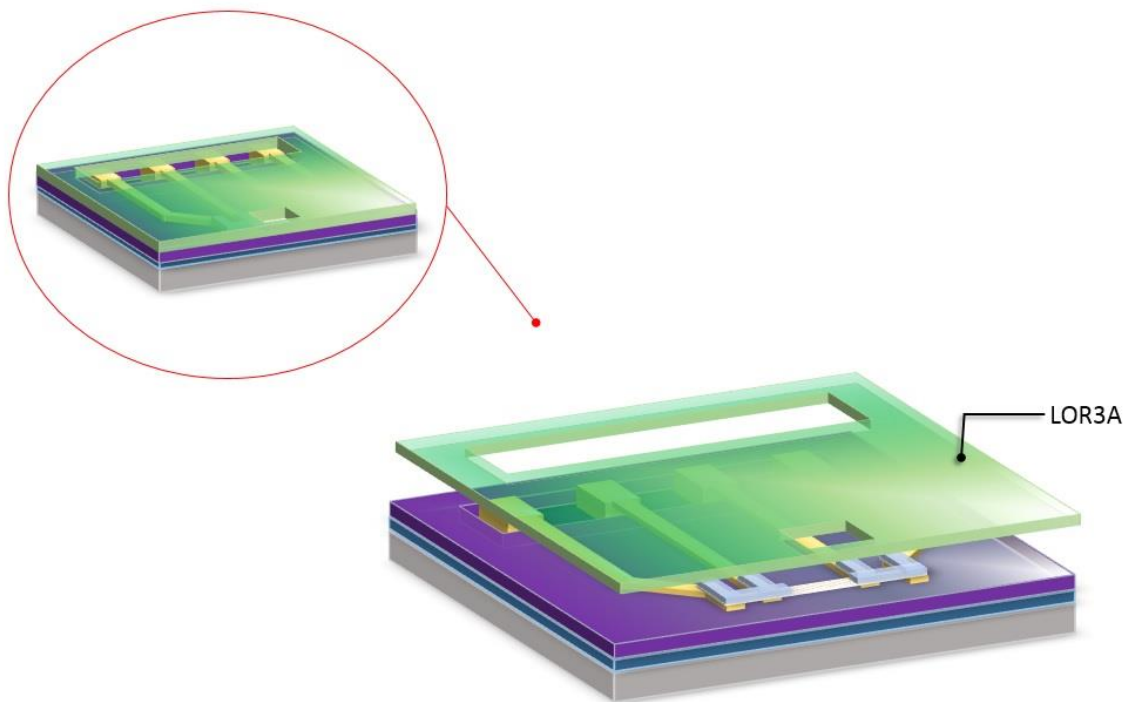


Figure 3.13 Overview of the biosensor appearance and structure after the realization of a protective layer.

The substrates obtained through the above described process undergoes two ulterior steps:

1. The devices, at the end of the processing, are tested to evaluate their functioning and quality. Further details on these controls are provided in Section 3.3 *Characterization*;
2. The devices that passed the first test are then mounted on a larger PCB support, as shown in Figure 3.14.

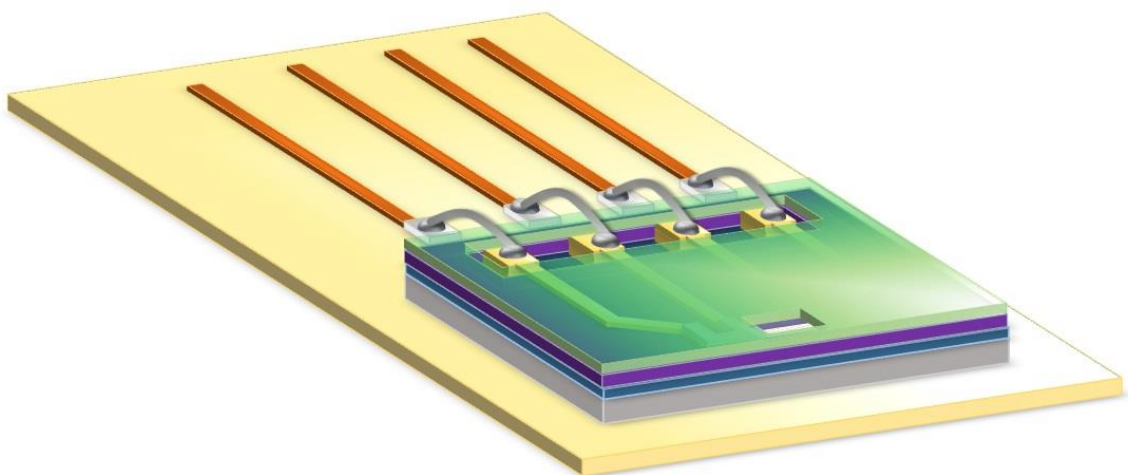


Figure 3.14 Overview of the biosensor appearance and structure after being mounted on the PCB support.

The final contacts are then realized through a silver paste, that connects the golden electrodes to the copper connectors on the plastic support. This final integration of the biosensor allows its insertion in the socket similarly to a USB drive into a plug. Eventually, the gold contacts are isolated from the working environment by covering with PDMS (PolyDiMethylSiloxane). This is necessary to ensure that the obtained results are void of any external factors.

The final appearance and structure of the biosensor realized through the photolithographic steps described along the Section is shown in Figure 3.15.

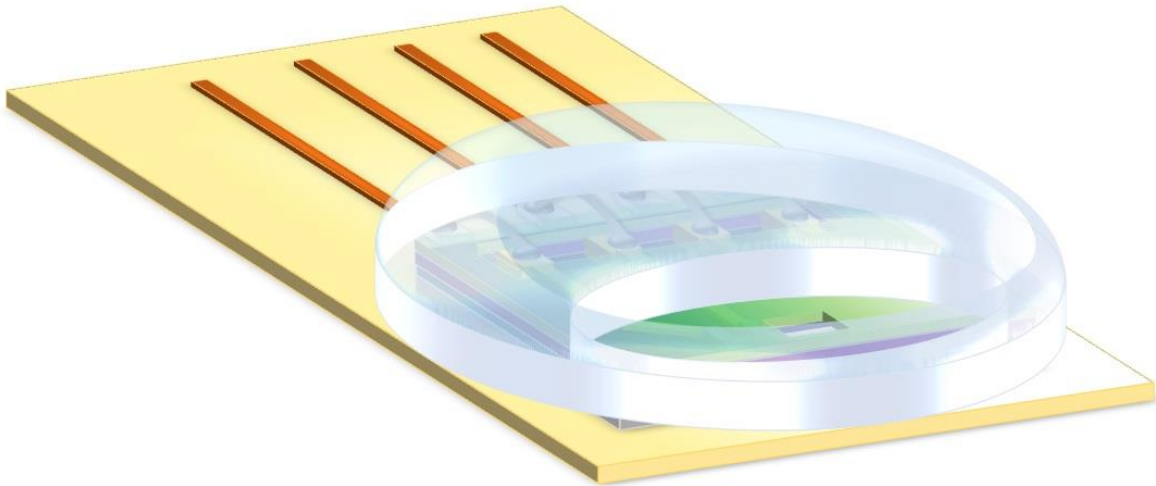


Figure 3.15 Overview of the final biosensor appearance and structure.

The devices thus obtained are safely stored under inert gas, so to prevent any form of oxidation or interaction with the exposed graphene.

In Figure 3.16 a brief summary of the entire process is described in 2D.

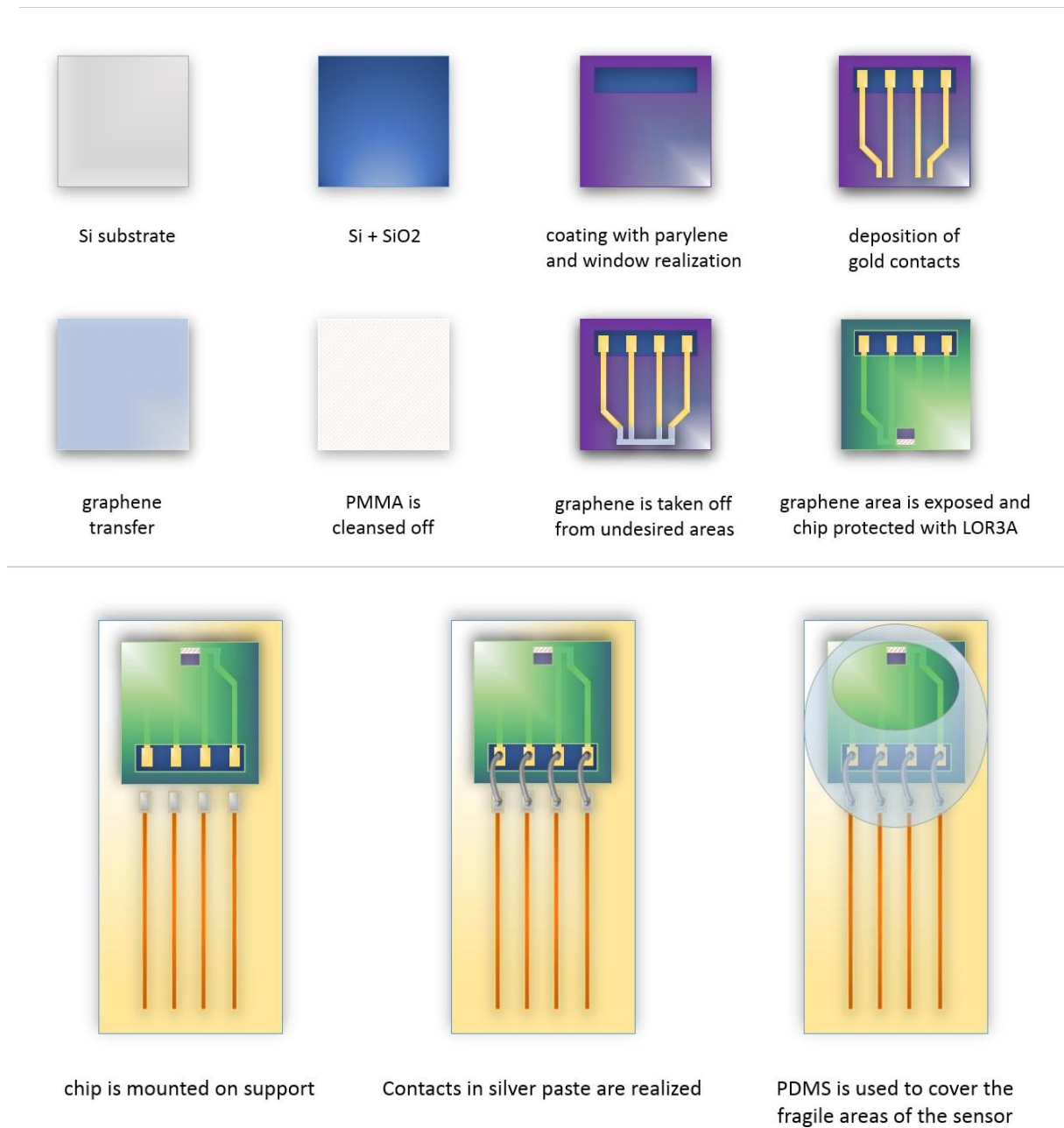


Figure 3.16 2D summary of the outcomes of the lithographic steps necessary to obtain the sensing device.

3.3. Characterization

3.3.1 Raman spectroscopy

As already announced in Section 2., Raman spectroscopy is a technique commonly used to verify the quality of graphene. In fact, it is both fast and non-destructive, and provides highly reliable information on both the structure and electronic configuration of the material [17, 117], thanks to the gapless nature of graphene, reason for which all incident wavelengths are resonant [117]. It allows univocal identification of the orientation and number of layers of the specimens [118] and of the presence of doping, grain boundaries, edges [119].

An example of Raman spectra of graphite and graphene can be seen in Figure 3.17. Using a laser of 514nm, it is possible to distinguish two main peaks, distinctive of graphite, one at around 1580 cm^{-1} (referred as G peak) and a second one around 2700 cm^{-1} (referred as G' peak).

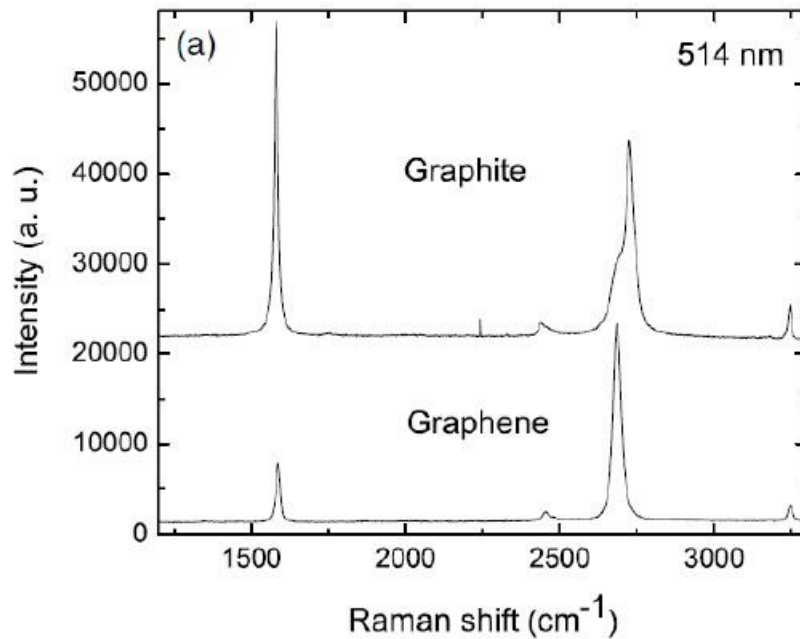


Figure 3.17 Raman spectra of graphite and graphene [reference]
The two spectra are scaled in order to have a similar height of the G' peak. [118]

When the number of graphene layers increases, the G' peak modifies its shape, full width at half maximum (FWHM) and position, as shown in Figure 3.18. The shift in peak position and the ratio of the peak intensities $I_{G'}/I_G$ can be reconnected to the number of graphene layers present [117,118].

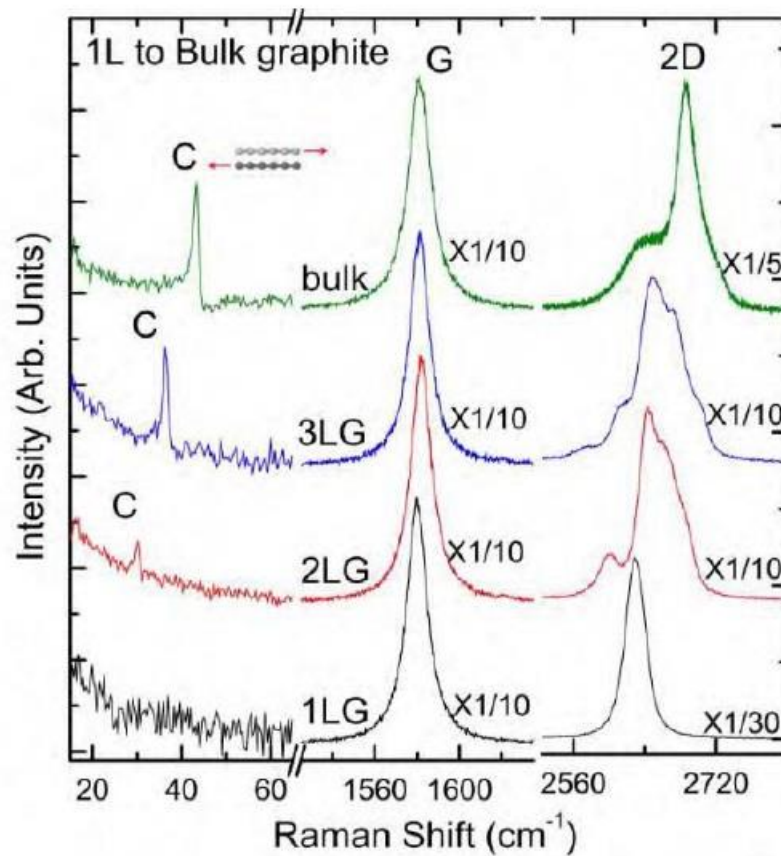


Figure 3.18 Stacking of Raman spectra describing the change in shape and intensity of the G' peak with increasing number of layers of graphene. [17]

Figure 3.19 provides an example of Raman Spectroscopy result obtained for graphene on a copper substrate, before the transfer process on the biosensor substrate. The two characteristic peaks G and G' are present, and the ratio of their intensities confirms the one-layer nature of the graphene. The presence of a peak at 1137 cm⁻¹ indicates, on the other hand, the presence of some defects of the CVD layer.

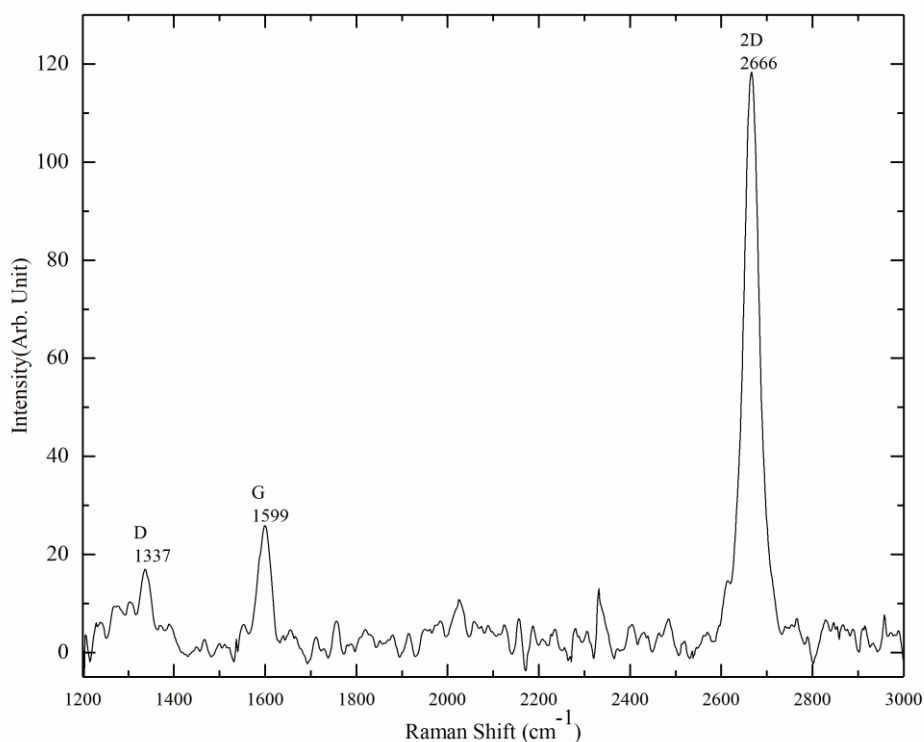


Figure 3.19 Raman spectrum of CVD-grown graphene on a copper substrate.

After the transfer process, a second characterization is done to check the quality of the transfer process. The outcome, shown in Figure 3.20, confirms the presence of a layer of graphene on the substrate, as proven by the presence and intensity of the two graphene main peaks. Although, other lower peaks at different wavelengths, typical of parylene (see Figure 3.21), indicate instead the presence of defects and unhomogeneity in the graphene layer. Unluckily, such variations of the quality of graphene depends on the technique adopted: while common and wide-spread, the transfer technique, mostly manual, implicates the chance of creating some defects in the very delicate layer.

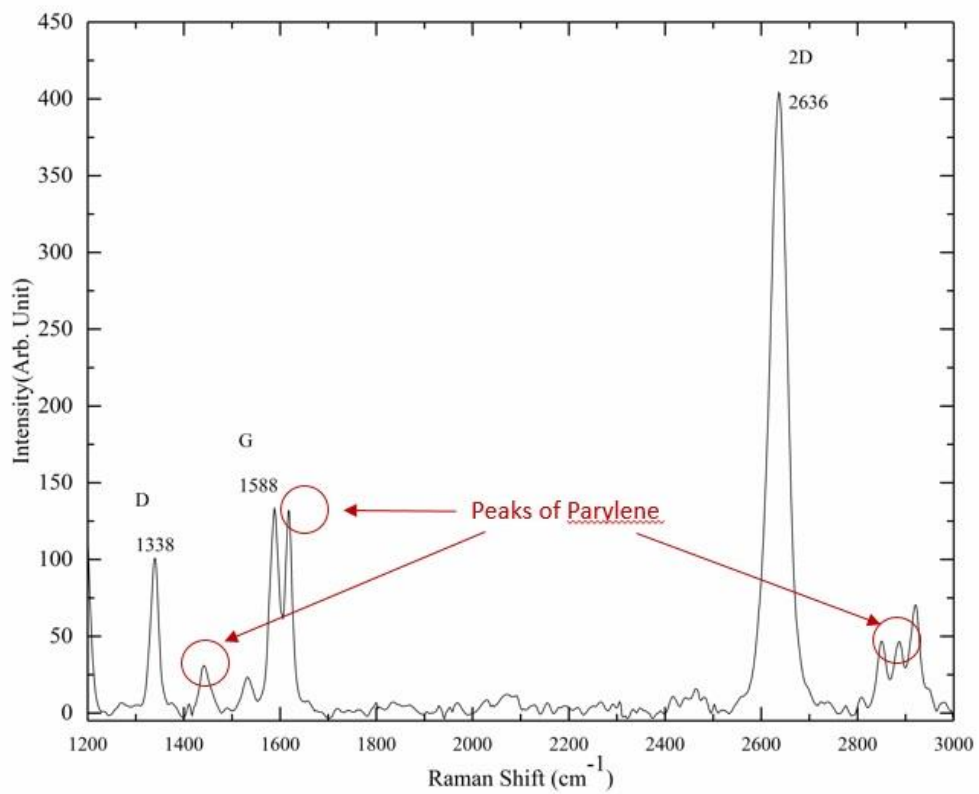


Figure 3.20 Raman spectrum of CVD-grown graphene on parylene.

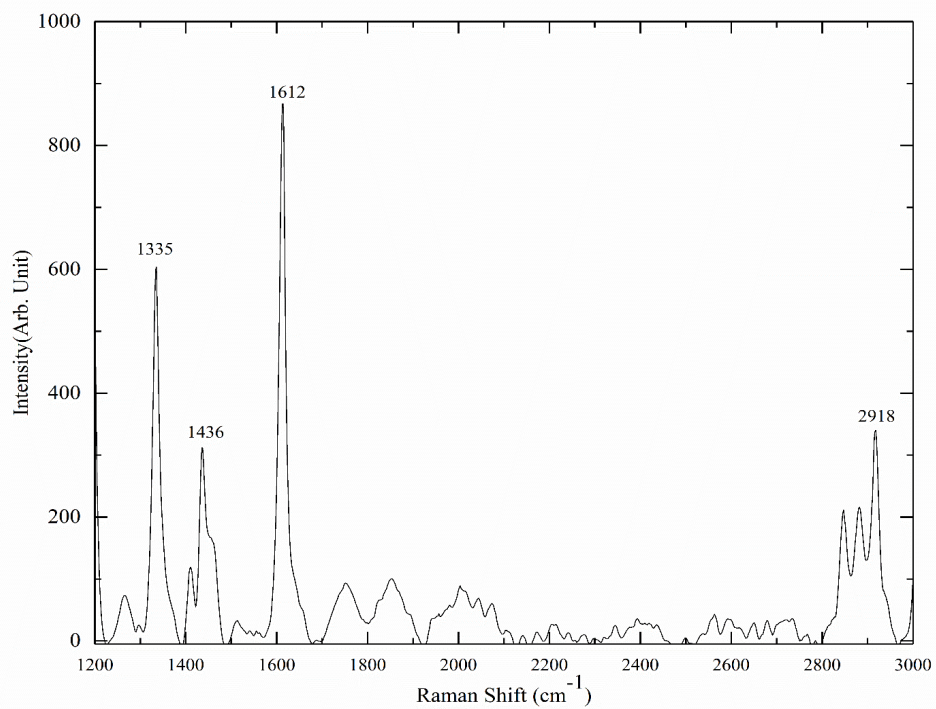


Figure 3.21 Raman spectrum of parylene.

3.3.2 R- V_G characteristics

In practice, every device contains two sensing circuits, coupled on the same substrate, referred to as Channel 1 and Channel 2 (see Figure 3.22).

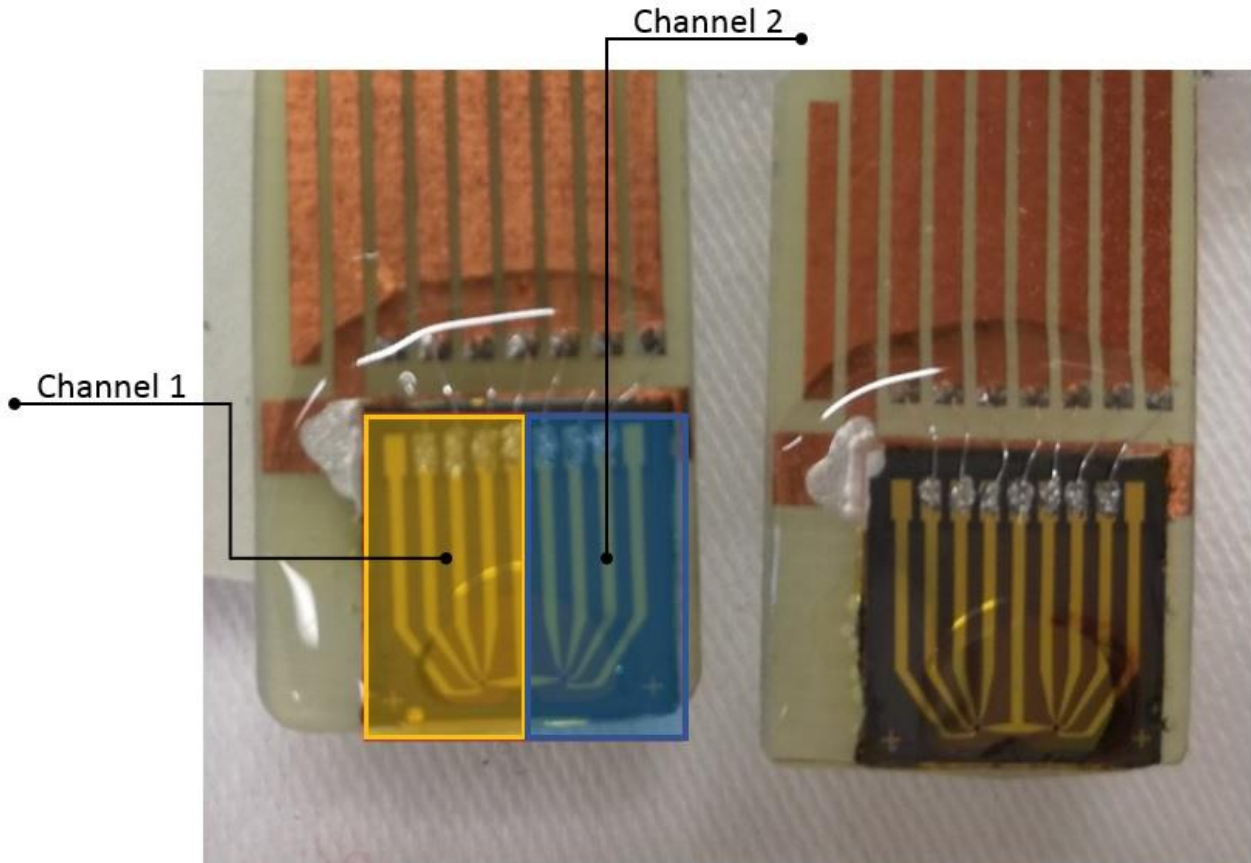


Figure 3.22 The picture shows the real structure of the biosensor: on the right, the sensing device as it appears at the end of the fabrication process, on the left two rectangles enclose and highlight the two channels present on the sensor.

In this way, the same sensor allows the testing on two different circuits, and such duplication permits the cross-check of the final results, for different behaviors in the outcome graphs would underline a malfunction in the experiment. Moreover, the presence of more than one detecting circuit increases statistically the number of times the biosensor can be reused, and thus writes off production costs. R- V_G characteristics are used to check the proper functioning of the two channels of the biosensor, and a couple examples of the test results are provided in Figure 3.23.

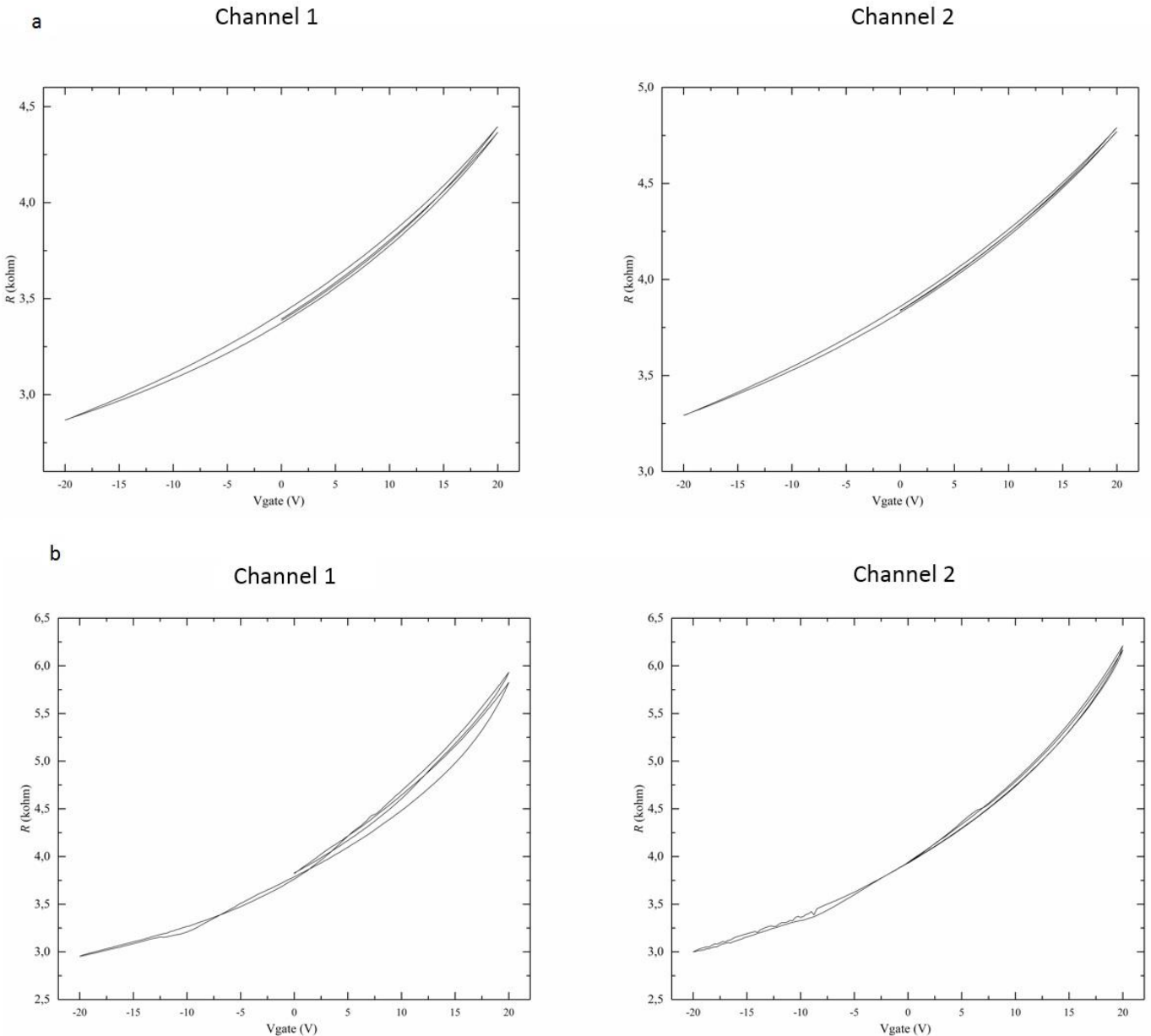


Figure 3.23 Representative Resistance (R) vs Gate Voltage (V) characteristics of two biosensors produced, *a* and *b*, for both the channels present on the device.

If compared to the Resistance vs Voltage Gate characteristics expected from theory (see Figure 2.24), where the point of maximum resistance should be found around 0V, it is possible to observe how, for the biosensor produced, the Dirac point does not correspond to any of the tested voltages. This would imply the presence of defects on the graphene surface which alter its R - V_G curve, shifting it to the right with respect to its normal position. In general terms, then, the biosensor will not be used around its most sensitive points, and the currents of the circuit may be higher than what expected theoretically and sustainable by the device. The second row of Figure 3.23 underlines also the presence of a slight hysteresis during the charge and discharge process, that

confirms how the single manufacturing of each device implies an unavoidable dispersibility in terms of quality of the final device.

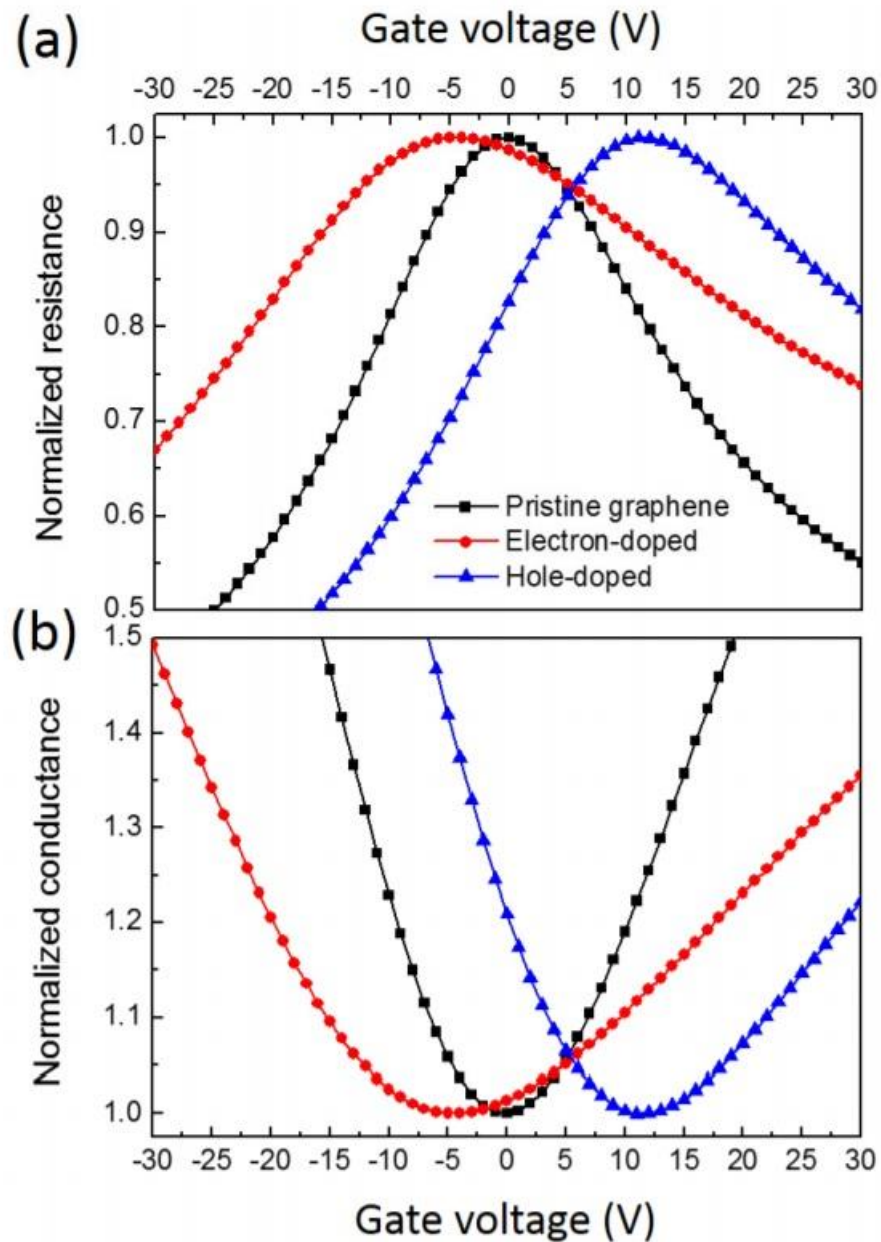


Figure 3.24 Characteristic Resistance vs Gate voltage (a) and Conductance vs Gate Voltage (b) of a standard G-FET [modified from 120].

3.4 Set-up

Once the proper functioning of the single biosensor is adequately tested, the device can be used for the bacterial growth testing.

First, a six well plate is placed inside an incubator with constant temperature maintained at 37°C, temperature needed by bacteria to grow and replicate. The plastic cover of the well-plate is discarded and substituted with a layer of aluminum foil covering the plate to avoid evaporation of the liquid and any possible contamination. In said aluminum foil a

small window, a little bigger than the lateral dimensions of the biosensor, is created (see Figure 3.25).

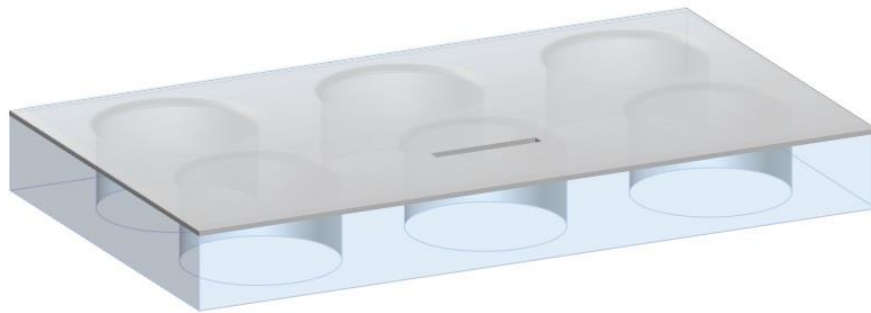


Figure 3.25 Six-well plate (in light blue) covered with aluminum foil (in grey), in which a small window is created to allow the passage of the device for the dipping in solution.

This opening will allow the dipping of the biosensor in the solution contained in one of the wells, while the coverage of the rest of the plate will avoid evaporation of the solution, thus maintaining the volume of media for the bacterial growth constant.

The device is plugged into a socket, like a USB drive would be plugged in a normal computer (see Figure 3.26). This way, the measurement circuit is then closed, and the biosensor connected to both the generator and the measuring device, as shown in Figure 3.27.

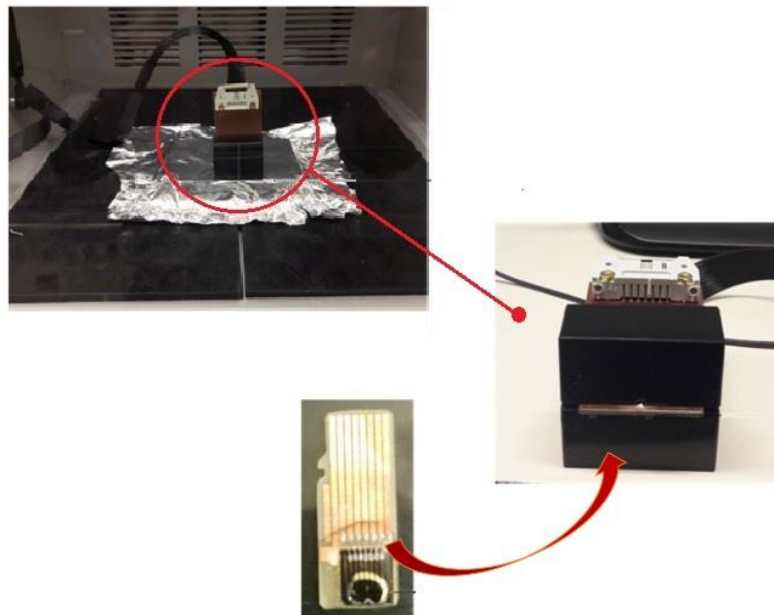


Figure 3.26 In the higher image the normal set-up for the experiment is shown. The Socket in which the biosensor is plugged in like a USB drive is shown on the right side.

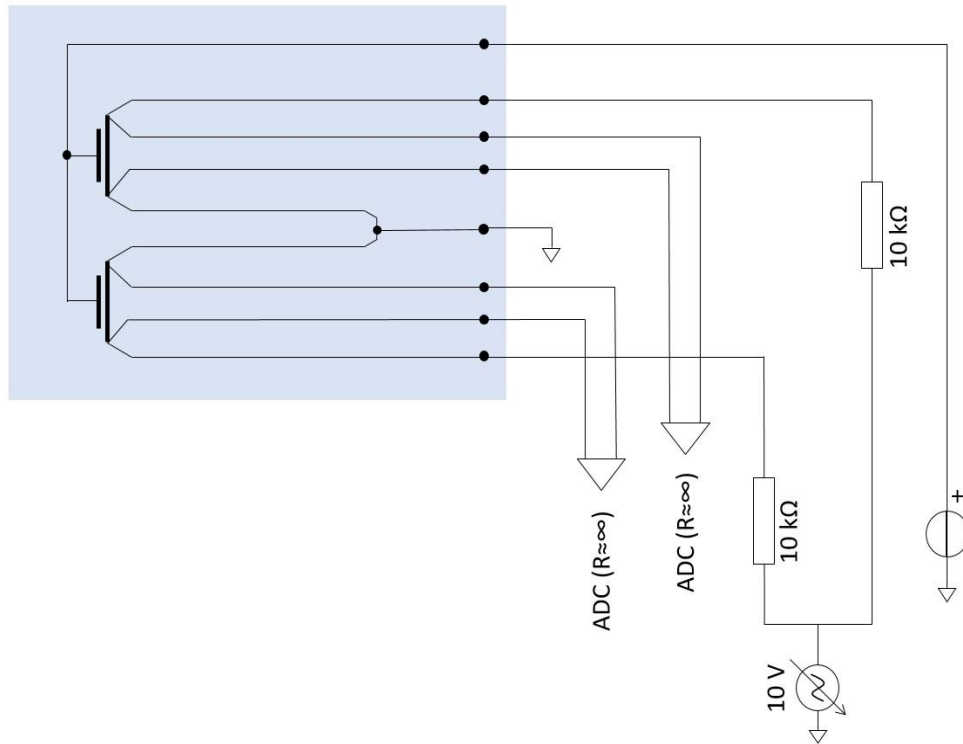


Figure 3.27 The circuit of the biosensor. The blue shaded area shows the circuit part on the biosensor.

An input voltage of 10V is used for the circuit (see Section 3.1 *The working principle*), and the measurement started so to sample the value of resistance every 30 seconds for the entire experiment.

For the first five minutes of the recorded measurements, the biosensor is kept outside the bacterial solution, at room temperature, to have a reference value of the initial resistance of the device prior the dipping into the solution. This initial resistance remains consistent during these five minutes.

The device is then carefully dipped in 12 ml of bacterial solution through the small window in the aluminum foil, making sure the exposed graphene area is entirely dipped in the bacterial solution.

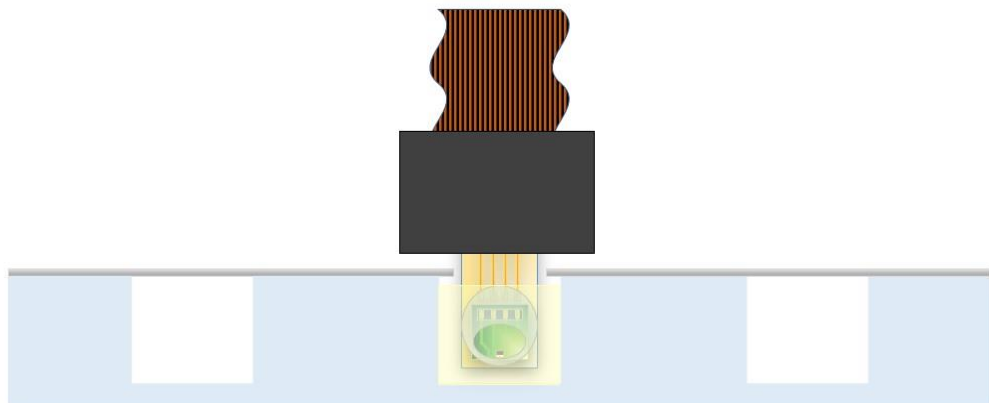


Figure 3.28 2D representation of the dipping process of the biosensor, required for the bacterial solution testing.

Following the dipping, which will be easily spotted on the final plots of resistance versus time because of a sudden change in resistance, the biosensor is kept in bacterial solution for 5 hours, considered to be an adequate time for the bacteria to grow and form a biofilm on the graphene.

After five hours, 120 μl of antibiotic, specifically 200 $\mu\text{g}/\text{ml}$ of ciprofloxacin, are added to the solution, without the extraction nor movement of the said biosensor, in order to kill the bacteria and stop their replication. In this case, the addition of a certain amount of antibiotic will create turbulence in the liquid, leading to a temporary perturbation that will show up quite clearly in the final graphs.

The quantity and concentration of the antibiotic was appropriately chosen so to guarantee the complete suppression of bacteria in solution [121]. The monitoring continues for other 3 hours, after which the measurement is stopped.

3.5 Bacterial colonization

3.5.1 Gram-positive and Gram-negative bacteria

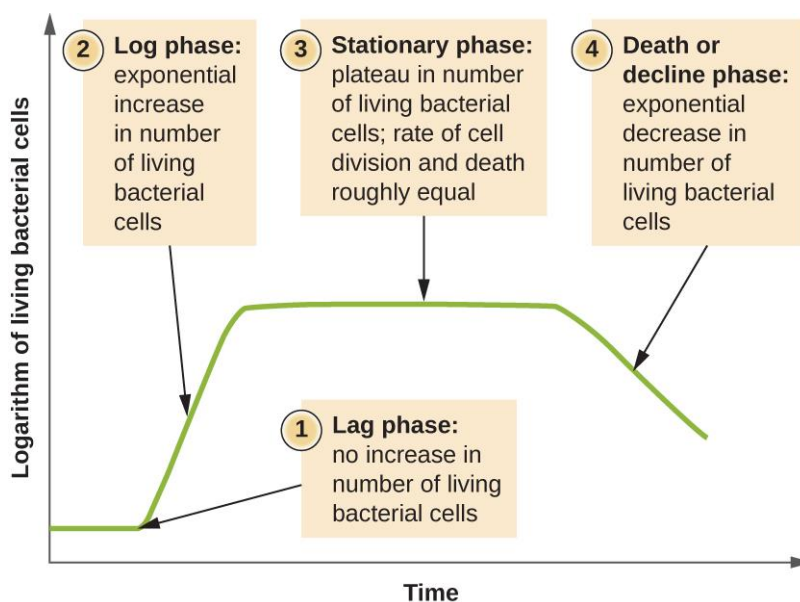


Figure 3.29 Typical bacterial growth curve. [122]

Bacteria are single-celled organisms with dimensions in the range of microns. Such cells replicate through binary fission to form two daughter cells that share the same genetic material as the parent cell, and the number of colonies over time follows a specific trend well represented in Figure 3.29.

The cell wall located on the outer layer of the bacteria, mainly composed of peptidoglycans, or mureins, provides the cell mechanical support and protection against stress or damage induced by osmotic pressure. Despite this similarity, not all bacterial cell walls are made up and organized in the same way, and such differences in the outer layers (see Figure 3.30) allow a generic division in two bacterial subgroups: according to a specific staining process, known as Gram staining, bacteria can in fact be divided into Gram-positive and Gram-negative bacteria thanks to the difference in chemical and physical properties of the cell wall.

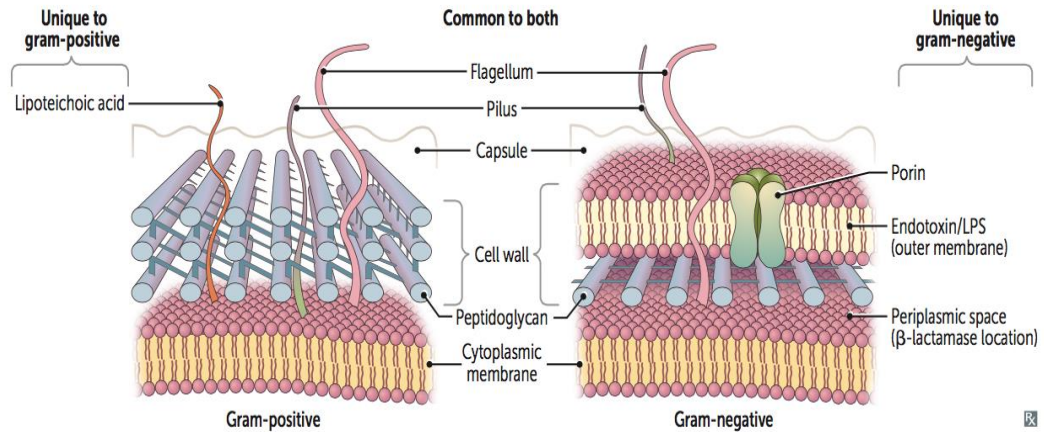


Figure 3.30 Representation of the outer membrane structures of gram-positive (on the left) and gram-negative (on the right) bacteria.

Summarily, the Gram staining process, graphically illustrated in Figure 3.31, consists of four steps:

- The bacterial culture is heat-fixed on the substrate, and the Crystal Violet dye is applied. The dying compound dissociates, in aqueous solutions, into two ions: CV^+ and Cl^- . The ions can thus penetrate through both the cell wall and cell membrane of both gram-positive and gram-negative cells: the interaction of CV^+ with negatively charged components of bacterial cells results in the purple staining of the cells.
- Addition of iodide, that interacts with CV^+ to form complexes of crystal violet and iodine ($CV-I$) in between the inner and outer layers of the cell that cannot be removed in the following steps, and thus maintain the coloring.
- Alcohol wash, which decolorizes the cells by interacting with their membrane. In case of a Gram-negative cell, the $CV-I$ complexes are washed away because of the loss of the outer membrane. For what concerns the Gram-positives, cells become dehydrated and the complexes are trapped in the cell.
- A final counterstaining, safranin, is used to color the gram-negative bacterial cells.

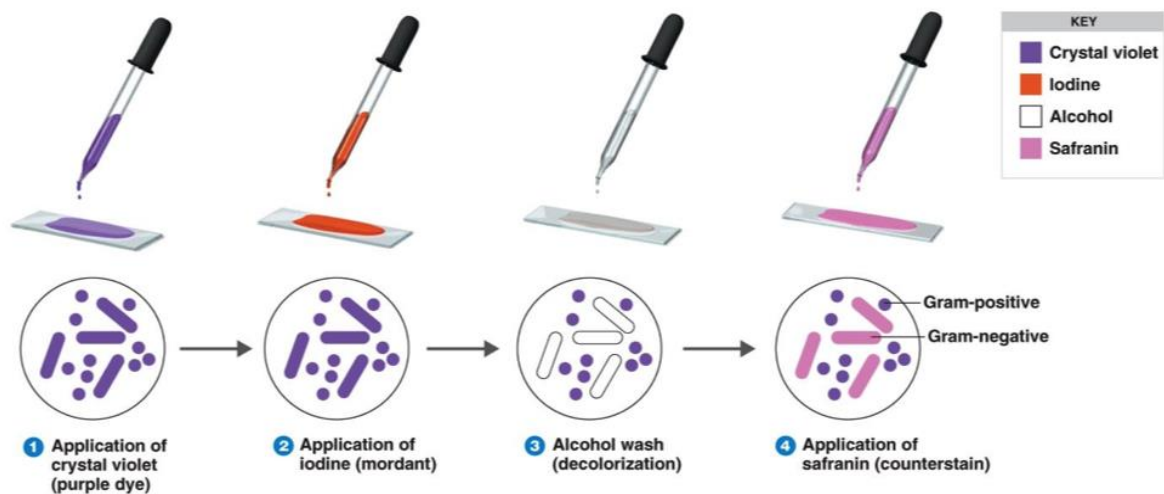


Figure 3.31 Schematic chart describing the steps of Gram staining process. [124]

In Gram-negative bacteria, the cell wall has a thickness of around 10 nanometers and is surrounded by a thin, single layer of peptidoglycans and another external membrane, known as outer membrane, made up of lipopolysaccharides, proteins and phospholipids. Sandwiched in between these layers there is the periplasm, a gel-like matrix containing numerous biological compounds necessary to the cell sustenance. The structure is well exemplified in the picture below.

For what concerns Gram-positive bacteria, in this case the cell wall is between 15 and 80 nm thick and is made up of multiple layers of peptidoglycan, with no presence of any outer membrane (see Figure 3.32). Specific of this subgroup is the presence of teichoic acids, linear polymers directed outward perpendicularly to the wall, which grant the cell walls a negative charge; the role of these acids is supposedly to anchor to the substrate, generally through a chelation reaction.

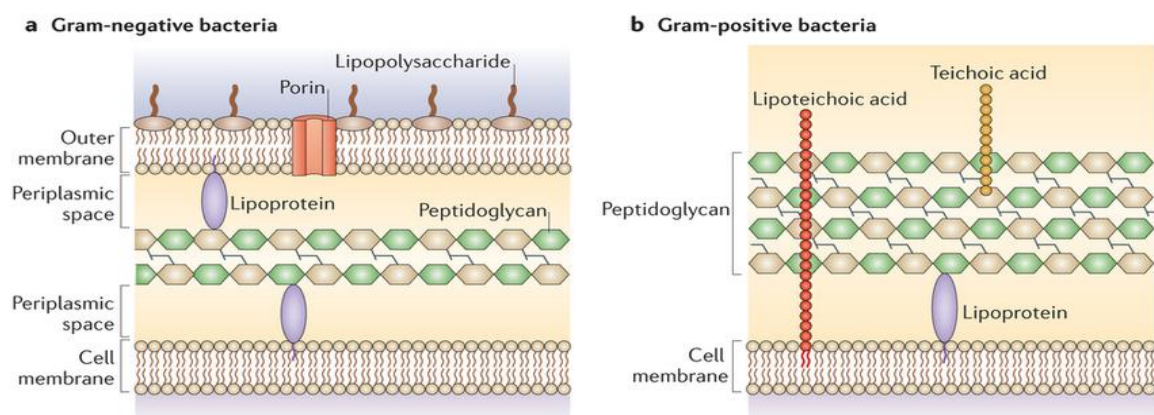


Figure 3.32 2D overview of the differences in composition and structure of gram-negative (on the left) and gram-positive (on the right) bacteria. [125]

3.5.2 Biofilm formation

Bacteria, like the ones used in our experiments, are the cause of the most common diseases, because of the outbreak of the infection caused by their colonization and replication inside the human body, that triggers the immune system and the inflammatory response and causes pain in the patient.

The bacterial colonization process, illustrated in Figure 3.33, is made up of four stages:

1. *Attachment to a surface*: The free-floating bacteria, in planktonic state, land on the surface and adhere through weak interactions such as Van Der Waals forces and hydrophobic effects.
2. *Formation of micro-colony*: The weak bonds are then stabilized and more bacteria adhere to the surface through cell adhesion structures, thus starting the colonization. At this stage the secretion of an external, gluy matrix made mainly of polysaccharides begins: it's the extracellular matrix, that encloses and protects the bacterial biofilm.
3. *Formation of a 3D structure*: the bacteria keep replicating and secrete the extracellular matrix, increasing the layers of the biofilm. The matrix formation is followed by water-filled channels for the transport of of nutrients within the biofilm.
4. *Maturation*: the bacterial biofilm reaches its moment of largest extension, with a typical fungus-shape.

5. *Detachment*: through a natural pattern of programmed detachment, some bacteria leave from the biofilm and return to a planktonic state for new colonization process.

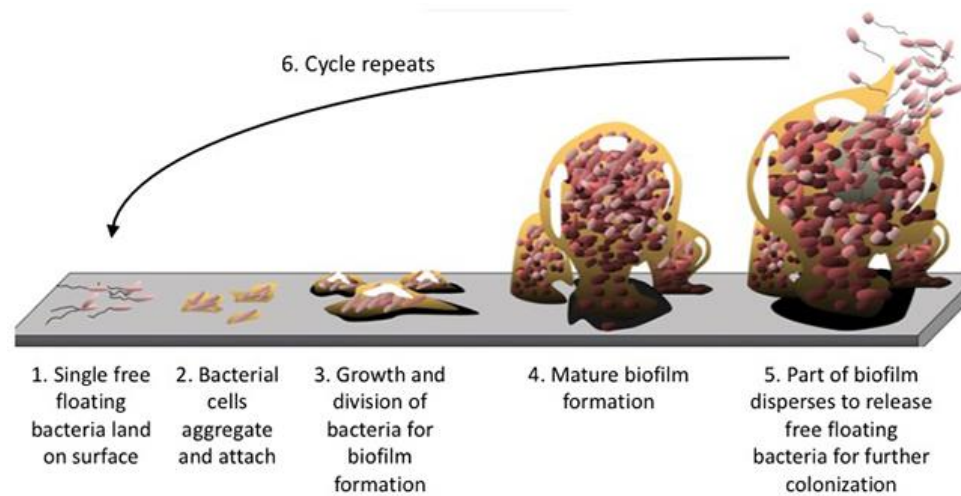


Figure 3.33 Stages of the bacterial colonization process. [126]

Interestingly, the ability to recognize a surface and colonize it is different between non-motile bacteria and motile bacteria.

3.6 Single bacteria test

As previewed, the aim of this experiment is, first, to univocally identify which kind of bacteria is growing in the solution and thus if it is possible or not to define, and thus forecast, a recurring shape in the obtained resistance vs time plot.

Summing up what described in more detail in section 3.4, the biosensor is first inserted into a socket to close the circuit and provide the necessary voltage, then dipped in 12 ml of solution, always inside an incubator maintained at 37°C. The biosensor solution is prepared as follows:

- 6 ml of sterilized de-ionized water;
- 6 ml of LB media;
- 20 µl of bacterial solution.

Bacterial solution is obtained by inoculation of two colonies of bacteria in 6 ml of media, where the media chosen is the most appropriate for the bacterial growth.

Each experiment lasts a total of 8 hours, where the values of resistance of the device are sampled every 30 seconds: for the first five hours the experiment runs normally, and the variation of resistance over time is impacted by the replication of bacteria and possible formation of a biofilm. After 5 hours, 120 µl of antibiotic are added to evaluate the impact of such addition on the bacterial replication and biofilm formation.

As examined more in depth in Section 3.5 *Biofilm formation*, the cell wall of bacteria might be a relevant variable in terms of interaction with the graphene layer. Consequently, two different kinds of bacteria were tested: gram-positive and gram-negative bacteria, that would allow to conclude if the bacterial cell wall might, in fact, univocally impact the result

of the resistance vs time plot, or if there are similarities in the results produced by bacteria belonging to the same one of these categories.

In particular, 2 types of bacteria for each of the above mentioned subgroups were tested: in this way it is possible to compare not only gram+/- bacteria, but also different kinds of bacteria belonging to one of these categories, and then underline similarities and differences in trends within bacteria of the same gram type.

Specifically, four bacteria were tested:

- Pseudomonas Aeruginosa
- Staphylococcus Epidermidis
- Escherichia Coli
- Staphylococcus Aureus

To allow the re-use of the single device, after every test the biosensor was rapidly stirred in 70% ethanol (EtOH), to kill all the bacteria present on the surface. The cleaning process required then the immersion of the chip in boiling water, to assure the kill of bacteria and favor the spontaneous detachment of the formed biofilm, then a rapid stirring in de-ionized water and blow-drying with nitrogen.

3.6.1 P. aeruginosa

3.6.1.1 Resistance vs time curve

Here the results of the R-time curves are plotted:

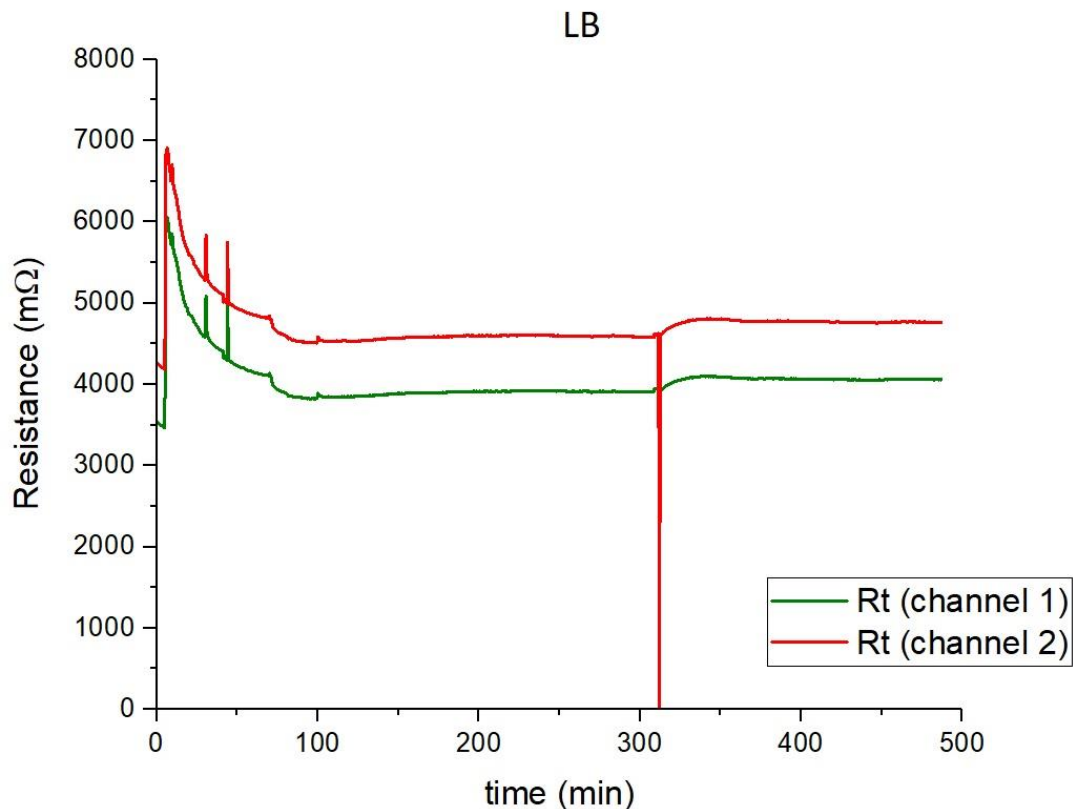


Figure 3.34 Resistance vs time plot for LB media.

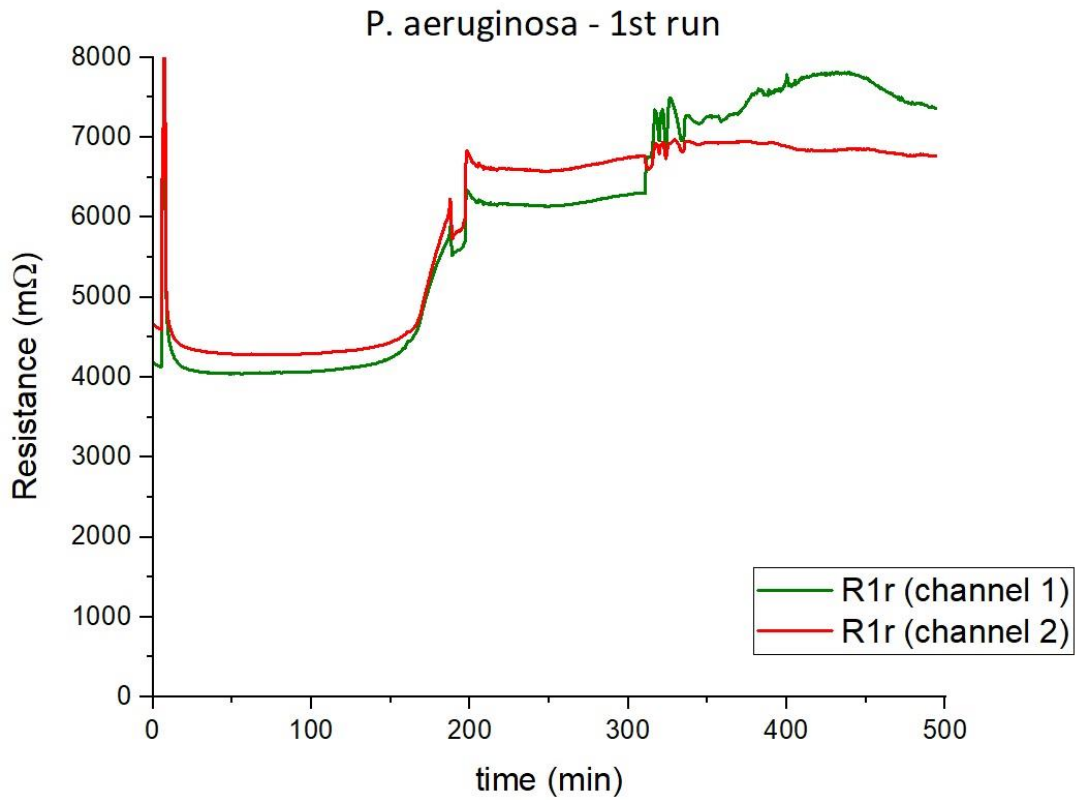


Figure 3.35 Resistance vs time plot for biosensor solution containing 20 μ l of bacterial solution with *Pseudomonas Aeruginosa* (1st run).

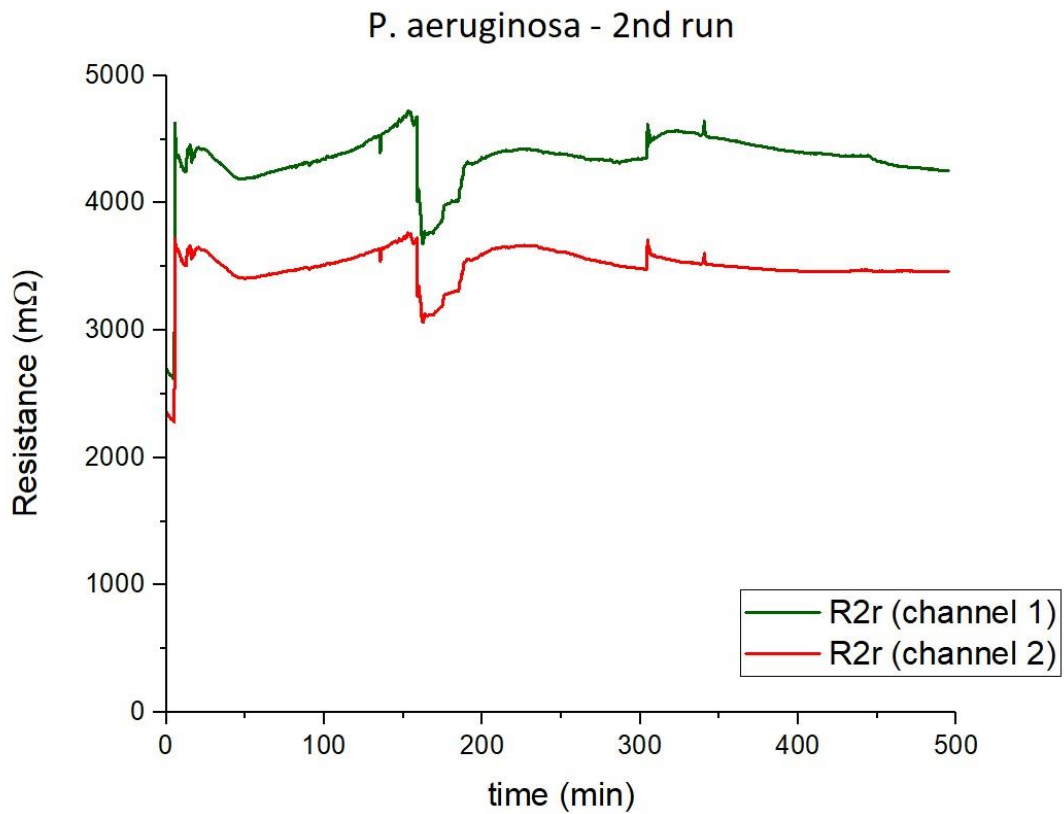


Figure 3.36 Resistance vs time plot for biosensor solution containing 20 μ l of bacterial solution with *Pseudomonas Aeruginosa* (2nd run).

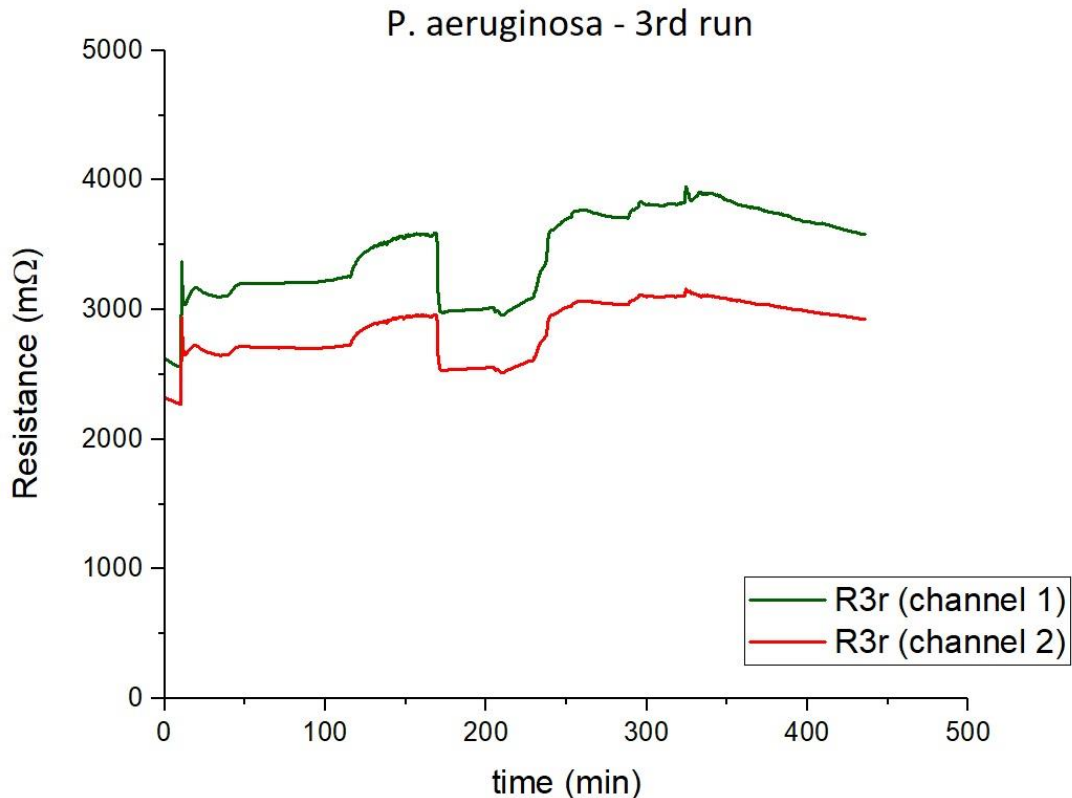


Figure 3.37 Resistance vs time plot for biosensor solution containing 20 μ l of bacterial solution with *Pseudomonas Aeruginosa* (3rd run).

3.6.1.2 Colony count

Independently from the outcome of the biosensor tests between different kinds of bacteria, it would be useful to be able to relate some trends in the curve to known variables, like the bacterial cell wall. For this reason, knowing the colony forming units (CFU) at different time intervals in the solution would first allow to confirm a normal behavior and replication of the cells, and secondly offer data that might explain some trends in the resistance vs time curves.

Colony counting is a common procedure in microbiology: definite amount of bacterial solution are plated in Agar plates in different dilutions, so to obtain single colonies on the plate, easily countable. The number of colonies in the plate, relatable to the number of colonies in the original solution, gives indications on the stage and quantity of bacterial growth.

To evaluate the number of colonies formed by the bacteria in solution, a solution similar to the one used for the biosensor was prepared:

- 6 ml of sterilized distilled water
- 6 ml of LB media
- 20 μ l of bacterial solution, obtained by the inoculation of two colonies of the bacteria in 6ml of media.

The plating of such solution would, although, deliver results impossible to interpret for the too high amount of CFUs. From this starting solution, progressive dilutions are thus obtained using:

- 900 μ l of buffer saline solution (0.9% NaCl)
- 100 μ l of biosensor solution

At stage one, 100 μL of the biosensor solution added to a 1,5ml Eppendorf tube containing 900 μL of buffer solution and the tube vortexed in order to homogenize the distribution of bacteria. The solution thus obtained was diluted ten times compared to the biosensor one. Then 100 μL can be drawn to be added to a second Eppendorf tube to obtain higher dilutions, as shown in Figure 3.38.

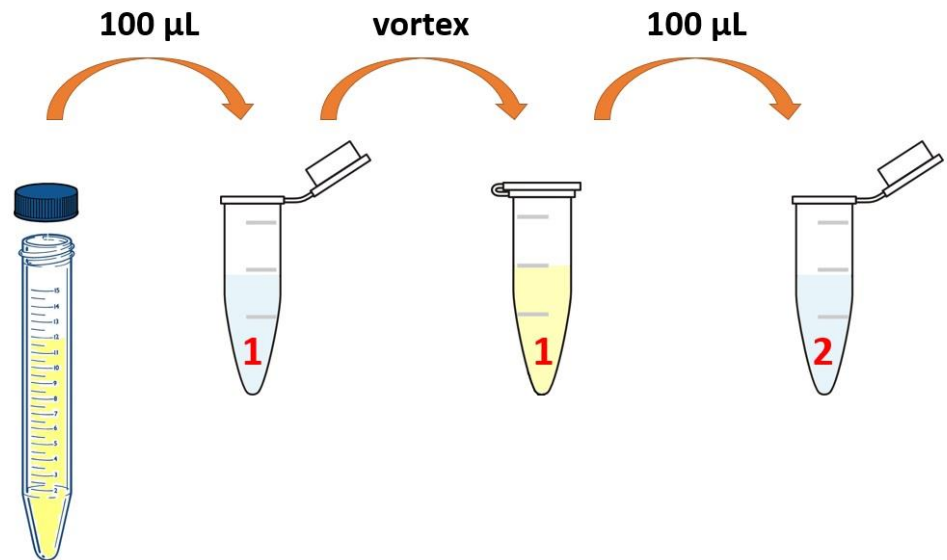


Figure 3.38 Figurative description of progressive dilutions.

The same procedure can be repeated for serial dilutions. If at step 1 the original solution is diluted ten times, it follows that for any further step the corresponding bacterial concentration will be $1/(10^{(\# \text{ dilution}))}$. Once dilutions were prepared, 100 μL of solution #2 and #3 were plated in Agar plates and incubated at 37°C overnight, to let the bacteria grow. Such Agar plates are labeled according to the time they were plated and the dilution used, so for example “0h, #2” indicates the plating of dilution 2 at time 0. An example of the solutions plated, their labels and compositions at time 0 is provided in Table 3.1.

Table 3.1 The table describes the dilutions prepared at time 0, with specific attention to their label (first column), their composition (second column) and their dilution with respect to the biosensor solution used for the testing (last column).

Label of dilution	Composition	Dilution [wrt biosensor solution]
#0	biosensor solution	-
0h, #1	<ul style="list-style-type: none"> 900 μL of buffer saline solution (0.9% NaCl) 	1/10

	<ul style="list-style-type: none"> • 100 µl of biosensor solution 	
0h, #2	<ul style="list-style-type: none"> • 900 µl of buffer saline solution (0.9% NaCl) • 100 µl of dilution #1 	1/100
0h, #3	<ul style="list-style-type: none"> • 900 µl of buffer saline solution (0.9% NaCl) • 100 µl of dilution #2 	1/1000

The biosensor solution was placed back in the 37°C incubator, without any rotation of the base: this way, the solution remains at 37°C for the same amount of time as the solution used for the biosensor testing, thus allowing an analogous growth of bacteria.

The procedure described above was repeated every hour, and every time 100 µL were sampled from the centrifuge tube to start the process. The plating was done every 60 minutes, for 8 hours, the same amount of time considered to monitor the growth of bacteria solution for the biosensor.

For each hour, the dilution process remained the same but generally the number of dilutions needed for plating may vary. In fact, following a normal growth curve of a bacteria of any kind (see Section 3.5 *Bacterial colonization*), the first 2-3 hours are characterized by a low rate of replication: the lower dilutions still allow an efficient plating, because the number of colonies present on the plate after incubation is countable and univocal. After that time, the multiplication of bacteria follows an exponential trend, and higher dilutions are needed for plating: lower dilutions, in fact, would result in too many colonies on a plate to allow proper counting.

Exactly as it happens in the case of the biosensor solution, 120 µl of antibiotic were added after 5h to the original solution, so to replicate the same conditions of the biosensor. An overview of the dilutions plated for each other is shown in Table 3.2.

Table 3.2 Overview of the biosensor solution dilutions prepared and plated every hour for colonies counting.

time	# dilutions prepared	dilutions plated
0 h	1,2,3,4	3,4
1 h	1,2,3,4	3,4
2 h	1,2,3,4	4,5
3 h	1,2,3,4,5	4,5
4 h	1,2,3,4,5,6	5,6
5 h	1,2,3,4,5,6	5,6
Addition of 120 µl of ciprofloxacin		
6 h	1,2,3	2,3
7 h	1,2	1,2
8 h	1,2	1,2

After around 20 hours of incubation at 37°C, colonies were counted on every Agar plate, and the labels and CFUs noted down, as shown in Table 3.3. If, for example, at time 1h and dilution 4 the number of colonies are 44, like in Table 3.3, then it means that to obtain the number of colonies in the original biosensor solution the number of colonies written down should be multiplied for the dilution with respect to the biosensor solution. More specifically:

$$\begin{aligned} & \# \text{ of colonies in diluted solution at a given time} \\ & * \text{ dilutions with respect to the biosensor solution} \\ & = \# \text{ of colonies in the biosensor solution at a given time} \\ & 44 * (10^4) = 440000 \text{ colonies in the biosensor solution} \end{aligned}$$

Table 3.3 Number of colonies (third column) counted for specific times (first column) and dilutions (second column).

time	dilution	# of colonies
0h	4	50
0h	5	1
1h	4	44
1h	5	3
2h	5	246
2h	6	187
3h	5	181
3h	6	15
4h	5	33
4h	6	1
5h	4	330
5h	5	36
5h	6	2
1h,a	3	0
1h,a	2	0
2h,a	1	0
2h, a	2	1
3h, a	1	0
3h, a	2	0

To attain further confirmation and higher reliability of the test outcomes, the plating was repeated in triplets and over multiple times, and the results obtained in the different colonies count were averaged to obtain a single final value.

In the case of Pseudomonas Aeruginosa, the number of colonies in solution are shown in Table 3.4.

Table 3.4 CFUs for biosensor solution containing 20 μ L of bacterial solution with *Pseudomonas Aeruginosa*.

Time (hours)	CFUs
0	1,42E+06
1	2,30E+06
2	9,00E+06
3	2,45E+07
4	3,48E+07
5	4,66E+07
1h, a	0
2h, a	0
3h, a	0

Results of the colony counting were eventually graphed in the histogram in Figure 3.39.

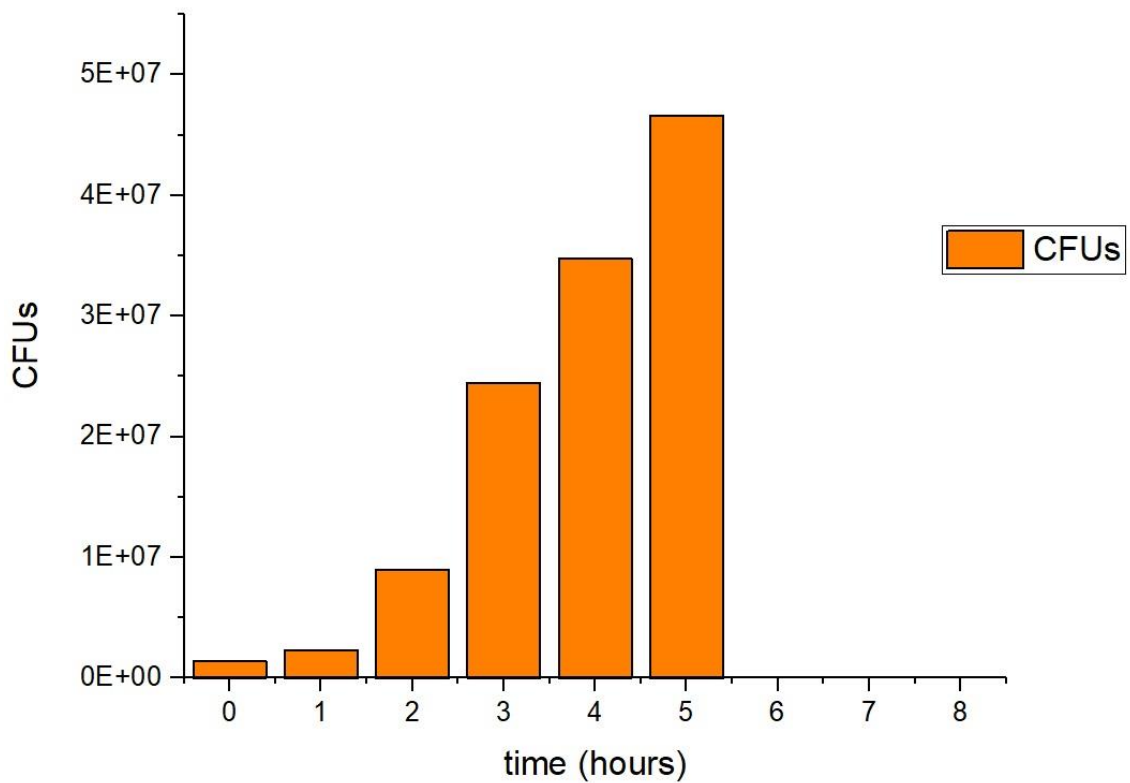


Figure 3.39 Average colony forming units vs time for biosensor solution containing 20 μ L of bacterial solution with *Pseudomonas Aeruginosa*.

3.6.2 Staphylococcus Epidermidis

3.6.2.1 Resistance vs time curve

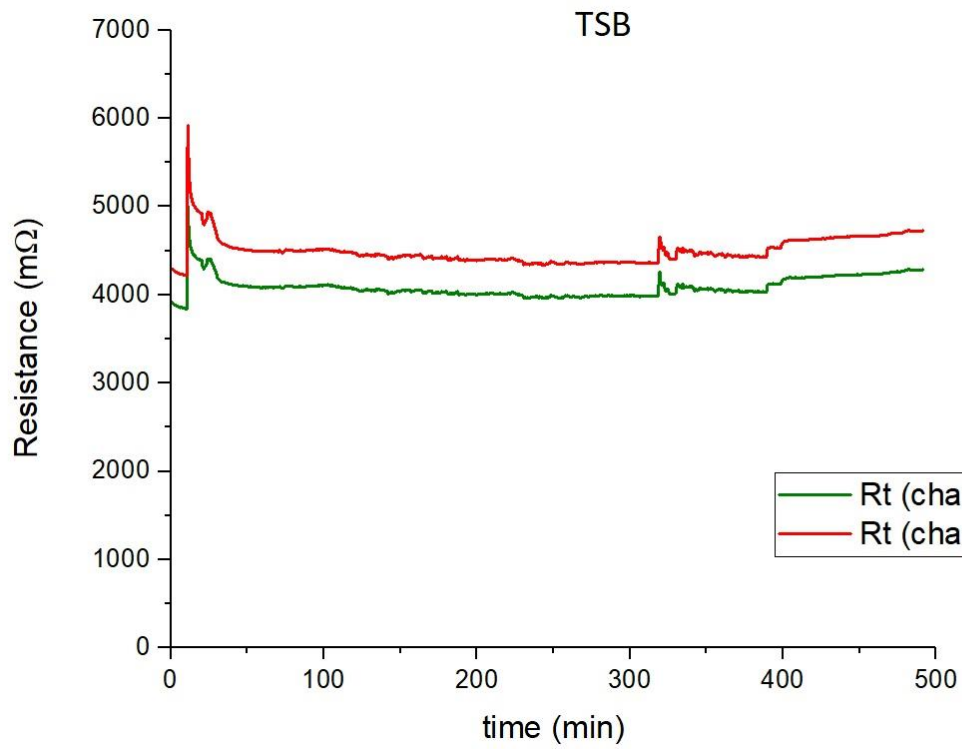


Figure 3.40 Resistance vs time plot for TSB media.

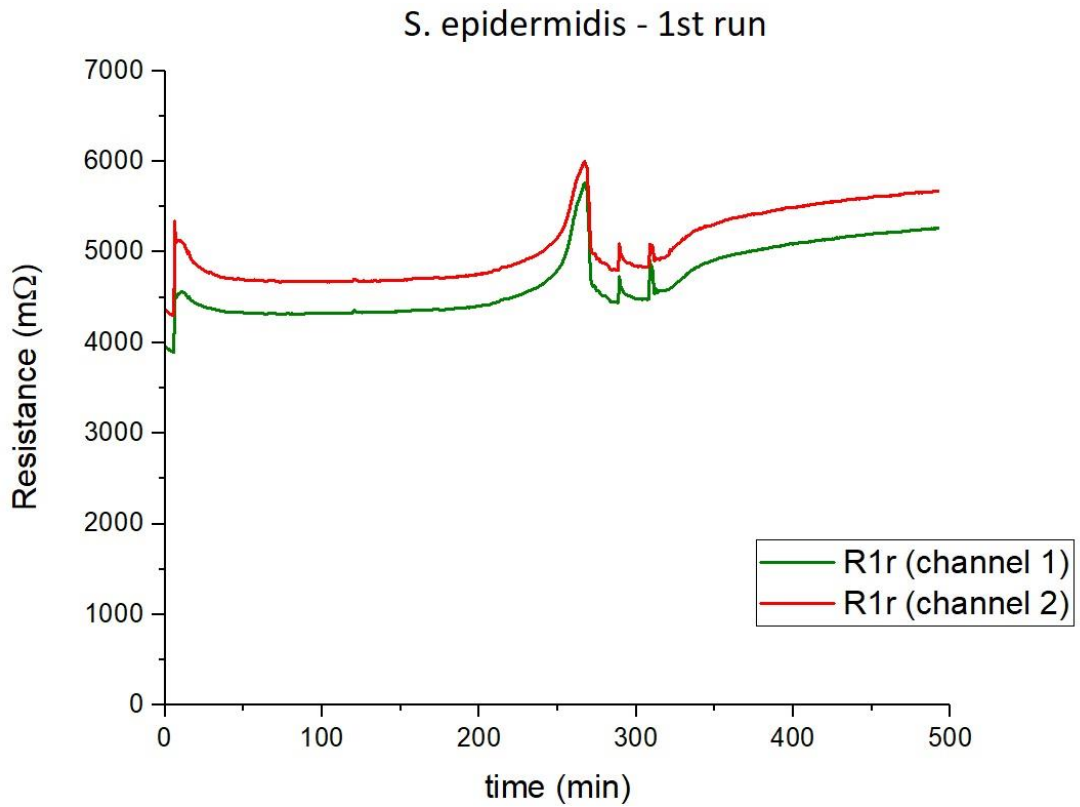


Figure 3.41 Resistance vs time plot for biosensor solution containing 20 µl of bacterial solution with Staphylococcus Epidermidis (1st run).

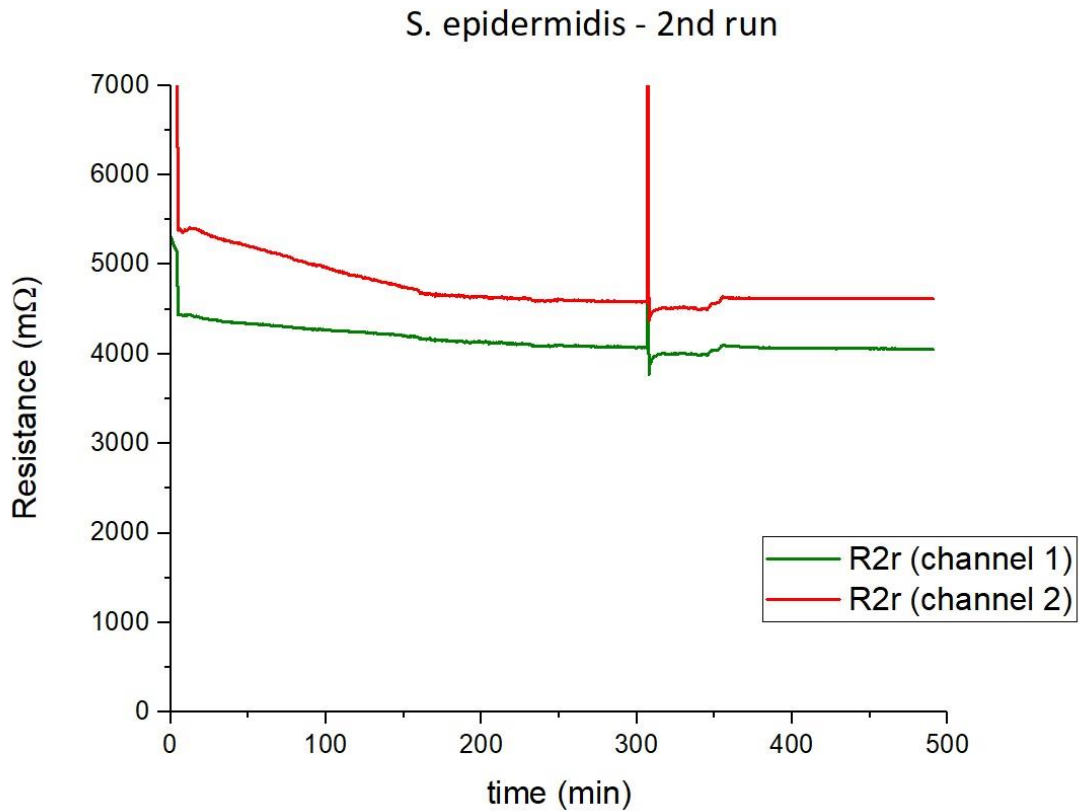


Figure 3.42 Resistance vs time plot for biosensor solution containing 20 μ l of bacterial solution with *Staphylococcus Epidermidis* (2nd run).

3.6.2.2 Colonies count

The colonies of *Staphylococcus Epidermidis* were counted and the results averaged as described in detail in Section 3.6.1.2. The final results are collected in Table 3.5 and represented in the histogram in Figure 3.43.

Table 3.5 CFUs for biosensor solution containing 20 μ l of bacterial solution with *Staphylococcus Epidermidis*.

Time (h)	CFUs
0	2,61E+04
1	3,54E+04
2	5,75E+04
3	2,73E+05
4	7,48E+05
5	1,56E+06
1h, a	0
2h, a	0
3h, a	0

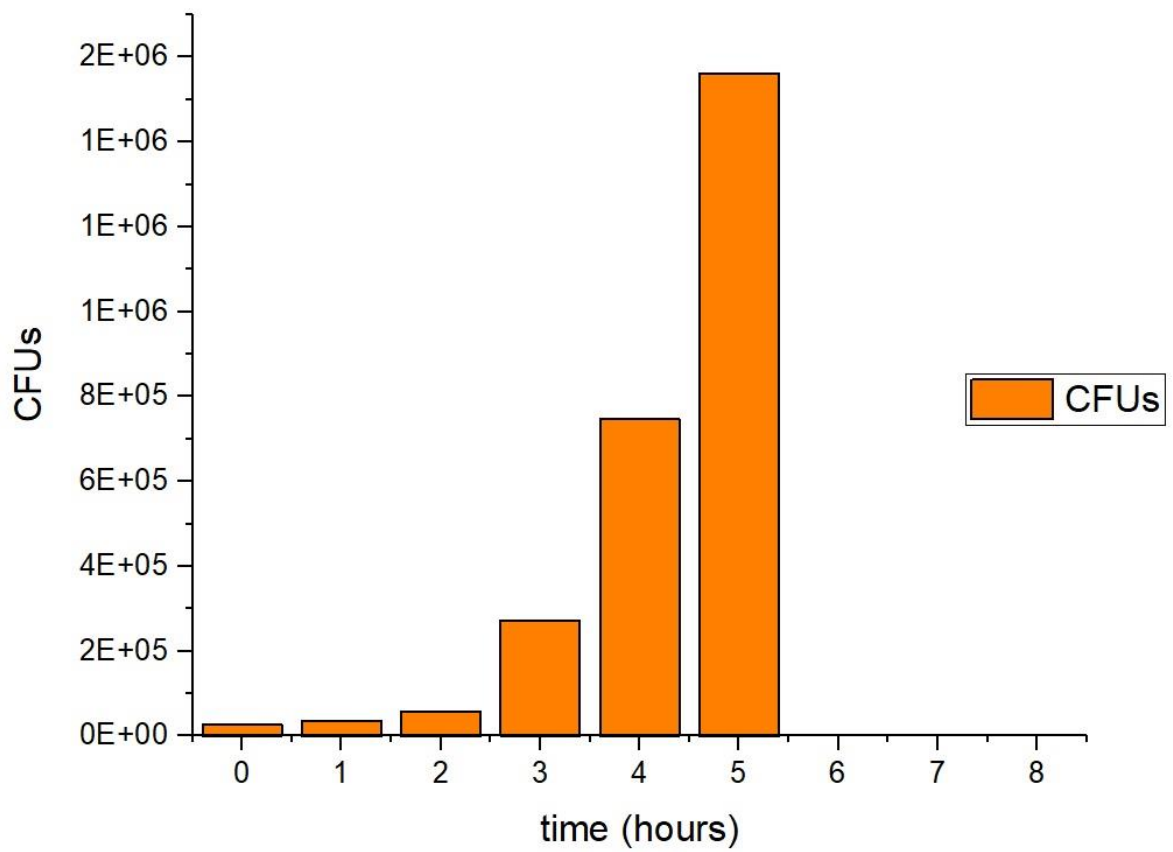


Figure 3.43 Average colony forming units vs time for biosensor solution containing 20 µl bacterial solution with Staphylococcus Epidermidis.

3.6.3 Escherichia coli

3.6.3.1 Resistance vs time curve

The outcomes of different runs on E.coli are represented in Figure 3.44, 3.45, 3.46, 3.47:

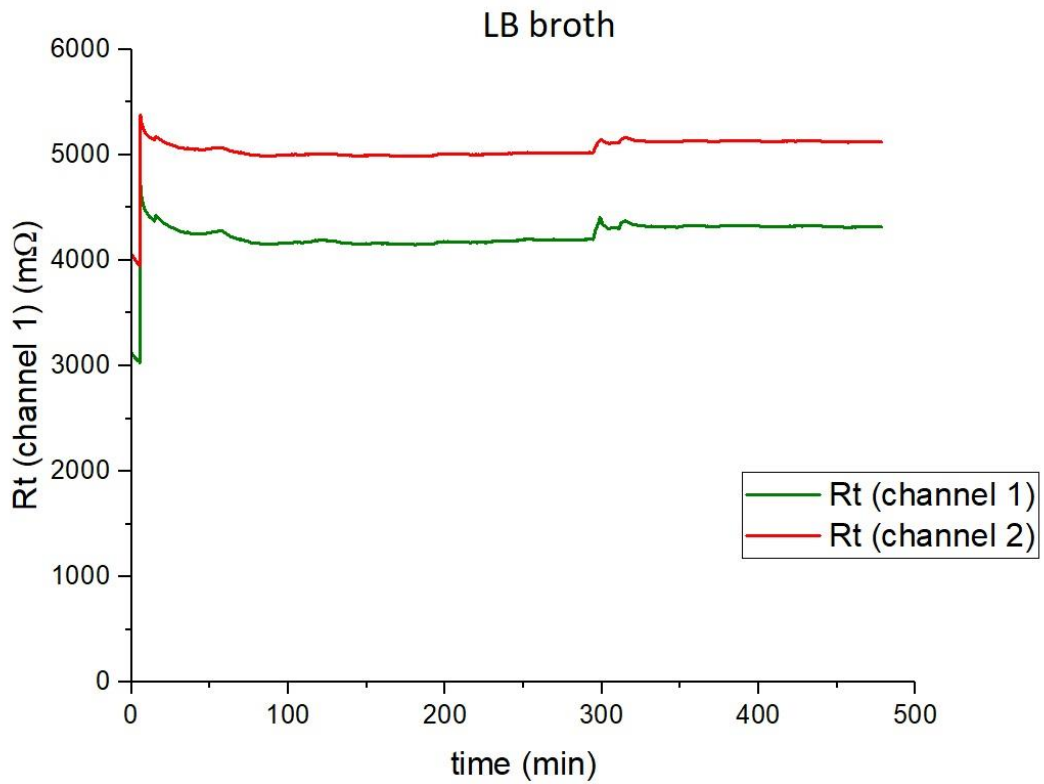


Figure 3.44 Resistance vs time plot for LB media.

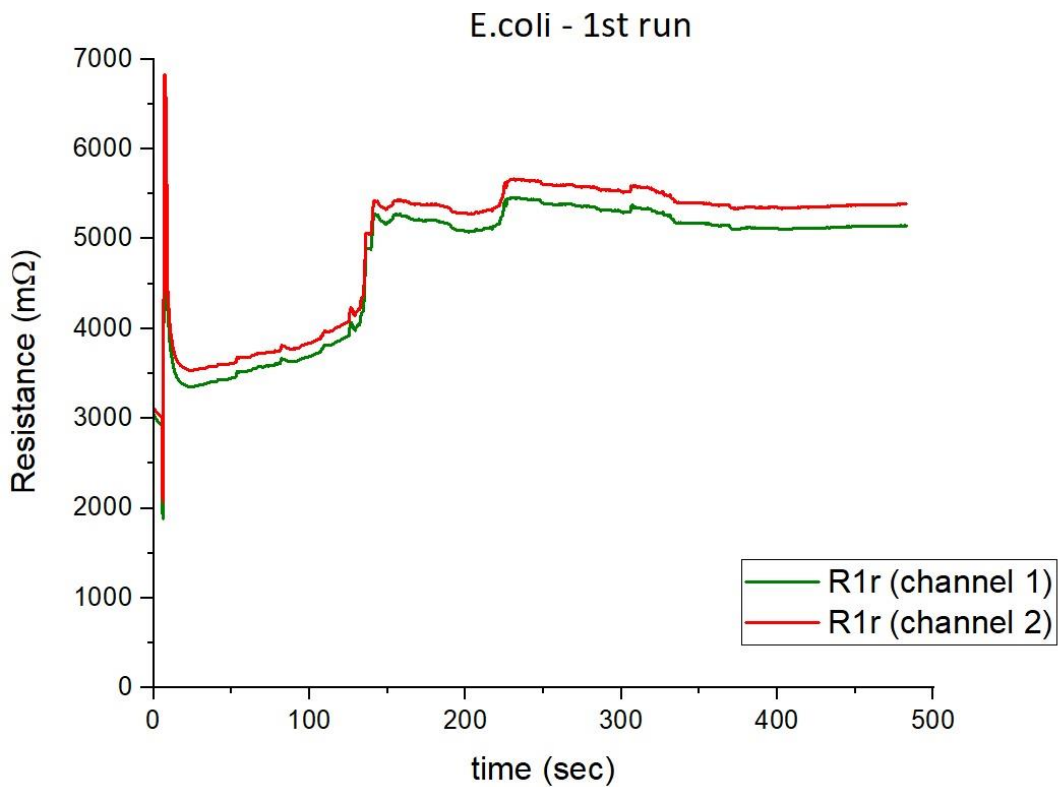


Figure 3.45 Average colony forming units vs time for biosensor solution containing 20 µl of bacterial solution with Escherichia Coli (1st run).

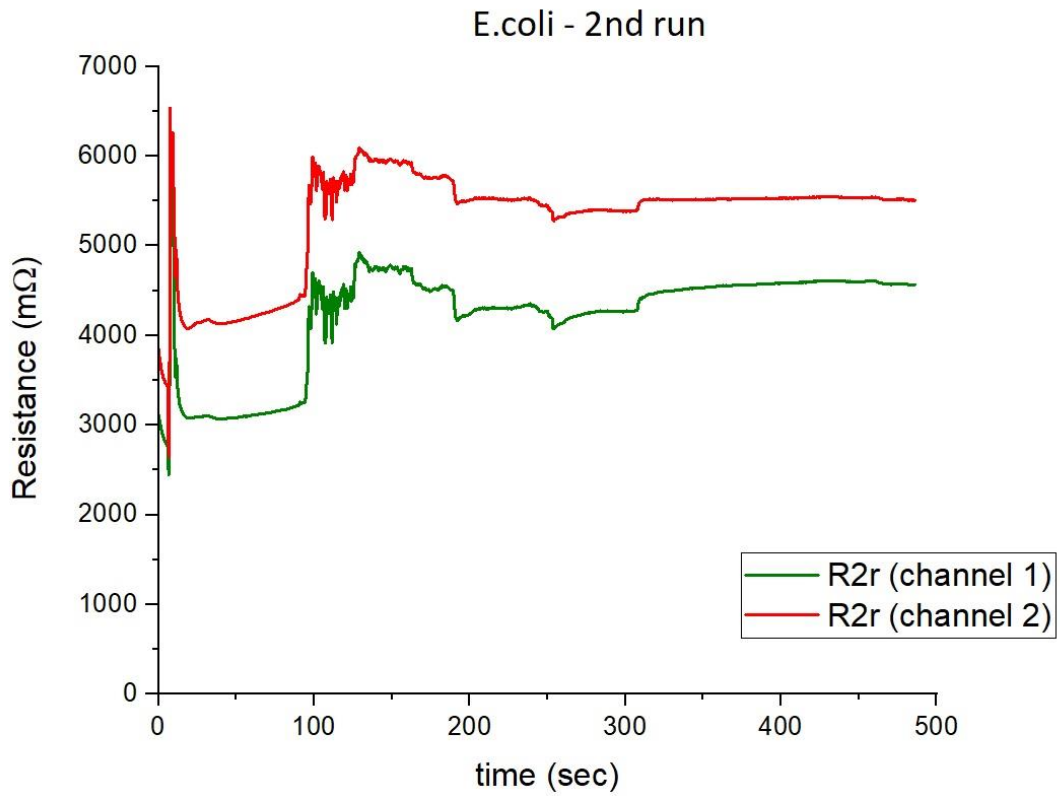


Figure 3.46 Resistance vs time plot for biosensor solution containing 20 μl of bacterial solution with Escherichia Coli (2nd run).

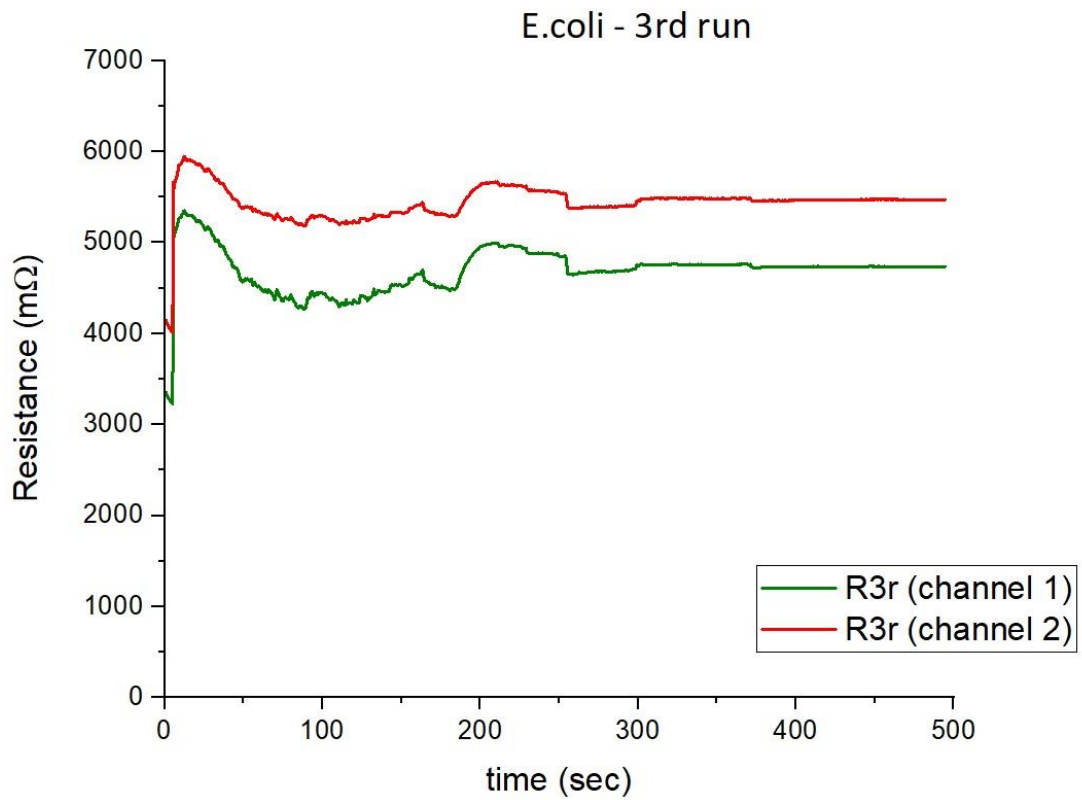


Figure 3.47 Resistance vs time plot for biosensor solution containing 20 μL of bacterial solution with Staphylococcus Epidermidis (3rd run).

3.6.3.2 Colonies count

The colonies of Escherichia Coli were counted and the results averaged as described in detail in Section 3.6.1.2. The final results are collected in Table 3.6 and represented in the histogram in Figure 3.47.

Table 3.6 CFUs for biosensor solution containing 20 µl of bacterial solution with Escherichia Coli.

time	CFUs
0	3,21E+05
1	2,95E+05
2	8,90E+05
3	5,30E+06
4	2,63E+07
5	1,31E+08
1h, a	5,47E+05
2h, a	2,87E+06
3h, a	2,86E+06

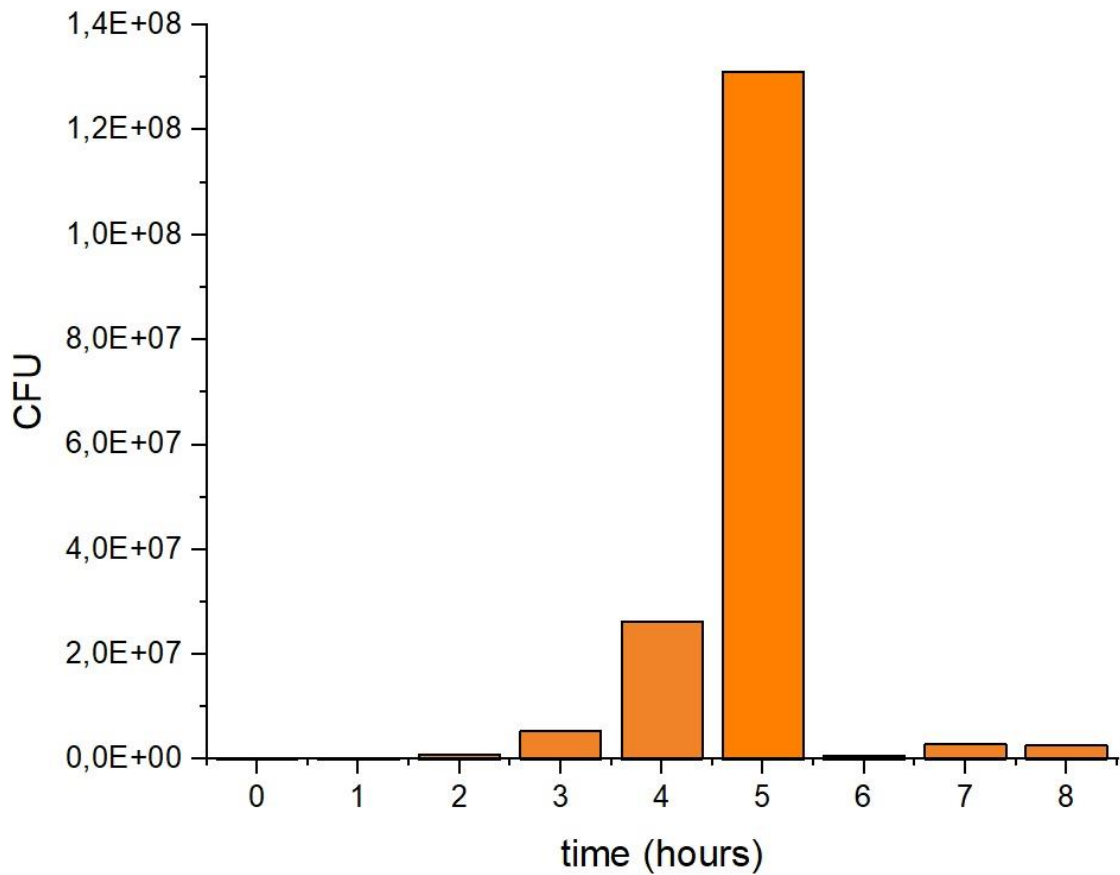


Figure 3.48 Average colony forming units vs time for biosensor solution containing 20 µl bacterial solution with Escherichia Coli.

3.6.4 Staphylococcus Aureus

3.6.4.1 Resistance vs time curve

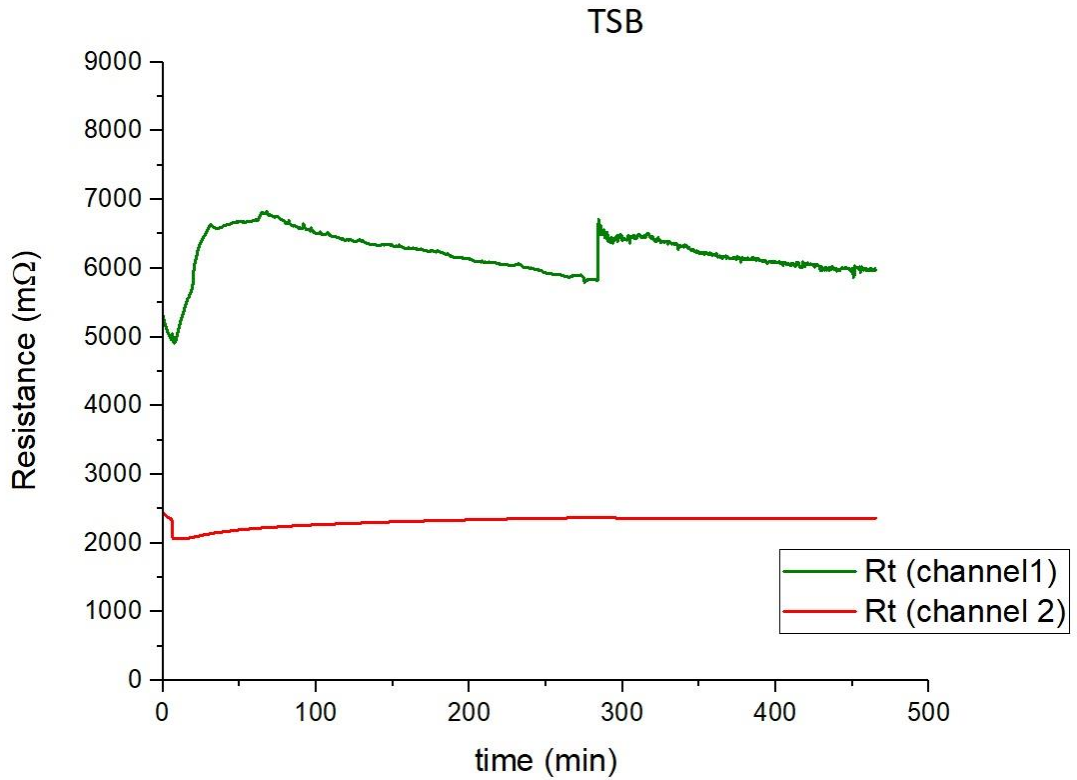


Figure 3.49 Resistance vs time plot for TSB media.

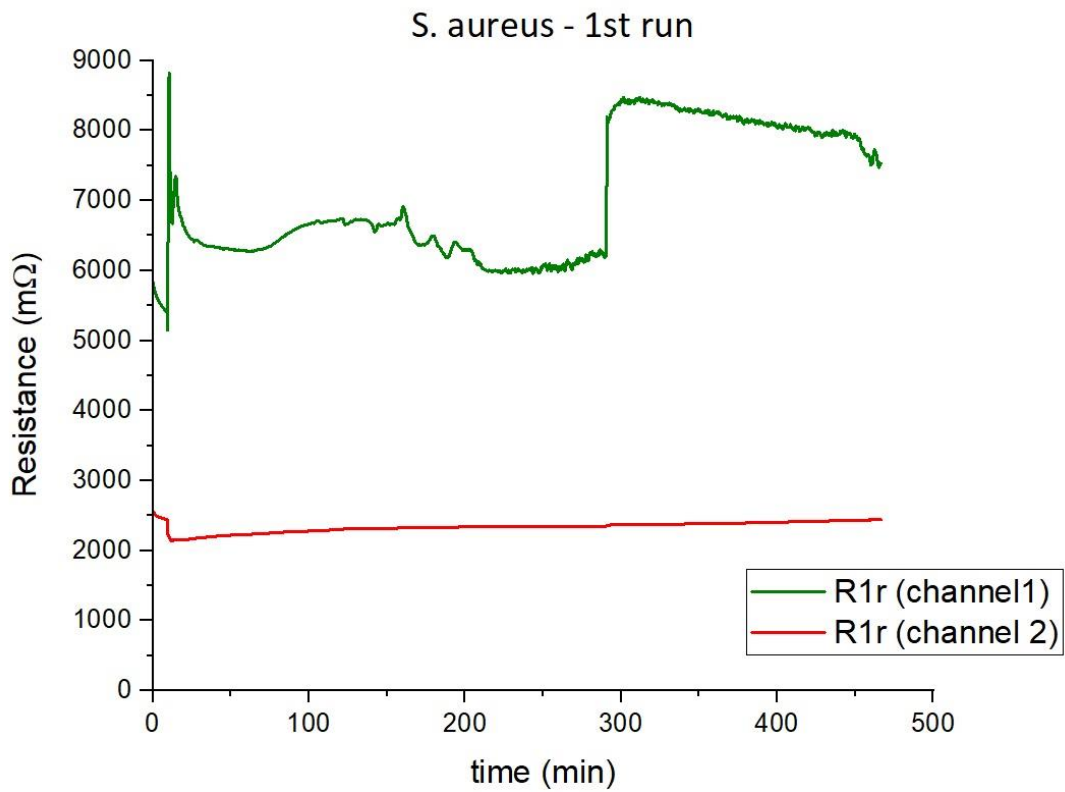


Figure 3.50 Resistance vs time plot for biosensor solution containing 20 μ l of bacterial solution with Staphylococcus Aureus (1st run).

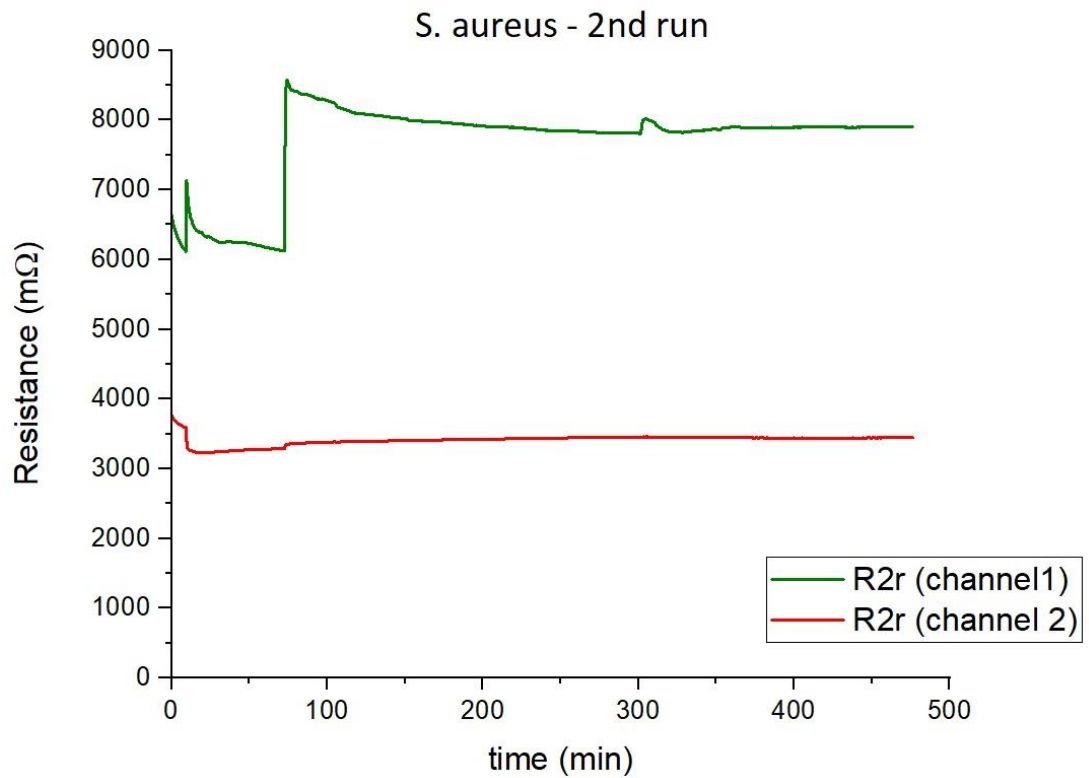


Figure 3.51 Resistance vs time plot for biosensor solution containing 20 μ l of bacterial solution with *Staphylococcus Aureus* (2nd run).

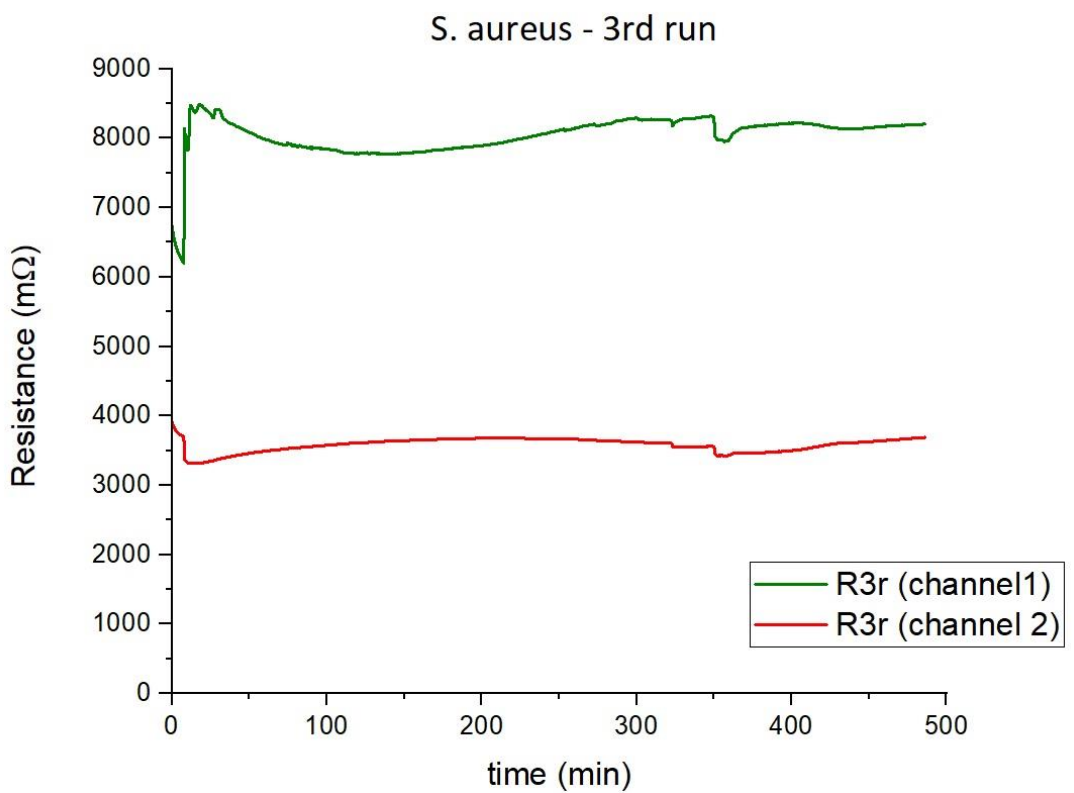


Figure 3.52 Resistance vs time plot for biosensor solution containing 20 μ l of bacterial solution with *Staphylococcus Aureus* (3rd run).

3.6.4.2 Colony count

The colonies of *Staphylococcus Aureus* were counted and the results averaged as described in detail in Section 3.6.1.2. The final results are collected in Table 3.7 and represented in the histogram in Figure 3.53.

Table 3.7 CFUs for biosensor solution containing 20 μ l of bacterial solution with *Staphylococcus Aureus*.

time	CFUs
0h	9,63E+05
1h	1,29E+06
2h	3,44E+06
3h	2,42E+07
4h	3,85E+07
5h	1,29E+08
1ha	5,13E+07
2ha	1,27E+07
3ha	1,01E+07

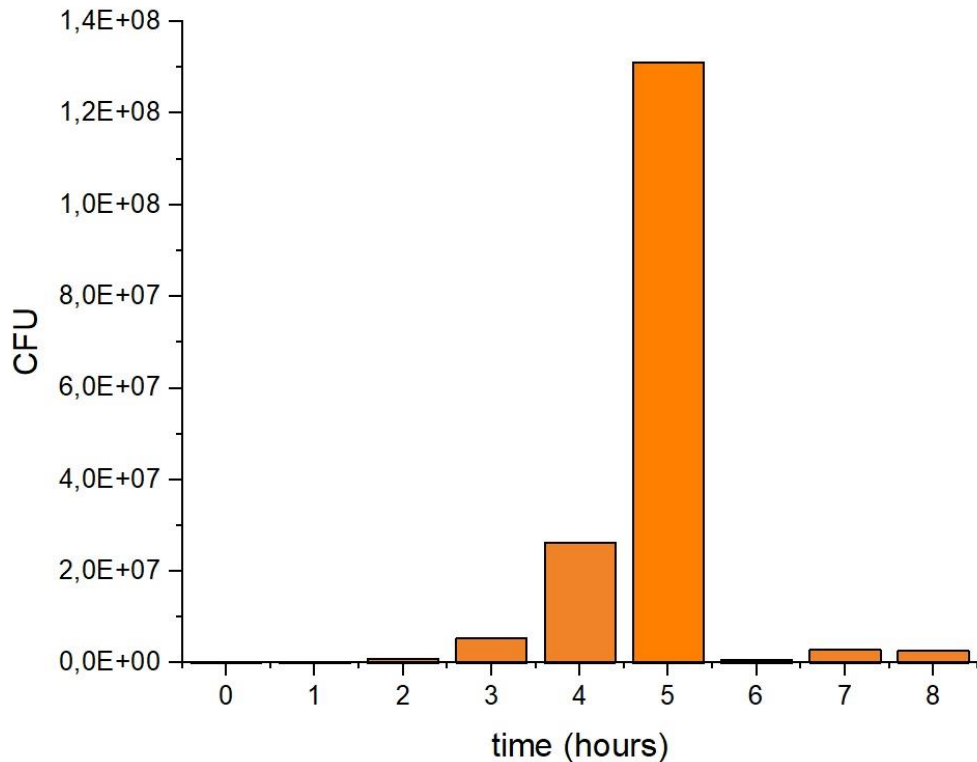


Figure 3.53 Average colony forming units vs time for biosensor solution containing 20 μ l bacterial solution with *Staphylococcus Aureus*.

3.7 Discussion of results

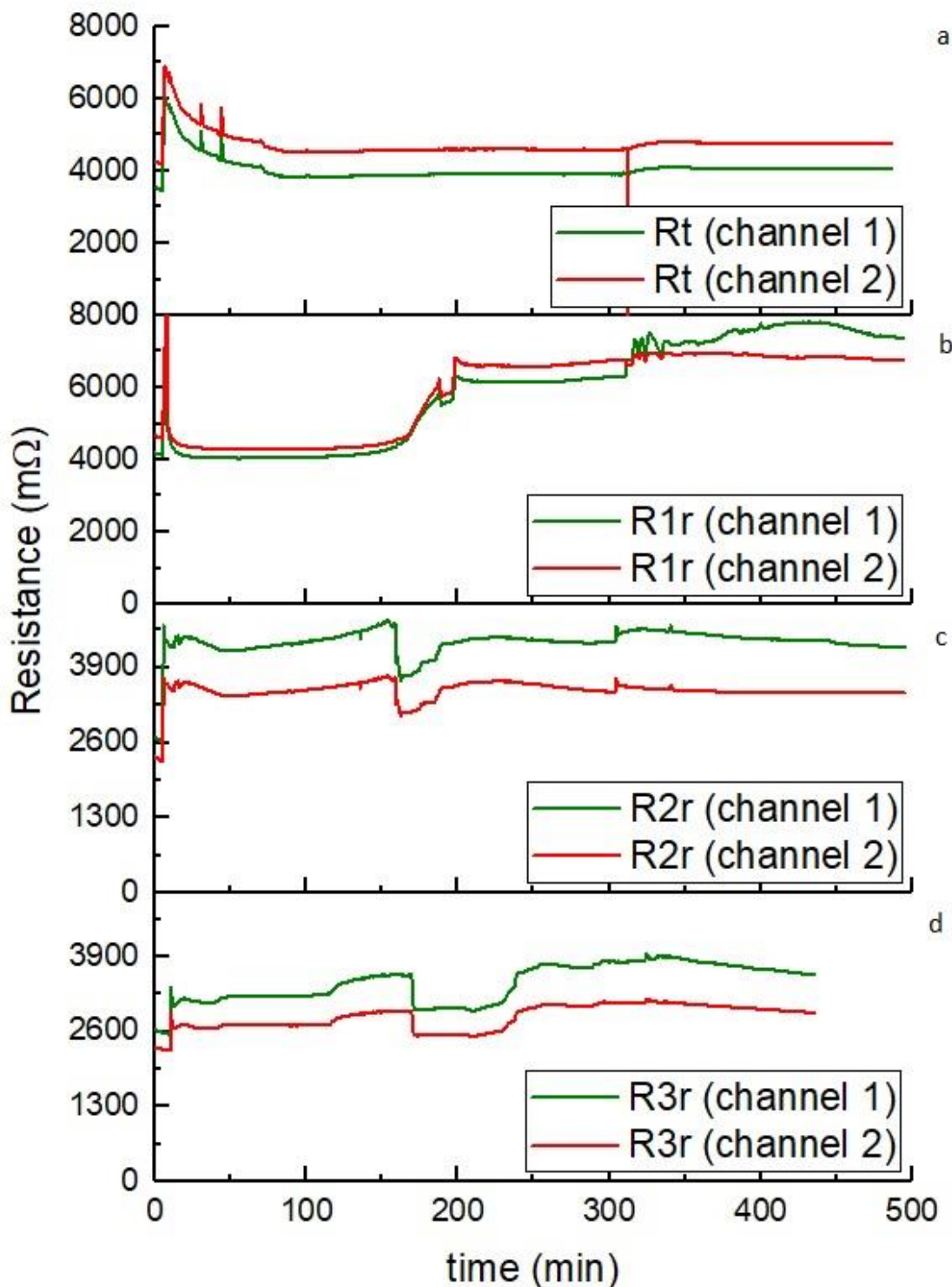


Figure 3.54 Comparison of the resistance vs time plots for TSB media (a), 1st (b) and 2nd (c) run of biosensor solution containing 20 μ l of bacterial solution with *Pseudomonas Aeruginosa*.

By comparing the results of P.A. (Figure 3.54), four things can be noticed. Firstly, the presence of the bacteria is evident in graph b, c and d: while in Figure 3.54a, representing the behavior of the control media, resistance remains approximatively constant over time, it changes in case of bacterial presence in solution (b,c,d). In addition, the change in resistance is characterized by a common pattern, with a

sudden change in resistance around 100-200 minutes, relatable, possibly, to the formation of a biofilm. The recurring peak at 300 minutes is instead due to the addition of the antibiotic.

The inversion in the peak direction for graph c and d is due to the different devices for testing, as proved by the relevant difference in initial resistance of the device (4Ω for a,b and $2,5\Omega$ for c,d), and probably to an inversion in the circuit connections. A slight change in initial resistance for consecutive runs is anyway normal: in fact, the cleaning process described in Section 3.6 *Single bacteria tests* did not completely succeed in removing the biofilm. The presence of biofilm residues on the graphene would then impact its initial resistance, and explain the small change in initial resistance for every re-use of the device, also with other bacteria.

Interestingly, it is not possible to correlate the characteristic peak between 100-200 mins of the resistance vs time graphs to the growth curve of the bacterium (Figure 3.39), nor the general behavior of the curve: the growth curve, in fact, keeps increasing exponentially even after that time, and the decrease in CFUs after 6 hours is due to the action of the antibiotic added, while no decrease appears on the R-t plot.

Similar conclusion can be drawn for E.coli (Figure 3.55): again the characteristic peak between 100-200 minutes can be noticed when bacteria are present in solution, and the resistance vs time plots show a common trend. The 100-200 minutes peak is a little less evident in Figure 3.55d, whose results may although be attributable to relevant damage of the biosensor, given the absence of the 300 minutes peak for the antibiotic addition, otherwise generally noticeable. For this bacterium too there is no evident correlation between the bacterial growth curve and the resistance vs time plots. For E.coli, on the other hand, the type and quantity of antibiotic seem to be less effective than in case of P.A., for a few bacterial colonized still survived even after its addition (Figure 3.48).

Dissimilar results are obtained for S.E. (Figure 3.56): in this case, there is no significant difference between the control media in Figure 3.55a and the runs in presence of bacteria (b and c). The resistance vs time plots are not consistent, and there is no characteristic peak underlining the presence of bacterial colonization.

S.A. (Figure 3.57) has an analogous behavior: aside from channel 2, which on this device was not functioning, channel 1 does not show a consistent behavior over different runs, and no characteristic peak can be pointed out for this bacterium either.

In both case, the growth curve of bacteria does not seem to explain the trend of the curves.

In conclusion, the repetitiveness of the resulting plot for P.A. and E.coli assures the possibility to distinguish on-going bacterial colonization, thanks to a characteristic peak between 100-200 minutes, present for both bacteria. Their resistance vs time plots are, on the other hand, not dissimilar enough to permit an unequivocal identification of the bacterium in solution. For S.A. and S.E., instead, no relevant difference can be found between the control curves and the runs with bacteria in solution, not permitting any conclusion on the presence of a bacterial colonization.

While it is then possible to conclude that the biosensor can recognize the presence and stage of bacterial colonization for gram-negative bacteria such as P.A. and E.coli, the biosensor is not optimized to detect the presence of an on-going infection for gram-positive bacteria such as S.E. and S.A. Moreover, it is not clear yet which parameters, and if one in particular, are impacting the resistance vs time plots: the lack of correlation between the bacterial growth curves and the R-t plots seem to suggest that the bacterial cycle does not have an impact on the final results, but the fact the biosensor detects gram-negative but not gram-positive bacteria might suggest the outer membrane of the cells is a key factor to interpret the results. Further experiments are in any case necessary to answer these questions and thus optimize the device to attain more univocal results.

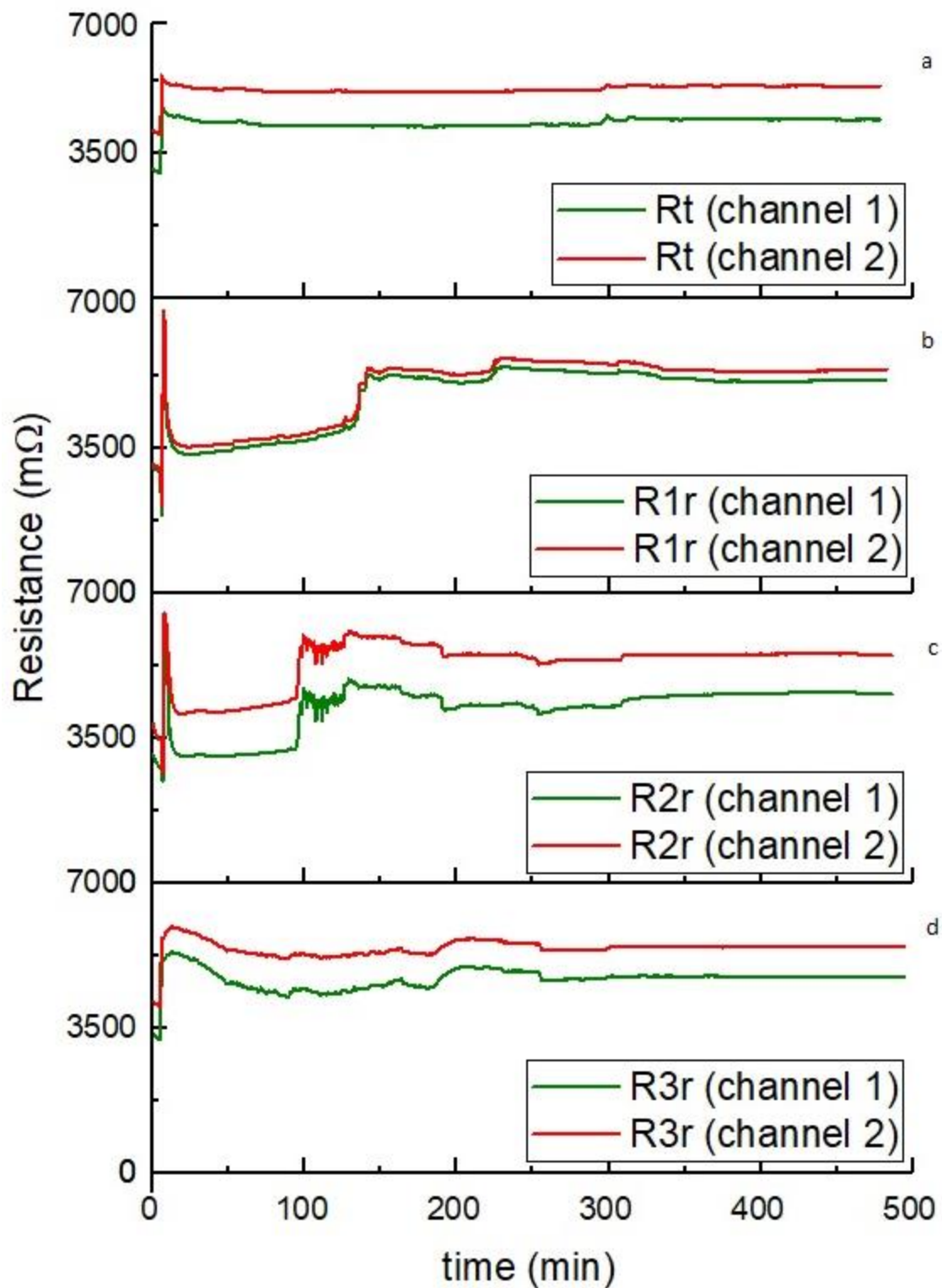


Figure 3.55 Comparison of the resistance vs time plots for TSB media (a) and 1st (b), 2nd (c) and 3rd (d) run of biosensor solution containing 20 μ l of bacterial solution with Escherichia Coli.

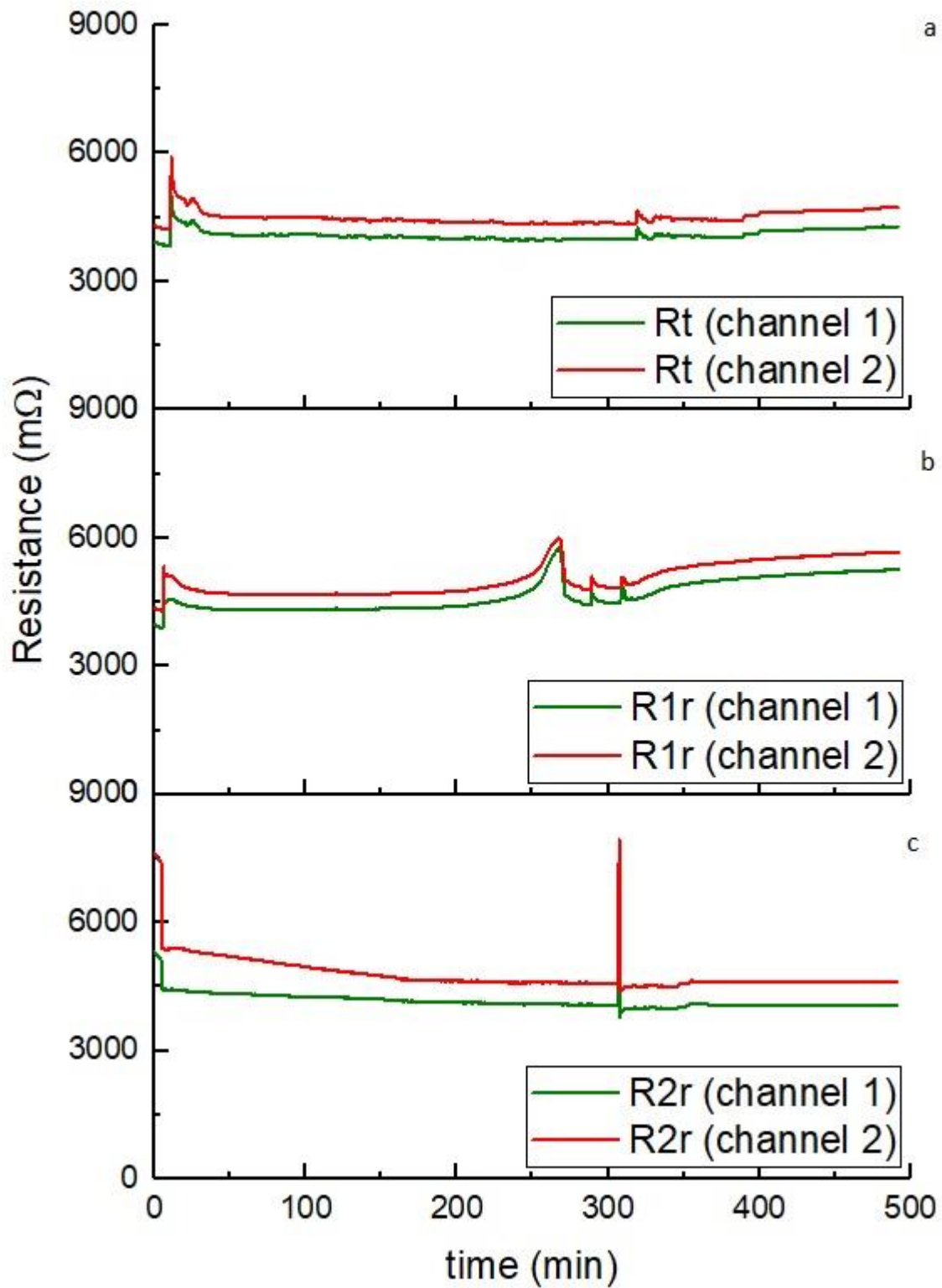


Figure 3.56 Comparison of the resistance vs time plots for TSB media (a), 1st (b) and 2nd (c) run of biosensor solution containing 20 μ l of bacterial solution with *Staphylococcus Epidermidis*.

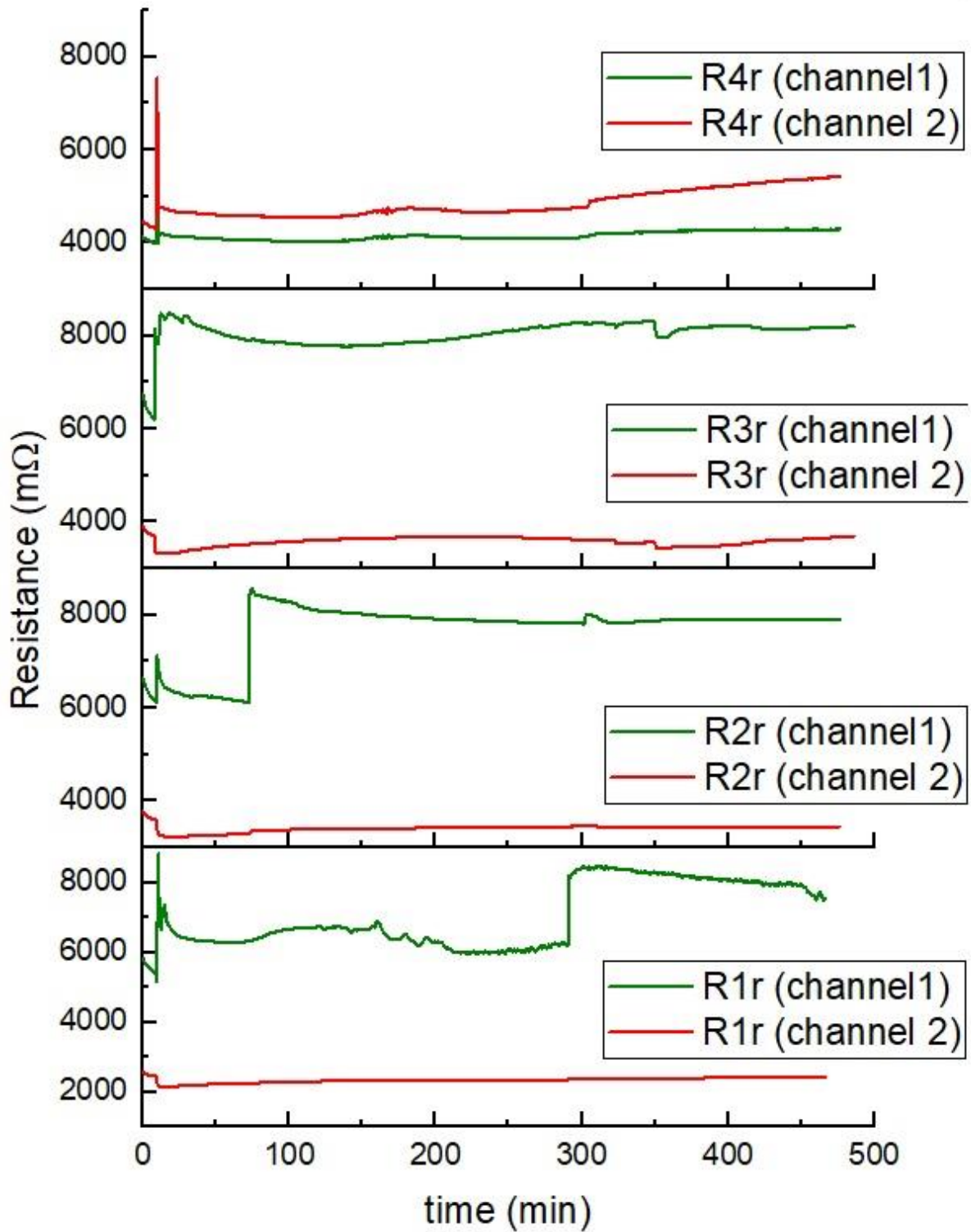


Figure 3.57 Comparison of the resistance vs time plots for TSB media (a) and 1st (b), 2nd (c) and 3rd (d) run of biosensor solution containing 20 μ l of bacterial solution with Staphylococcus Aureus.

4. Conclusions

After the analysis of results done in Section 3.7 *Discussion of Results*, it is possible to conclude that graphene can be a good choice as material in terms of the studied biomedical application. Firstly, the material can be easily integrated in the device by simple transfer technique, a well-known and mastered process in the manufacturing of electronic devices such as the biosensor in analysis. For what discussed in Section 3. *Antibacterial properties of graphene*, it seems quite reasonable to assume, also, that the planar structure of CVD graphene permits the exclusion of phenomena such as membrane penetration or damaging of cells, and the damage and death registered on bacteria cells in colony forming units numbers is attributable to the use of ciprofloxacin, an antibiotic, and not ascribable to graphene.

Given the results, it can be primarily concluded that the different resistance versus time plots show different trends for different bacteria, thus proving that graphene field effect transistor has good credentials to become a reliable device for the detection of bacterial infections in real-time analysis.

More specifically, consistent results were obtained with gram-negative bacteria. Referring to the peaks between 100 and 200 minutes in Figure 3.54, 3.55, it is possible to state that the bacterial colonization and biofilm formation takes place between 100 and 200 minutes from the beginning of the test, which is comparable in both the cases. The presence of such peaks, identified only in *Pseudomonas Aeruginosa* and *Escherichia Coli* but missing in the *Staphylococci* strains, allow to define which gram-type of bacteria is colonizing the graphene surface (with a little less confidence exactly which bacteria), thus providing a first indication of which kind of antibiotic may be necessary, but also allows to determine the stage and progress of the infection.

On the other hand, given the preliminary phase of the project, a few considerations are in order to better understand the reliability of results and how the device, production process and data analysis could be furtherly improved to optimize the device.

At this stage, the device does not seem to be able to detect univocally the presence of gram-positive bacteria (in our study, *S. epidermidis* and *S. aureus*) in solution and their formation of a biofilm: the trend of the line in the resistance vs time plot do no differ noticeably from the cases in which only media (control) is present. Such similarity, then, does not permit to draw conclusions on the presence, type and stage of the infection. Further tests led on other gram-positive bacteria would allow to define whether this problem is detected only for some gram-positive bacteria or for all of them. If the uncharacteristic trend was confirmed, then, it would be interesting to compare the different resistance vs time plots to define whether some small but still relevant (as in not attributable to noise) discrepancies can be detected among the different bacteria. Where even the latter hypothesis was not attested, that would restrict the range of applications of the device, for it would only be possible to have real-time analysis of certain strands of bacteria.

In addition, while it is possible to distinguish quite clearly gram-positive from gram-negative bacteria, it is more complicated to define specific peculiarities for single bacteria, as specific peaks or trends in the line that would allow the univocal identification of a specific bacterium. In this case also, then, the subministration of the antibiotic would not be a secondary issue: the same quantity and concentration of ciprofloxacin, for example, proved to be efficient in killing most of the *Pseudomonas Aeruginosa* bacterial cells, but far less effective in case of *Escherichia Coli*. The possibility to tell apart the different bacteria seems then to be of crucial importance in the definition of the possible applications of the device, and would then deserve further investigation.

While the results would suggest a marked dependence of the final plot on the type of bacteria analyzed, and subsequently on the structure of their outer membrane (see Section), other variables might prove relevant in the definition of a specific trend for bacteria. Considering that bacteria feed on the components of the media to survive and proliferate, the media used for cultivation is an important variable to define how the bacteria behave in solution: how quickly the log phase of the growing curve starts and if a different composition may impact the time at which the peak indicating a biofilm formation appears. At the same time, the quality of distilled water, the efficiency of the sterilization process (whose inefficiency may induce contamination), random phenomena connected with the normal routine of a lab all constitute factors that impact the final results, and strongly decrease the reproducibility of the tests in similar conditions. The listed variables would prove possibly even more significant in light of the fact that the real-time analysis would imply the presence not of media but presumably of blood, whose composition is much more diverse and complex than the one of the media.

Even if it can already be excluded that the shape of the curve depends on the evolution of the bacteria and the number of colonies present in solution, additional work is required to understand what other factors impact the curve, and on what degree. In fact, even if it was confirmed that the outer membrane composition plays a role in determining the resulting plot of a test, it can hardly be considered the only variable important, for otherwise all of the results on the same gram-type bacteria would offer identical shape.

Into the bargain, two more details are worth a more in-depth sight: the definition of a proper cleaning process for the device and the reproducibility of the obtained results.

For what concerns the former one, the device, after each test, was initially rinsed in ethanol to kill all the bacteria, followed by cleaning in boiling water for 5 minutes, stirred in distilled water and air-blow dried, which necessarily impacted the device state in two ways: first, the cleaning process did not guarantee the complete removal of the biofilm formed on graphene, and secondly some parts of the biosensor, like the protective layers or the connectors may be slightly damaged by the conditions of the process, thus changing the starting conditions for the next test. The definition of a less aggressive and more effective cleaning process would then be extremely important and tailors directly into the reproducibility issue.

The manufacturing of single devices is both material and time-consuming, and the fabrication of reusable sensors was necessary, in the experiment, to allow multiple tests on different bacteria in a limited time. The presence of residues of biofilm on the biosensor, on the other hand, determines a change in the initial conditions of the chip that may result in different final shapes of the resistance vs time curves. In the practical use, for hygiene reasons, the reuse of such devices would not be possible, and the definition of an effective cleaning process is then necessary to prove the obtainment of recurring curves on a single use device.

The reproducibility of results is, as already stated, impacted by many factors: different initial conditions due to the cleaning process and the composition of the biological components play an important role in the definition of final and reliable results. Moreover, the manual fabrication of the devices is connected with a higher variability on the quality of the devices produced: only during the transfer process, which is only one of the many steps necessary to obtain the final device (see Section 3.5 Device Manufacturing), the variability on the final device is strongly impacted by the formation of defects on the graphene layer. Such defects are generally randomly distributed, but can impact the sensing of the device, and, in case of the formation of peaks on the graphene surface, may induce cell damage. An optimized production process, maybe on a larger scale and more precise, would permit a better

reproducibility of the entire sensing process, making the biosensor more univocal and reliable in its results. For this, other fabrication method may be considered in order to produce disposable sensors.

Regardless of the underlined issues, further analysis, tests and optimization of the process remain strong and concrete possibilities. The definition of the relevant variables impacting the system, the confirmation of a normal growth of cells on the device, the delineation of an adequate cleaning process would all permit further confirmations of the results thus far obtained, and candidate the biosensor as an effective and reliable detector.

In conclusion, even if still a lot needs to be done in order to draw definite conclusions of the reliability and efficacy of the biosensor, the preliminary results are then, thus far, quite encouraging.

As future perspectives, it would then be interesting to test mixed bacterial colonies during the same test and analyze the final curves to check whether it would be a linear combination of the two curves of the single bacterium, thus allowing the distinction of single from multiple bacterial infections, or if one bacteria would just repress the other, which would make the distinction between single and multiple infections a lot more complicated.

Appendix I: Boron doped graphene Biosensor

I. The working principle

The aim of this experiment was to develop a more sensitive, label-free biosensor of small dimensions and practical use adapt to the use in the medical field for testing outside of clinical laboratories that would deliver results with good reliability but in a shorter time with respect with the normal analysis procedures, possibly in real time. In particular, the developed biosensor would allow the specific binding of certain biomolecules and a quantitative evaluation of such bindings.

This biosensor is, to be truthful, the re-adaptation of a biosensor realized using magnetic nanorods produced by nano-imprint lithography. In this case, although, instead of using nanoparticles, those were substituted with magnetized boron doped graphene flakes, first to see whether the same principle could be adapted to a different material, and then to evaluate the sensitivity of the device with respect to the previous form.

The working principle is well described in the image below: the incoming light, collimated and linearly polarized, interacts with the magnetic nanoparticles in solution inside a cuvette, which are rotating due to the applied external magnetic field, realized through two Helmholtz coils. This interaction results in a null, partial or total transmission of the incident polarized light, whose intensity is recorded by the photodetector (see Figure I). The nanoparticles have a small delay in their rotation with respect to the magnetic field, relatable to a phase lag in the oscillating function that describes the rotation of the nanoparticles. Such delay is dependent on the hydrodynamic volume of such particles. In case of adhesion and attachment of biological molecules, and subsequent change in hydrodynamic volume of the total aggregate composed of graphene flakes + molecules, a change in phase lag would be recorded.

This biosensor could then be surface functionalized in order to allow the attachment of specific molecules, whose adhesion would be confirmed and detected via change in the phase of the curve describing the motion of the magnetic nanoparticles.

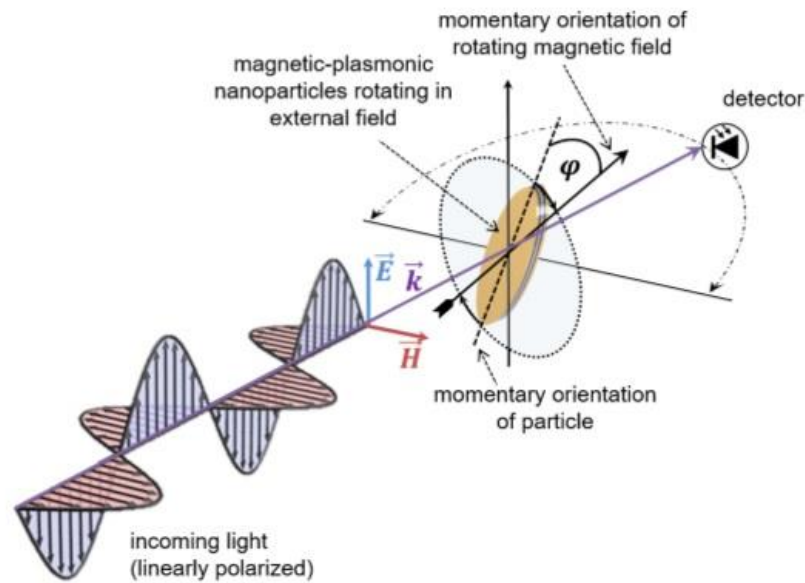


Figure I Overview of the working principle of the biosensor. [127]

Due to optical anisotropy, at a given wavelength, the scattered component of the incident light is lowest when the major axis of the flake is oriented perpendicular to the polarization direction, as shown in Figure II.A, while it is highest when the major axis of the nanoparticle is parallel to the polarization direction of the light: referring to Figure I, the polarization direction E coincides with the minor axes in the upper picture, and with the major axes in the lower picture. Within a single rotation cycle of the magnetic field, the light scattering of the particle reaches two times maximum and minimum values: this results in a frequency-doubling of the photodetector signal compared to the frequency of the rotating magnetic field (Figure II.B).

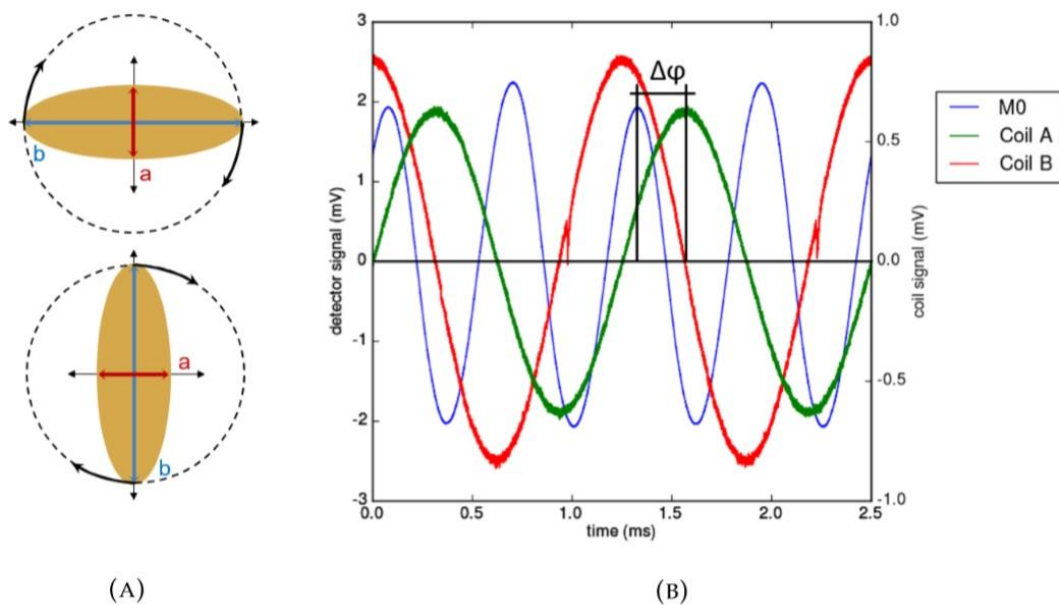


Figure II (A) The scattering of the nanoparticle is highest or lowest when its major or minor axis is oriented parallel to the polarization direction of light. (B) Typical measurement signals 90° phase shifted coil currents required for the rotating magnetic field (red and blue curves) and the frequency-doubled photodetector signal (M0). The phase lag angle corresponds to the phase shift between the coil and detector signal. [127]

II. The structure of the flakes

For the device to perform adequately, the flakes need to have two specific characteristics:

1. Flakes need to have magnetic properties
2. Flakes need to have plasmonic properties

The employed boron doped graphene flakes are optically anisotropic and consist of different overlapping layers: a ferromagnetic coating is needed to induce magnetism, and thus motion and rotation in response to the external magnetic field. Additionally, a second layer constituted of a noble metal, gold in the examined case, is deposited. The addition of this second metal coating can be explained thanks to two different reason: first, the layer prevents the oxidation of the ferromagnetic material in the underlayer, secondly, it enhances the plasmonic effect.

A localized surface plasmon is an electron density oscillation in an electrical conductor (like Au, in this case) excited by the interaction with an electromagnetic wave. Assuming the atomic cores to be in fixed positions and the negative charges to constitute an electron cloud around them, like in the classical physics model, then this density oscillation involves the negative charges. Such movement induces the polarization of the coated flake because of the displacement of free electrons in the electric field of the electromagnetic wave, which induces a restoring force in response to the polarization. The phenomenon results, then, in the occurrence of resonant oscillations at distinct frequencies. In a short, simple form, then, when the frequency of the incident light is distant from the resonance frequency of the flake, no real change in the system can be perceived, while in case of similar frequencies to the resonance one, the absorption cross-section is largely increased.

The flakes surface can then be functionalized with biomolecules, generally referred to as ligands, to elicit the specific binding of target biological molecules, generally referred to as analyte, most commonly biomarkers specific for certain diseases. Upon the addition of analyte solution, the binding events lead to an increase of the hydrodynamic volume which further impacts the rotational dynamics of the particle: the rotational motion lags behind that of the rotating magnetic field more than in the case of just the flake. The optically measured phase lag signal is directly proportional to the amount of bound target molecules on the particle surface.



Figure III Specific binding mechanism of analyte and ligand for the detection of specific biomarkers. [128]

III Preparation for testing

III.I Samples preparation

The sample preparation involves multiple steps:

1. Membrane fabrication using BDG flakes
2. Metal evaporation (Fe, CO or Ni)
3. Dis-mantling the membrane in to powder
4. Testing of induced magnetism
5. Preparation of dilutions for testing

Boron doped graphene flakes could not be coated in their native powder form: the material, is, in fact, extremely volatile and polarizable. Even not considering the possible health risks connected to the use of a volatile compound, the deposition of the metal can guarantee uniform thickness only in case of homogenous substrate surface, that needs to be compact and consistent, and not in the powder form. The integration of boron doped graphene flakes in a membrane was then identified as a good solution to allow the following deposition of metals on top of the flakes.

First a solution of boron doped graphene flakes and ethanol was prepared as described:

- 2 mL of EtOH;
- 8 scoops of BDG powders (around 9,6 mg).

The solution was then sonicated for 1h.

A standard glass substrate of dimensions 75 mm x 25 mm was first cleansed with ethanol and then allowed to dry at room temperature below a perspirant cover, to impede the deposition of particulate in air on the glass substrate again.

On this substrate 1 mL of di-water and 1mL of BDG solution (from the above stock) was added and left over night for drying at room temperature under a perspirant cover to allow the evaporation of water and formation of a membrane of BDG on the substrate.

The membrane fabrication process has been depicted in the Figure IV.

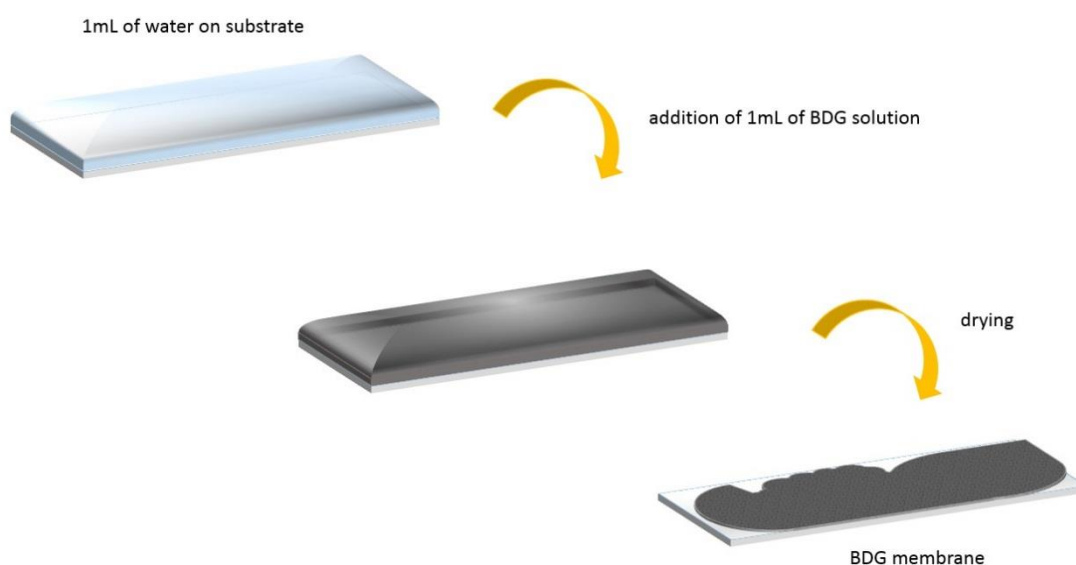


Figure IV. Overview of the preparation process of the BDG membranes.

Once dried, the membranes are ready for the second step: the deposition of metals. Different metals were deposited on the glass substrate in different sessions in order to obtain a variability on samples in terms of thickness and presence of certain layers, and possibly evaluate whether these variables may interfere with the results. The composition of the membranes realized for testing are depicted in Table I.

Table I. Synthesis of the prepared samples (first column) and their compositions (second column).

Label of sample	Layers composition
Ti5Fe10Ti5	<ul style="list-style-type: none"> • BDG membrane • 5 nm of titanium • 10 nm of iron • 5 nm of titanium
Ti5Fe20Ti5	<ul style="list-style-type: none"> • BDG membrane • 5 nm of titanium • 20 nm of iron • 5 nm of titanium
Ti5Fe10Au15	<ul style="list-style-type: none"> • BDG membrane • 5 nm of titanium • 10 nm of iron • 15 nm of gold
Ti5Fe10Au25	<ul style="list-style-type: none"> • BDG membrane • 5 nm of titanium • 10 nm of iron • 25 nm of gold
Ti5Fe10Au35	<ul style="list-style-type: none"> • BDG membrane • 5 nm of titanium • 10 nm of iron • 35 nm of gold
Ti5Fe10Au45	<ul style="list-style-type: none"> • BDG membrane • 5 nm of titanium • 10 nm of iron • 45 nm of gold
Ti5Ni10Au15	<ul style="list-style-type: none"> • BDG membrane • 5 nm of titanium • 10 nm of nickel • 15 nm of gold

Since the material for the final testing is required in powder form, the membranes were scratched-off from the glass substrate and the obtained powder was collected in small glass containers correctly labeled.

The glass containers were weighed before and after filling with the powder to evaluate the net weight of the powders obtained for each kind of coating. Even if this step adds an error on the quantity of powders in each container, as already stated, powders

could not be weighted in normal weighing boats as they are highly polarized. Final weights of the BDG powders coated with metal are presented in Table II.

Table II. Overview of the prepared samples in powder form (first column) and their net weight (second column).

Label of sample	BDG powder weight [mg]
Ti5Fe10Ti5	6,605
Ti5Fe20Ti5	10,500
Ti5Fe20Au15	3,025
Ti5Fe10Au25	1,765
Ti5Fe10Au35	11,630
Ti5Fe10Au45	4,650
Ti5Ni10Au15	5,255

Qualitatively, the induced magnetism was successfully evaluated by visualizing the BDG flakes response to an external magnet.

After this, the preparation of the samples for the final testing can begin.

The first powders tested were 10,5 mg of Ti5Fe20Ti5. The powders were added in 2 mL of purified water for a final stock concentration of 5,25 mg/mL, and the solution were mixed to attain homogeneity.

It is important to know the ideal concentration in order to have a clear outcome and as these are the first of its kind tests and no literature study available, we opted to use similar concentrations as that of magnetic-nanorods that were used in earlier studies (129).

To obtain a concentration in that range, 100 μ L are drawn from 5,25 mg/mL solution:

$$0,1 \text{ mL} * 5,25 \frac{\text{mg}}{\text{mL}} = 0,525 \text{ mg}$$

And then diluted with di-water to 2 mL, for a final concentration of:

$$\frac{0,525 \text{ mg}}{2 \text{ mL}} = 0,2625 \text{ mg/mL}$$

The solution is then sonicated for 5 minutes to attain good homogeneity. Said solution is made up, although, by a variety of particles, different not only in dimensions, but also in their constituting layers: regardless of the presence of the titanium to improve adhesion, some metal layers, the titanium one included, might divide during the sonication process necessary to properly disperse the powders in solution. This division results then in the formation of particles that are not necessarily

ferromagnetic, and thus the solution needs to undergo a cleaning process in order to separate the ferromagnetic ones from the waste.

The solution with a concentration 0,2625 mg/mL, was kept inside an Eppendorf tube of 2 mL volume. Two strong magnets were taped to the tube and the solution kept resting in vertical position for approximately 30 minutes: this way, the ferromagnetic particles would be attracted to the magnets on the side, while the non-ferromagnetic residue would sediment at the bottom of the tube. After 30 minutes, the supernatant was discarded, and the tube was diluted to 2mL with di-water.

To attain optimal cleaning, the same cleaning process described above was repeated 3 times.

After the final cleaning step, the final solution was diluted to 2mL and sonicated again for 2 minutes to guarantee a better suspension.

After the separation of magnetized particles from non-magnetized, the particles needed to be separated according to their size. In order to divide the flakes of different size, the 3-times cleansed solution, already diluted to 2mL, rested in steady vertical position for around 20 mins. This way, bigger particles would sediment at the bottom of the Eppendorf tube, while the smaller particles would remain in suspension. At the end of this sedimentation process, the solution was divided as follows: the upper 1,5 mL of solution, which will contain the smaller particles, are taken out and transferred to another Eppendorf tube. This solution will be identified as FSS (Final Solution Small of Ti5Fe20Ti5). According to theoretical calculations, we presumed that this solution would contain 10% of the initial powder weight present at point 4, thus a final weight of 52,5 μ g of powder.

The remaining 0.5 mL of the after-sedimentation solution, containing the bigger flakes, are diluted to 2 mL, and the solution identified as FSL (Final Solution Large of Ti5Fe20Ti5).

III.II The setup

In Figure V the actual setup of the experiment is shown: from the left, the lamp, lens and polarizer to collimate and polarize the light entering the analysis chamber. To the right, inside the chamber, two Helmholtz coils are present, with a space in between to accommodate the sample. The walls of the analysis chamber also serve as support for the movable detector (red line), to extreme right.

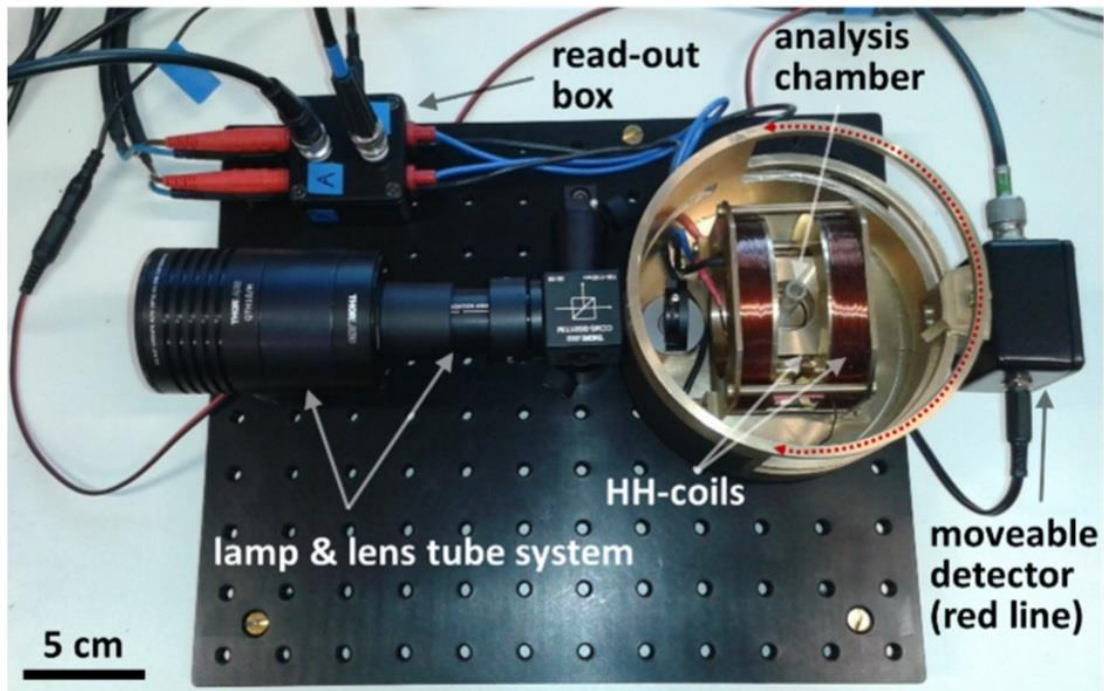


Figure V Set-up of the experiment. [127]

The final solution (2mL) containing the separated smaller flakes are used for testing. Before testing, the solution was sonicated again for a couple of minutes in order to evenly disperse the particles, followed by taking 500 μ L of this FSS solution in a glass cuvette. The glass cuvette was then placed between the two coils, where the white cross sign is seen (Figure VI). In this position, polarized light is aligned accurately to the sample, and the two coils, once feeded, would generate a magnetic field that induced the rotation of the particles in solution.

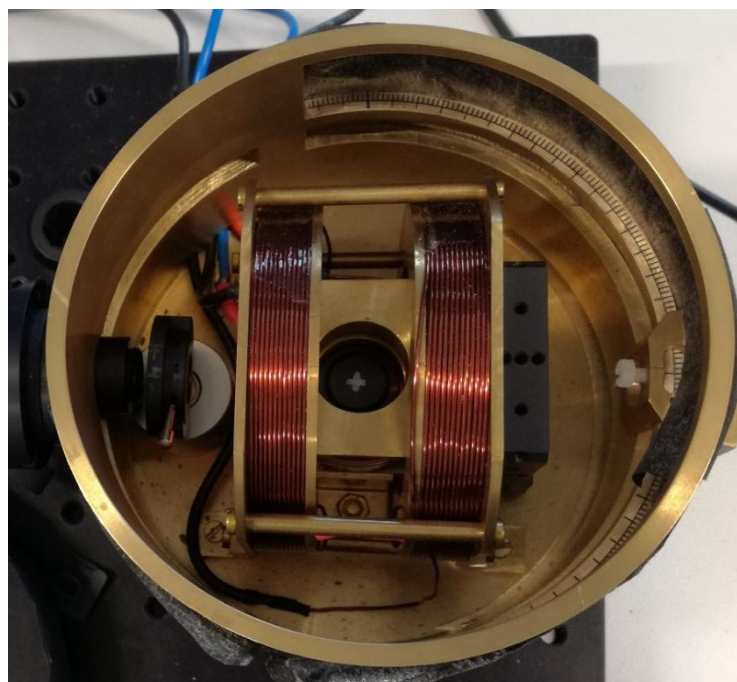


Figure VI Main chamber containing the two Helmholtz coils and in between them, marked by a white cross, the designated place for the sample.

Testing was run for multiple combinations of frequencies and magnetic field intensities, as shown in Table III.

Table III. Frequencies and magnetic field intensities used for the biosensor testing.

Tested frequencies [hz]	Tested \vec{B} [mT]
<ul style="list-style-type: none"> • 300 • 400 • 600 • 800 • 900 • 1000 	<ul style="list-style-type: none"> • 1 • 2,5 • 5 • 7,5

IV. Verification of induced magnetism

flake concentration 50 $\mu\text{g/ml}$

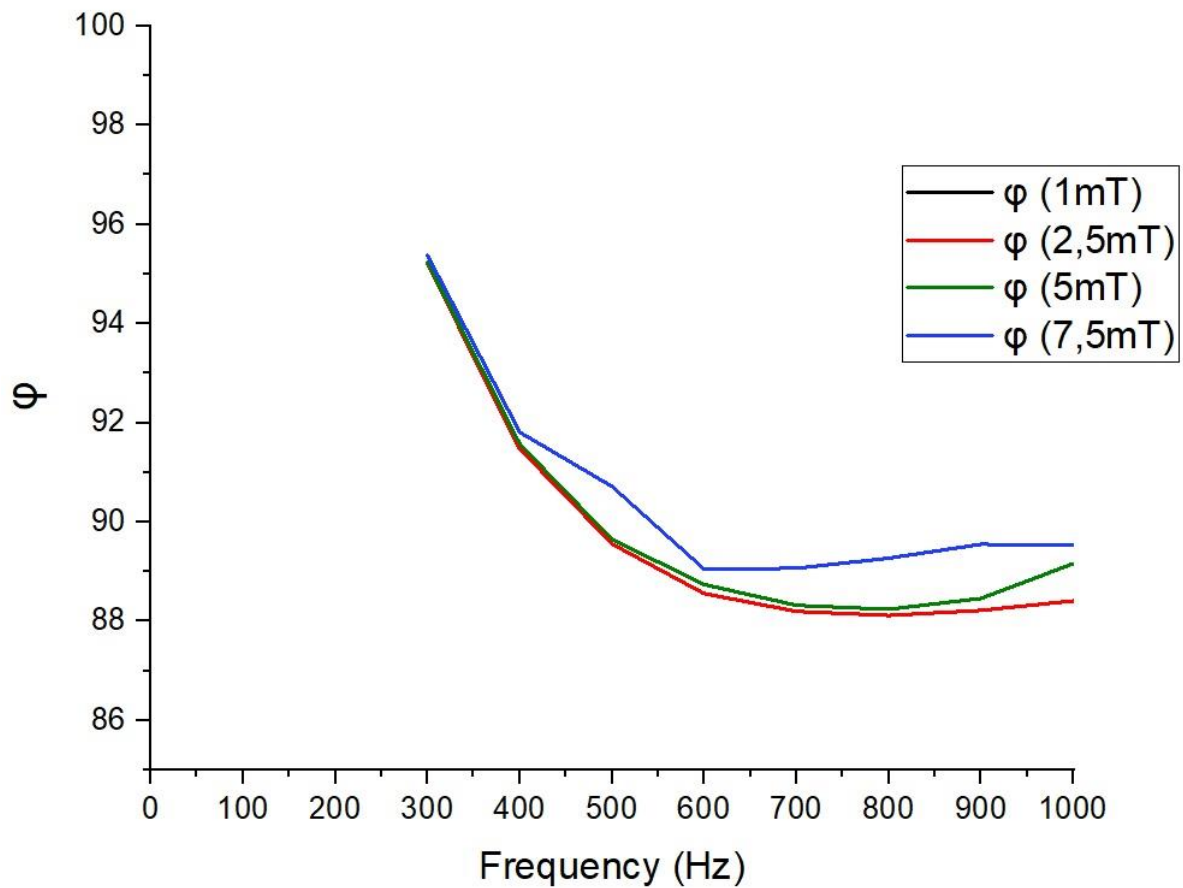


Figure VII Phase vs Frequency plot of FSS solution (concentration of 50 $\mu\text{g/ml}$) at different \vec{B} .

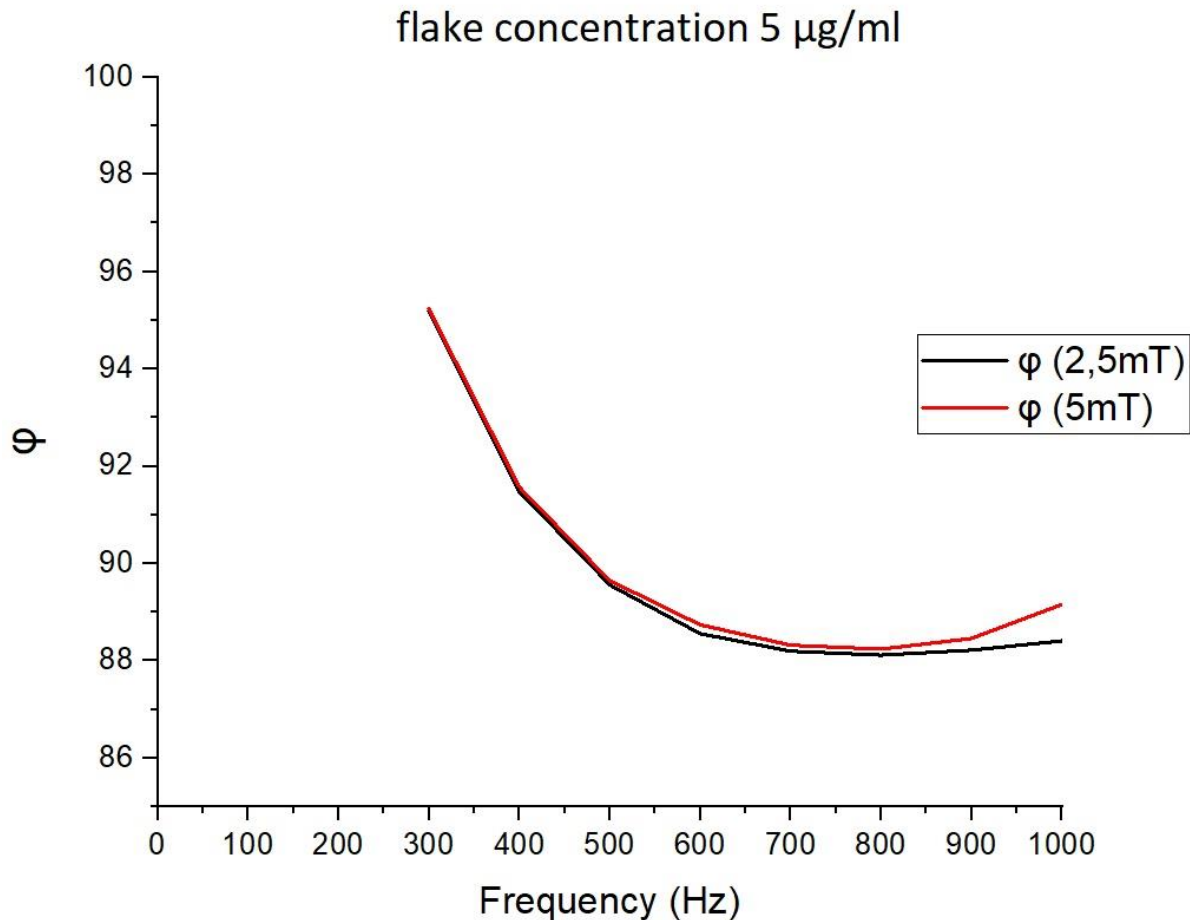


Figure VIII Phase vs Frequency plot of FSS solution (concentration of 50 $\mu\text{g}/\text{ml}$) at different \vec{B} .

V. Conclusions and future prospects

From the first pilot investigation described above, and whose results are showed in Figure VII and VIII, it seems possible to conclude that the BDG particles in solution responded to an external magnetic field, and thus the method adopted to induce ferromagnetism was successful. As obvious, the data thus far obtained with this proof of concept are few and only preliminary, thus inadequate to come to definitive conclusions, but still enough for a cautious optimism.

Further analysis and tests are necessary to prove the magnetism of all the samples prepared, and not only of those containing iron, but especially those containing cobalt and nickel, whose biocompatibility should be higher than the one of Fe. The biocompatibility of the materials used might also be a factor worth researching on in future studies on this biosensor.

In addition, the confirmation of induced magnetism still doesn't respond to the main aim of the experiment, whose goal was to produce a more sensitive, label-free biosensor for the detection of biological molecules. While no data are yet available to answer the main question, a good candidate for preliminary tests could be identified in Bovine Serum Albumine (BSA), a plasma protein commonly used in medical testing with good binding properties. Further and more comprehensive studies are necessary, then, to confirm the magnetism and discuss further whether this biosensor is suitable for the sensing of biomolecules and with which sensitivity.

References

- [1] "The Nobel Prize in Physics 2010 - Press Release," Nobelprize.org [Online]. Available at: https://www.nobelprize.org/nobel_prizes/physics/laureates/2010/press.pdf [Last Accessed 31/05/2018].
- [2] K. Novoselov, A. Geim, S. Morozov, D. Jiang, Y. Zhang, S. Dubonos, I. Grigorieva and A. Firsov, "Electric Field Effect in Atomically Thin Carbon Films," *Science*, vol. 306, no. 5696, pp. 666-669, 22 10 2004.
- [3] Wang J., Ma F., Sun M., Graphene, hexagonal boron nitride, and their heterostructures: properties and applications, 2017, *RSC Advances*, 7, 16801-16822.
- [4] "Graphene in Autospace Industry", Cambridgenanosystems.com [Online]. Available at: <https://cambridgenanosystems.com/graphene-aerospace-industry/> [Last Accessed 31/05/2018].
- [5] "Graphene aerospace strategy launched", Manchester.ac.uk [Online]. Available at: <http://www.manchester.ac.uk/discover/news/graphene-aerospace-strategy-launched/> [Last Accessed 31/05/2018].
- [6] Elmarakbi A.M., Azoto W.L., Novel composite materials for automotive applications: concepts and challenges for energy-efficient and safe vehicles, 2015, *10th International Conference on Composite Science and Technology*.
- [7] Reddy D., Register L.F., Carpenter G.D., Banerjee S.K., Graphene field-effect transistors, 2011, *Journal of Physics D: Applied Physics*, 31.
- [8] Zhan B., Li C., Yang J., Jerkins G., Huang W., Dong X., Graphene Field-Effect Transistor and its applications of electronic sensing, 2014, *Small*, 10, 4042-4065.
- [9] Mikhailov S.A., Non-linear graphene optics for terahertz applications, 2009, *Microelectronics Journal*, 40, 712-715.
- [10] Yang Y., Asiri A.M., Tang Z., Du D., Lin Y., Graphene based materials for biomedical applications, 2013, *MaterialsToday*, 16, 365-373.
- [11] Farshid B., Lalwani G., Mohammadi M.S., Simonsen J., Sitharaman B., Boron nitride nanotubes and nanoplatelets as reinforcing agents of polymeric matrices for bone tissue engineering, 2015, *Journal of Biomedical Materials Research B: Applied Biomaterials*, 105B, 406-419.
- [12] Mateti S., Wong C.S., Liu Z., Yang W., Li Y., Li L.H., Chen Y., Biocompatibility of boron nitride nanosheets, 2018, *NanoResearch*, 11, 334-342.
- [13] Manzeli S., Ovchinnikov D., Pasquier D., Yazyev O.V., Kis A., 2D transition metal dichalcogenides, 2017, *Nature Reviews Materials*, 2.
- [14] Choi W., Choudhary N., Han G.H., Park J., Akinwande D., Lee H.Y., Recent development of two-dimensional transition metal dichalcogenides and their applications, 2017, *MaterialsToday*, 20, 116-130.
- [15] "Graphene: 2D carbon", GraphITA 2015, Graphita.bo.immm.cnr.it [Online]. Available at: <http://graphita.bo.immm.cnr.it/graphita2011/graphene.html> [Last Accessed: 11/05/2018]

- [16] V. Singh, D. Joung, L. Zhai, Das S., S. Khondaker and Seal, Graphene based materials: Past, present and future, *Progress in Materials Science*, no. 56, pp. 1178-1271, 2011.
- [17] A. C. Ferrari, F. Bonaccorso, V. Fal'ko, K. Novoselov, S. Roche, P. Boggild, S. Borini, F. Koppens, V. Palermo and N. Pugno, 2015, Science and technology roadmap for graphene, related two-dimensional crystals, and hybrid systems, *Nanoscale*, 7, 4598-4810.
- [18] Bhuyan M.S.A., Uddin M.N., Islam M.M., Bipasha F.A., Hossain S.S., Synthesis of graphene, 2015, *International Nano Letters*, 6, 65-83.
- [19] Avouris P., Dimitrakopoulos C., Graphene: synthesis and applications, 2012, *MaterialsToday*, 15,86-97.
- [20] Allen M.J., Tung V.C., Kaner R.B., Honeycomb carbon: a review of graphene, 2010, *Chemical Reviews*, 110, 132-145.
- [21] Bharech S., Kumar R., A review on the properties and applications of graphene, 2015, *Journal of Material Science and Engineering*, 2, 70-73.
- [22] Taghioskoui M., Trends in graphene research, 2009, *MaterialsToday*, 12, 34-37.
- [23] Novoselov K., Fal'ko V.I., Colombo L., Gellert P.R., Schwab M.G., Kim K., A roadmap for graphene, 2012, *Nature*, 490, 192-200.
- [24] Berry V., Impermeability of graphene and its applications, 2013, *Carbon*, 5, 52.
- [25] Yoo B.M., Shin H.J., Yoon H.W., Park H.B., Graphene and Graphene oxide and their uses in barrier polymers, 2014, *Journal of Applied Polymer Science*, 131.
- [26] Wassei J.K., Kaner R.B., Graphene, a promising transparent conductor, 2010, *MaterialsToday*, 13, 52-59.
- [27] Kim H., Ahn J.H., Graphene for flexible and wearable applications, 2017, *Carbon*, 120, 244-257.
- [28] Bolotin K.I., Sikes K.J., Jiang Z., Klima M., Fudenberg G., Hone J., Kim P., Stomer H.L., Ultrahigh electron mobility in suspended graphene, 2008, *Solid State Communications*, 146, 351-355.
- [29] E. McCann, "Electronic properties of monolayer and bilayer graphene", 2011, *Graphene Nanoelectronics: Metrology, Synthesis, Properties and Applications*, Springer, Berlin, Heidelberg, 235-275.
- [30] Schwierz F., Graphene transistors, 2010, *Nanotechnology*, 5, 487-496.
- [31] Geim A., Novoselov K., "The Rise of Graphene", 2007, *Nature Materials*, 6, 183-191.
- [32] Novoselov K., Geim A., Morozov S., Jiang D., Katsnelson M., Grigorieva I., Dubonos S. and Firsov A., Two-dimensional gas of massless Dirac fermions in graphene, 2005, *Nature*, 438, 197-200.
- [33] Baudino L., Electronic Properties of graphene-based field effect transistor, Master of Science Thesis, 2018.
- [34] Castro Neto A., Guinea F., Peres N.M.R., Novoselov K.S., Geim A.K., The electronic properties of graphene, 2009, *Reviews of Modern Physics*, 81, 109-162.

- [35] Ju L., Shi Z., Nair N., Lv Y., Jin C., Velasco J. J., Ojeda-Aristizabal C., Bechtel H., Martin M., Settl A., Analytis J., Wang, F., Topological Valley Transport at Bilayer Graphene Domain Walls, 2015, *Nature*, 520, 650-655.
- [36] Li J., Wang K., McFaul K., Zern Z., Ren Y., Watanabe K., Taniguchi T., Qiao Z. and Zhu J., Gate-controlled Topological Conducting Channels in Bilayer Graphene, 2016, *Nature Nanotechnology*, 11, 1060-1065.
- [37] Wang J., Ma F., Liang W., Sun M., Electrical properties and applications of graphene, hexagonal boron nitride (h-BN) and graphene/hBN heretostructures, 2017, *MaterialsToday Physics*, 2, 6-34.
- [38] Du X., Skachko I, Baker a., Andrei E.Y., Approaching ballistic transport in suspended graphene, 2008, *Nature Nanotechnology*, 3, 491-495.
- [39] Zhu Y., Murali S., Cai W., Li X., Suk J.W., Potts J.R., Ruoff R.S., Graphene and graphene oxide: synthesis, properties and applications, 2010, *Advanced Materials*, 22, 3906-3924.
- [40] Baladin A.A., Suchismita G., Wenzhong B., Calizo I., Desalegne T., Miao F., Lau C.N., Superior thermal conductivity of Single-Layer graphene, 2008, *Nanoletters*, 8, 902-907.
- [41] Pop E., Varshney V., Roy A.K., Thermal properties of graphene: fundamental and applications, 2012, *MRS Bulletin*, 37, 1273-1281.
- [42] Marambio-Jones C., Hoek E.M.V., A review of the antibacterial effects of silver nanomaterials and potential implications for human health and environment, 2010, *Journal of Nanoparticle Research*, 12, 1531-1551.
- [43] Morones J.R., Elechiguerra J.L., Camacho A., Holt K., Kouri J.B., Ramirez J.T., Yacaman M.J., The bactericidal effect of silver nanoparticles, 2005, *Nanotechnology*, 16.
- [44] Zhao H., Ding R., Zhao X., Li Y., Qu L., Pei H., Yildirim L., Wu Z., Zhang W., Graphene-based nanomaterials for drug and/or gene delivery, bioimaging and tissue engineering, 2017, *Drug Discovery Today*, 22, 1302-1317.
- [45] Zhang B., Wang Y., Zhai G., Biomedical applications of the graphene-based materials, 2016, *Materials Science and Engineering C*, 61, 953-964.
- [46] Yousefi M., Dadashpour M.m Hejazi M., Hasanzadeh M., Behnam B., del la Guarda M., Shadjou N., Mokhatarzadeh A., Anti-bacterial activity of graphene oxide as a new weapon nanomaterial to combat multidrug-resistance bacteria, 2017, *Materials Science and Engineering C*, 74, 568-581.
- [47] McCallion C., Burthem J., Rees-Unwin K., Golovanov A., Pluen A., Graphene in therapeutics delivery: problems, solutions and future opportunities, 2016, *European Journal of Pharmaceutics and Biopharmaceutics*, 104, 235-250.
- [48] Zhang Q., Wu Z., Li N., Pu Y., Wang B., Zhang T., Tao J., Advanced review of graphene-based nanomaterials in drug delivery systems: synthesis, modification, toxicity and application, 2017, *Materials Science and Engineering C*, 77, 1363-1375.
- [49] Yousefi M., Dadashpour M., Hejazi M., Hasanzadeh M., Behnam B., De la Guardia M., Shadjou N., Mokhatarzadeh A., Anti-bacterial activity of graphene oxide as a new weapon nanomaterial to combat multidrug-resistance bacteria, 2017, *Materials Science and Engineering C*, 74, 568-581.

- [50] Seo D.H., Woo Y.C., Xie M., Murdock A.T., Ang E.Y.M., Jiao Y., Park M.J., Lim S.I., Lawn M., Borghi F.F., Hanz Z.J., Gray S., Millar G., Du A., Shon H.K., Ng T.Y., Ostrikov K.K., Anti-fouling graphene-based membranes for effective water desalination, 2018, *Nature Communications*, 9, 683.
- [51] Mokkaṡati V.R.S.S., Imer D.Y.K., Yilmaz N., Ozguz V., Koyuncu I., Protein mediated textile dye filtration using graphene oxide-polysulfone composite membrane, 2015, *RSC Advances*, 5, 71011-71021.
- [52] Ji H., Sun H., Qu X., Antibacterial applications of graphene-based nanomaterials: recent achievements and challenges, 2016, *Advanced Drug Delivery Reviews*, 105, 176-189.
- [53] Liu S., Zeng T.H., Hofmann M., Burcombe E., Wei J., Jiang R., Kong J., Chen Y., Antibacterial activity of graphite, graphite oxide, graphene oxide, and reduced graphene oxide: membrane and oxidative stress, 2011, *ACS Nano*, 5, 6971-6980.
- [54] Ruiz O.N., Fernando K.A.S., Wang B., Brown N.A., Luo P.G., McNamara N.D., Vangsness M., Sung Y.P., Bunker C.E., Graphene oxide: a nonspecific enhancer of cellular growth, 2011, *ACS Nano*, 5, 8100-8107.
- [55] Hegab H.M., ElMejawy A., Zou L., Mulcahy D., Saint C.P., Ginic-Markovic M., The controversial antibacterial activity of graphene-based materials, 2016, *Carbon*, 105, 362-376.
- [56] Moritz M., Geszke-Moritz M., The newest achievements in synthesis, immobilization and practical applications of antibacterial nanoparticles, 2013, *Chemical Engineering Journal*, 228, 596-613.
- [57] Perreault F., De Faria A.F., Nejati S., Elimelech M., Antimicrobial properties of graphene oxide nanosheets: why size matters, 2015, *ACS Nano*, 9, 7226-7236.
- [58] Zhu Z., Su M., Ma L., Ma L., Liu D., Wang Z., Preparation of graphene oxide-silver nanoparticle nanohybrids with highly antibacterial capability, 2013, *Talanta*, 117, 449-455.
- [59] Nguyen V.H., Kim B.-K., Jo Y.-L., Shim J.-J., Preparation and antibacterial activity of silver nanoparticles decorated graphene composites, 2012, *The Journal of Supercritical Fluids*, 72, 28-35.
- [60] Kavitha T., Gopalan A.I., Lee K.P., Park S.Y., Glucose sensing, photocatalytic and antibacterial properties of graphene-ZnO nanoparticle hybrids, 2012, *Carbon*, 50, 2994-3000.
- [61] Chang Y.N., Ou X.M., Zeng G.M., Gong J.L., Deng C.H., Jiang Y., Liang J., Yuan G.Q., Liu H.Y., He X., Synthesis of magnetic graphene oxide-TiO₂ and their antibacterial properties under solar irradiation, 2015, *Applied Surface Science*, 343, 1-10.
- [62] Mazaheri M., Akhavan O., Simchi A., Flexible bactericidal graphene oxide-chitosan layers for stem cell proliferation, 2014, *Applied Surface Science*, 301, 456-462.
- [63] Zhang Z.B., Wu J.J., Su Y., Zhou J., Gao Y., Yu H.Y., Gu J.S., Layer-by-layer assembly of graphene oxide on polypropylene macroporous membranes via click chemistry to improve antibacterial and antifouling performance, 2015, *Applied Surface Science*, 332, 300-307.
- [64] L. Duan, Y. Wang, Y. Zhang, J. Liu, Graphene immobilized enzyme/polyethersulfone mixed matrix membrane: Enhanced antibacterial, permeable and mechanical properties, 2015, *Applied Surface Science*, 355, 436-445
- [65] Surudzic R., Jankovic A., Bibic N., Vukasinovic-Sekulic M., Peric-Grujic A., Miskovic-Stankovic V., Park S.J., Rhee K.Y., Physico-chemical and mechanical properties and antibacterial activity of

silver/poly(vinyl alcohol)/graphene nanocomposites obtained by electrochemical method, 2015, *Composites Part B: Engineering*, 85, 102-112.

[66] Fan Z., Liu B., Wang J., Zhang S., Lin Q., Gong P., Ma L., Yang S., A Novel Wound Dressing Based on Ag/Graphene Polymer Hydrogel: Effectively Kill Bacteria and Accelerate Wound Healing, 2014, *Advanced Functional Materials*, 24, 3933-3943.

[67] Pandit S., Cao Z., Mokkalapati V.R.S.S., Celauro E., Yurgens A., Lovmar M., Westerlund F., Mijakovic I., Vertically aligned graphene coating is bactericidal and prevents the formation of bacterial biofilms, 2018, *Advanced Materials Interfaces*, 5.

[68] Tu Y., Lv M., Xiu P., Huynh T., Zhang M., Castelli M., Liu Z., Huang Q., Fan C., Fang H., Zhou R., Destructive extraction of phospholipids from Escherichia coli membranes by graphene nanosheets, 2013, *Nature Nanotechnology*, 8, 594-601.

[69] Li Y., Yuan H., Von dem Bussche A., Creighton M., Hurt R.H., Kane A.B., Gao H., Graphene microsheets enter cells through spontaneous membrane penetration at edge asperities and corner sites, 2013, *Proceeding of the National Academy of Sciences*, 110, 12295-12300.

[70] Liu S., Zeng T.H., Hofmann M., Burcombe E., Wei J., Jiang R., Kong J., Chen Y., Antibacterial activity of graphite, graphite oxide, graphene oxide, and reduced graphene oxide: membrane and oxidative stress, 2011, *ACS Nano*, 5, 6971-6980.

[71] Perreault F., De Faria A.F., Nejati S., Elimelech M., Antimicrobial Properties of Graphene Oxide Nanosheets: Why Size Matters, 2015, *ACS Nano*, 9, 7226-7236.

[72] Khilaid P., Hussain M.A., Suman V.B., Arun A.B., Toxicology of carbon nanotubes – a review, 2016, *International Journal of Applied Engineering Research*, 11, 148-157.

[73] Kobayashi N., Izumi H., Morimoto Y., Review of toxicity studies of carbon nanotubes, 2017, *Journal of Occupational Health*, 59, 394-407.

[74] Liu Y., Zhao Y., Sun B., Chen C., Understanding the toxicity of carbon nanotubes, 2013, *Accounts of Chemical Research*, 19, 702-713.

[75] Liu Y., Zhang Y. et al., Synthesis, characterization and cytotoxicity of phosphorylcholine oligomer grafted graphene oxide, 2014, *Carbon*, 71, 166-75.

[76] Waiwijit U., Kandhavivorn W. et al., Cytotoxicity assessment of MDA-MB-231 breast cancer cells onscreen-printed graphene-carbon paste substrate, 2014, *Colloids Surf B Biointerfaces*, 113, 190-97.

[77] Chowdhury S.M., Lalwani G. et al., Cell specific cytotoxicity and uptake of graphene nanoribbons, 2013, *Biomaterials*, 34, 283-293.

[78] Ludowiak A. Kedziora A. et al., Antimicrobial graphene family materials: progress, advances, hopes and fears, 2016, *Advances in Colloid and Interface Science*, 236, 101-12.]

[79] Akhavan O., Ghaderi E. et al., Size dependent genotoxicity of graphene nanoplatelets in human stem cells, 2012, *Biomaterials*, 33, 8017-25.

[80] Xie Y., Wu B. et al., Influence of graphene on microbial community and antibiotic resistance genes in mouse gut as determined by high-throughput sequencing, 2016, *Chemosphere*, 144, 1306-11.

- [81] “Basic Electronics – Types of Transistors”, Tutorialspoint.com [Online]. Available at: https://www.tutorialspoint.com/basic_electronics/basic_electronics_types_of_transistors.htm [Last accessed 31/05/18]
- [82] “Power Semiconductor Devices”, Allaboutcircuits.com [Online]. Available at: <https://www.allaboutcircuits.com/technical-articles/a-review-on-power-semiconductor-devices/> [Last accessed 31/05/2018]
- [83] Bondavalli P., Carbon-nanotubes based transistors composed of single-walled carbon nanotubes as gas sensors: a review, *Comptes Rendus Physique*, 11, 389-396.
- [84] Tran T.T, Mulchandani A., Carbon nanotubes and graphene nano field-effect transistor-based biosensors, 2016, *Trends in Analytical Chemistry*, 79, 222-232.
- [85] Song Y., Luo Y., Zhu C., Li H., Du D., Lin Y., Recent advances in electrochemical biosensors based on graphene two-dimensional nanomaterials, 2016, *Biosensors and Bioelectronics*, 76, 195-212.
- [86] Chen Z., Appenzeller J., Knoch J., Lin Y., Avouris P., The Role of Metal–Nanotube Contact in the Performance of Carbon Nanotube Field-Effect Transistors, 2005, *Nano Letters*, 5, 1497-1502.
- [87] Andronescu C., Schuhmann W., Graphene-based field effect transistors as biosensors, 2017, *Current Opinion in Electrochemistry*, 3, 11-17.
- [88] Tejeda A., Soukiassian P.G., Graphene: from functionalization to devices, 2014, *Journal of Physics D: Applied Physics*, 47, 90201.
- [89] Kuila T., Bose S., Khanra P., Mishra A.K., Kim N.H., Lee J.H., Recent advances in graphene-based biosensors, 2011, *Biosensors and Bioelectronics*, 26, 4637-4648.
- [90] Pumera M., Graphene in biosensing, 2011, *MaterialsToday*, 14, 308-315.
- [91] Schwierz F., Graphene Transistors, 2010, *Nature Technology*, 5, 487-496.
- [92] Ohno Y., Maehashi K., Yamashiro Y., Matsumoto K., Electrolyte-gated graphene field-effect transistor for detecting pH and protein adsorption, 2009, *Nanoletters*, 3318-3322.
- [93] Mackin C.E., “Electrolyte-gate graphene field-effect transistors modeling and applications”, 2015, S.M., Massachusetts Institute of Technology, Department of Electrical Engineering and Computer Science [Online]. Available at: <https://dspace.mit.edu/handle/1721.1/97815> [Last accessed 31/05/2018].
- [94] Mackin C., Palacios T., Large-scale sensor systems based on graphene electrolyte-gate field-effect transistors, 2016, *Analyst*, 141, 2704-2711.
- [95] Ohno Y., Maehashi K., Matsumoto K., Chemical and biological sensing applications based on graphene field-effect transistors, 2010, *Biosensors and Bioelectronics*, 26, 1727-1730.
- [96] “Graphene applications in Electronics”, Slideshare.net [Online]. Available at: <https://www.slideshare.net/researcher1234/graphene-applications-in-electronics> [Last accessed 18/05/2018]
- [97] “Changing charge-doping in graphene”, Nanotechweb.org [Online]. Available at: <http://nanotechweb.org/cws/article/tech/46912> [Last accessed 18/05/2018].
- [98] Lu N., Wang L., Li L., Liu M., A review for compact model of graphene field-effect transistors, 2017, *Chinese Physics B*, 26.

- [99] Lin C.T., Loan P.T., Chen T.Y., Liu K.K., Chen C.H., Wei K.H., Li L.J., Label-free electrical detection of DNA hybridization on graphene using hall effect measurements: revisiting the sensing mechanism, 2013, *Advanced Functional Materials*, 23, 2301–2307.
- [100] Zheng C., Huang L., Zhang H., Sun Z., Zhang Z., Zhang G.J., Fabrication of ultrasensitive field-effect transistor DNA biosensors by a directional transfer technique based on CVD-grown graphene, 2015, *Applied Materials & Interfaces*, 7, 16953-16959.
- [101] Green N.S., Norton M.L, Interactions of DNA with graphene and sensing applications of graphene field-effect transistor devices: a review, 2015, *Analytica Chimica Acta*, 853, 127-142.
- [102] Cai B., Huang L., Zhang H., Sun Z., Zhang Z., Zhang G.-J., Gold nanoparticles-decorated graphene field-effect transistor biosensor for femtomolar MicroRNA detection, 2012, *Biosensors and Bioelectronics*, 74, 329–334.
- [103] He Q., Sudibya H.G., Yin Z., Wu S., Li H., Boey F., Huang W., Chen P., Zhang H., Centimeter-long and large-scale micropatterns of reduced graphene oxide films: fabrication and sensing applications, 2010, *ACS Nano*, 4, 3201–3208.
- [104] Xie H., Li Y-T., Lei Y-M., Liu Y-L., Xiao M.M., Gao C., Pang D.W., Huang W.H., Zhang Z.Y., Zhang G.J., Real-time monitoring of nitric oxide at single-cell level with porphyrin-functionalized graphene field-effect transistor biosensor, 2016, *Analytical Chemistry*, 88, 11115–11122.
- [105] Chen Y., Ren R., Pu H., Guo X., Chang J., Zhou G., Mao S., Kron M., Chen J., Field-effect transistor biosensor for rapid detection of Ebola antigen, 2017, *Scientific Reports*, 7, 10974.
- [106] Kim Y.W., Sardari S.E., Iliadis A.A., Ghodssi R., A bacterial biofilm surface acoustic wave sensor for real time biofilm growth monitoring, 2010, *IEEE SENSORS 2010 Conference*, 1568-1571.
- [107] Shan C., Yang H., Han D., Zhang Q., Ivaska A., Niu L., Graphene/AuNPs/chitosan nanocomposites film for glucose biosensing, 2010, *Biosensors and Bioelectronics*, 25, 1070-1074.
- [108] Ohno Y., Maehashi K., Matsumoto K., Chemical and biological sensing applications based on graphene field-effect transistors, 2010, *Biosensors and Bioelectronics*, 26, 1727-1730.
- [109] Levy S.B., Marshall B., Antibacterial resistance worldwide: causes, challenges and responses, 2004, *Nature Medicine*, 10, 122-129.
- [110] Kardas P., Devine S., Golembesky A., Roberts C., A systemic review and meta-analysis of misuse of antibiotic therapies in the community, 2005, *International Journal of Antimicrobial Agents*, 26, 106-113.
- [111] Martin M.J., Thottathil S.E., Newman T.B., Antibiotics overuse in animal agriculture: a call to action for health care providers, 2015, *American Journal of Public Health*, 105, 2409-2410.
- [112] Chang Q., Wang W., Regev-Yochay G., Lipsitch M., Hanage W.P., Antibiotics in agriculture and the risk to human health: how worried should we be?, 2015, *Evolutionary Applications*, 8, 240-247.
- [113] “Semiconductor Lithography (Photolithography) – The Basic Process”, Lithoguru.com [Online]. Available at: <http://www.lithoguru.com/scientist/lithobasics.html> [Last Accessed 31/05/2018].
- [114] “Developers, Metal Ion Free (Organic) Developers”, Micromaterialstech.com [Online]. Available at: <http://micromaterialstech.com/products/photoresist-developers-tmah-koh-naoh/> [Last Accessed 31/05/2018].

- [115] “Microposit® S1800® Series Photo Resist”, Cmnst.ncku.edu.tw [Online]. Available at: <http://cmnst.ncku.edu.tw/ezfiles/23/1023/img/127/s1800seriesDataSheet.pdf> [Last Accessed 31/05/2018]
- [116] “LOR Lift-Off Resists”, Nanofab.utah.edu [Online]. Available at: <https://www.nanofab.utah.edu/svn/public/documents/Non%20SOPs/Photoresist/LOR%20resist%20spec%20sheet2.pdf> [Last Accessed 31/05/2018]
- [117] Ferrari A., Basko D., Raman spectroscopy as a versatile tool for studying the properties of graphene, 2013, *Nature Nanotechnology*, 8, 235-246.
- [118] Ferrari A., Meyer J., Scardaci V., Casiraghi C., Lazzeri M., Mauri F., Piscanec S., Jiang D., Novoselov K., Roth S., Geim A., Raman Spectrum of Graphene and Graphene Layers, 2006, *Physical Review Letters*, 97, 187401-187404.
- [119] Childres, Jauregui L., Park W., Cao H., Chen Y., Raman Spectroscopy of Graphene and Related Materials, *New Developments in Photon and Materials Research*, Binghamton, NY, USA, Nova Science Publishers, Incorporated, 2013.
- [120] Chang J.K., Hsu C.C., Liu S.Y., Wu C.I., Gharib M., Yeh N.C., Spectroscopic studies of the physical origin of environmental aging effects on doped graphene, 2016, *Journal of Applied Physics*, 119.
- [121] Zelenitsky S., Ariano R., Harding G., Forrest A., Evaluating Ciprofloxacin dosing for *Pseudomonas Aeruginosa* infection by using clinical outcome-based Monte Carlo simulations, 2005, *Antimicrobial Agents and Chemoteraphy*, 4009-4014.
- [122] “How microbes grow”, Lumenlearning.com [Online]. Available at: <https://courses.lumenlearning.com/microbiology/chapter/how-microbes-grow/> [Last Accessed 31/05/2018].
- [123] “Step 1: Microbiology”, Memorangapp.com [Online]. Available at: <https://www.memorangapp.com/flashcards/50975/Step+1%3A+Microbiology/> [Last Accessed 31/05/2018].
- [124] Anna Science Lab, annapiquelab.blogspot.com [Online]. Available at: <http://annapiquelab.blogspot.com/2017/05/iougurt.html> [Last Accessed 31/05/2018].
- [125] “Bacteria structure diagram”, Csmmith.co [Online]. Available at: <http://csmmith.co/bacteria-structure-diagram/bacteria-structure-diagram-through-the-wall-extracellular-vesicles-in-gram-positive-and-fungi-nature-reviews-microbiology/> [Last Accessed 31/05/2018].
- [126] “Batteri”, Chimica-online.it [Online]. Available at: <http://www.chimica-online.it/biologia/batteri.htm> [Last Accessed 31/05/2018].
- [127] Schneeweiß P., Magneto-Plasmonic Nanoparticles for molecular detection, Bachelor of Science Thesis, 2017, University of Vienna.
- [128] “How surface plasmon resonance works”, Nicoya Lifesciences [Online]. Available at: <https://nicoyalife.com/technology/surface-plasmon-resonance/how-surface-plasmon-resonance-works/> [Last Accessed 03/06/2018]
- [129] Schrittwieser S., Palaz B., Parak W.J., Lentijo-Mozo S., Soulantica K., Dieckhoff J., Ludwig F., Altantzis T., Bals S., Schotter J., Homegeous protein analysis by magnetic core-shell nanorod probes, 2016, *ACS Applied Materials & Interfaces*, 8, 8893-8899.

List of symbols and acronyms

APS	Ammonium Persulfate
CFU	Colony Forming Units
CVD	Chemical Vapour Deposition
E.coli	Escherichia Coli
EtOH	Ethanol
FET	Field-Effect Transistor
G	Graphene
G-FET	Graphene Field-Effect Transistor
GO	Graphene Oxide
Gt	Graphite
GtO	Graphite Oxide
i	Current [A]
IPA	Isopropyl Alcohol
l	Liter [l]
LB	Lysogeny Broth
MOSFET	Metal-Oxide-Semiconductor Field-Effect Transistor
P. A.	Pseudomonas Aeruginosa
PDMS	Polydimethylsiloxilane
PMMA	Polymethylmethacrylate
R	Resistance [Ω]
r-GO	Reduced-Graphene Oxide
S. A.	Staphylococcus Aureus
S. E.	Staphylococcus Epidermidis

t	Time [s]
TSB	Tryptic Soy Broth
V	Voltage [V]

Aknowledgments

For the present work of Thesis I have to thank first my home supervisor, Professor Marco Sangermano, for all the help provided in these months. I am also grateful to Professor Ivan Mijakovic and his collaborators Raghu Mokkaapati and Santosh Pandit, of Chalmers University of Technology, in Göteborg, for giving me the chance to collaborate with their research group and widen my background. An honorable mention for Professor Avgust Yurgens, of Chalmers University of Technology, in Göteborg, is also due, for the all the patience and help.

Per la realizzazione del presente elaborato di Tesi devo ringraziare il mio relatore, il Professor Marco Sangermano, per l'aiuto profuso in questi mesi. Contestualmente ringrazio altresì il Professor Ivan Mijakovic della Chalmers University of Technology di Göteborg, e i suoi collaboratori Raghu Mokkaapati e Santosh Pandit, per avermi dato la possibilità di collaborare col loro gruppo di ricerca ed espandere il mio background culturale.

Una menzione speciale la devo al Professor Avgust Yurgens, per la pazienza e l'aiuto.

Ringraziamenti

A mio papà, per tutte le letture notturne della Barba del Conte, per il sostegno e per tutte le cose che mi ha insegnato, e a mia mamma, per la fiducia incrollabile che ha sempre riposto in me, tutto affetto sempre dimostrato, per le passeggiate distensive e il comfort food.

A mio fratello, per essere stato una grande fonte di ispirazione nella mia vita, per i pareri sempre onesti, e per i biglietti pre partenze.

A i nonni per tutti i pranzi, tutte le partite a carte, tutti i parbundi ogni Capodanno, tutte le zucchine con la panna e tutte le fricasà ad patate, per le 7 Goccioline del mattino e per essere stati fieri delle più piccole conquiste.

A mia madrina, per essere stata la migliore madrina che una bambina potesse desiderare prima, e poi la migliore madrina che una ragazza potesse desiderare.

A Evelyn, perchè abbiamo iniziato con Wildfire e poi non ci siamo più fermate. Ammiro davvero la tua risolutezza e determinazione, senza però dimenticare la giusta gaiezza. A Ilaria, per i momenti più seri e quelli più gioiosi, sempre condivisi. Sono profondamente contenta di essere vostra amica.

A Franz, Ire, Franci, Peppe e Fede. Avete reso le giornate al Poli un ottimo diversivo allo studio, e per giunta in gran bella compagnia. Per i pranzi assieme, per le discussioni di serie tv, per quelle di calcio, quelle di PokemonGo, quelle sul futuro, quelle sugli esami presenti, per gli unicorni rosa e gli scarabocchi a margine, per le giornate in terza fila e quelle nascosti in mezzo all'aula, per Gardaland e per i messaggi vocali prima degli esami.

A Carro e Mani, per aver reso il periodo da lowans sia epico che trash, per aver fatto di me un uomo, per le serate ad un dollaro e per i viaggi in giro per il continente.

A Angie, Alice, Gabri, Luca, Mauri e Olga, per aver reso l'esperienza svedese un'avventura goliardica in multiplayer. Per tutti i giochi di società, per le partite di pallavolo, per le cene assieme e le discussioni su qualsivoglia argomento, per le insinuazioni sulla mia vera essenza, per esservi presi cura di me ed essere sopravvissuti alla mia cucina.

Ai compagni di corso del primo anno, quelli del primo anno in inglese e nello specifico le mie Pretty Girls, che seppure sparse per il mondo rimangono legate da profondo affetto e ci sono sempre l'una per l'altra.

A tutti i compagni di corso degli anni successivi, per le risate, i kebab, i panini oleosi, per l'aiuto e il tempo trascorso assieme.

A tutti gli amici dell'avventura americana: Val per le eterne chiacchierate, Fra per le risate e la compagnia, Leo per aver compreso più dai silenzi che dalle parole, Manuel per le avventure in California, Shanti per il suo unire un animo leggero ad un cuore grande. Agli AKL per avermi fatto sentire la benvenuta, a Arianna e Tirra per la loro allegria e a tutto il gruppo di foreign students.

A My, Ignis, Martin, Max, Johannes, Zeinab e tutti gli studenti del Dungeon, per aver reso l'ambiente di lavoro gioioso e formativo, pur sempre spalleggiandosi vicendevolmente. A tutti gli altri membri del Sysbio, Facundo, Francesca, Jin, Pinar, e tutti coloro che si sono impegnati a farmi sentire a casa.

A Ghibo, Luca e Fabio per aver condiviso con me le mie avventure, e soprattutto le mie sventure, e per aver sempre riso con me e di me. Gli amici li riconosci dal fatto che bevono vino e preparano pizzette prima della carbonara.

A tutti gli amici al di fuori dell'università, su tutti Buidas, per aver imparato ad usare la matita nera prima di me, ad Anto, per non mollare mai, a Carla per il tutoring vidding, e per il tutoring in tutto il resto.

Siete stati, e confido continuerete ad essere, cioè che di veramente importante mi ha lasciato il percorso universitario.

A tutti voi, grazie. Di cuore.

To my dad, for all the times you read me La Barba del Conte before going to bed, for your support and for all the things you taught me, and to my mom, for the unshakable faith she always had in me, and the unconditional love she has always shown, for the relaxing walks and the comfort food.

To my brother, for being a huge inspiration for me throughout all my life, for his always honest opinions, and for his notes before I was leaving.

To my grandparents, for all the card games, for all the “parbundi” on New Year’s Day, for all the zucchini with sour cream and all the fricasà with potatoes, for the seven Gocciolate I could have in the morning, and for being proud even of the slightest improvements.

To my godmother, for being the best godmother a little girl could ever hope for first, and then the best godmother a grown up girl could ever hope for.

To Evelyn, because we started with Wildfire and now we’re still here. I admire your resolution and decisiveness, especially since you never forget how to laugh. To Ilaria, for all the serious moments and the not-so-serious ones, and for always sharing them. I am so happy I get you call you girls my friends.

To Franz, Ire, Franci, Peppe e Fede. You guys have been an incredible diversion during classes, and always in cheerful company. For all the times we had lunch together, for the discussion on tv shows, soccer or PokemonGo, for the discussions about the future, or those about the present, for the pink unicorns and the doodles in the margins, for the days we spent in third row and those we hid at the back of the class, for Gardaland and all the vocal recordings before an exam.

To Carro and Mani, for making my time as lowan filled with both epicness and trash, for making a man out of me, for all the one dollar nights and the trips around the continent.

To Angie, Alice, Gabri, Luca, Mauri and Olga, per making the Swedish experience an exuberant game in multiplayer. For all the board games, all the volleyball tournaments, for all the time we had dinner together and the discussion about absolutely anything that would pop up in our minds, for the insinuations about my true nature, for taking care of me and for surviving my cooking.

To all my classmates during the “first” first year, for those during the year in English, and specifically to my Pretty Girls. We’re all spread around the globe, but still bound by deep love and always there for each other.

To all of the classmates I had during the following years, for the laughs, for the Jungle Speed games, for all the kebabs and oily sandwiches, for the help and all the time spent together.

To all of the friends I made during the American adventure: Val for the superlong and open-hearted talks, Fra for the company and the laughs, Leo for getting to know me better from what I didn’t say than what I expressed out loud, Manuel for all the adventures in California, Shanti, for her light heart and deep soul. To the AKLs, for always making me feel welcome, to Tirra and Arianna for their cheerfulness and to all the other foreign students.

To My, Ignis, Martin, Max, Johannes, Zeinab and all the other students in the Dungeon, for making the work environment both easy-going and formative, for always having each other’s back. To all the other members in SysBio, Facundo, Francesca, Jin, Pinar, and all the other people who made me feel at ease, and at home.

To Luca, Ghibo e Fabio, for sharing with me all my adventures, and especially my misfortunes, for laughing with me and at me, both. You can recognize a friend from the friend they drink wine and prepare pizzette before making carbonara.

To all those friends I met outside of university, and especially Buidas, for learning how to use eye make up before I did, to Anto, for never giving up, and to Carla, for the vidding tutoring, and the tutoring about everything else especially.

You people have been, and I'm positive you will continue to be, the really irreplaceable gift my university years left me.

To each and every one of you, thank you, from the very bottom of my heart.